SILVA FENNICA

Monographs 3 · 2004

Ilkka Korpela

Individual Tree Measurements by Means of Digital Aerial Photogrammetry

Abstract

Korpela, I. 2004. Individual tree measurements by means of digital aerial photogrammetry. Silva Fennica Monographs 3. 93 p.

This study explores the plausibility of the use of multi-scale, CIR aerial photographs to conduct forest inventory at the individual tree level. Multiple digitised aerial photographs are used for manual and semi-automatic 3D positioning of tree tops, for species classification, and for measurements on tree height and crown width. A new tree top positioning algorithm is presented and tested. It incorporates template matching in a 3D search space. Also, a new method is presented for tree species classification. In it, a partition of the image space according to the continuously varying image-object-sun geometry of aerial views is performed. Discernibility of trees in aerial images is studied. The measurement accuracy and overall measurability of crown width by using manual image measurements is investigated. A simulation study is used to examine the combined effects of discernibility and photogrammetric measurement errors on stand variables. The study material contained large-scale colour and CIR image material and 7708 trees from 24 fully mapped plots in Southern Finland. The results of the discernibility analysis suggest that 88–100% of the total stem volume is measurable when using multiple aerial photographs. The structure and density of the forest were found to affect discernibility. The best hit-rates when using the semi-automatic tree top positioning algorithm ranged from 77 to 100% of the visually discernible trees. Systematic underestimation of the crown width was observed and the measurability of crown width was best near the image nadir. Species classification was tested in mixed stands of Scots pine, Norway spruce, and silver birch. The Kappa-coefficients ranged from 0.71 to 0.86. The results of the simulation suggest that very high accuracy at the individual tree level cannot be expected. However, if the photogrammetric measurements are unbiased, the aggregate stand variables can be very accurate. An accurate species recognition method is needed in the mixed stands in order to achieve unbiased estimates for the small strata.

Author's address Department of Forest Resource Management, POB 27, FIN-00014 University of Helsinki, Finland
Fax +358 9 191 58174 **E-mail** Ilkka.Korpela@hut.fi

Contents

Definitions

Discernibility. Property of a tree. A tree is discernible if given several aerial images an operator can manually measure it in 3D for tree top position. This requires that the tree is seen on at least two images, which view the tree from different directions.

Photograph. Herein vertical aerial photographs are referred to as photographs. Photographs represent *views*.

Image (*function*). Used also as a synonym for an aerial photograph but the use of the word image emphasises that the digital version is somehow essential. The word image is used also with templates (template image) and cross-correlation functions (cross-correlation image).

Template. A sub-image representing a tree top (in general, any object to be detected from an image).

Matching. Used in template matching (TM) and image-matching (IM). In TM the similarity of the template and the image are computed for a point in the image. TM is a pattern recognition method in image analysis. TM converts the image into a similarity or dissimilarity image, which in this study is a cross-correlation image and cross-correlation is the measure of similarity. IM is synonymous with the correspondence problem in the field of 3D machine vision. In IM, corresponding entities are matched between images, and solved for 3D locations.

Precision. An estimate is impresice if it fluctuates considerably about its mean. An impresice estimate is affected by random errors. A precise estimate is not necessarily accurate. Standard deviation is used as a measure of precision.

Accuracy. An estimate is inaccurate if it in a systematic manner deviates from the true (field measurement) value, or, if it is imprecise. Root mean square error (RMSE) is a measure for accuracy used in this study. Mean difference of true and estimated values is used for measuring systematic deviation. An inaccurate estimate is affected by random errors and/or systematic errors (bias).

Relative height. The ratio from zero to one (truncated for high trees) between tree's height and the dominant height of trees in a set which it belongs to. See H_{dom}.

Dominant tree. A tree with the relative height of above 0.9.

Co-dominant tree. A tree with the relative height of between 0.8 and 0.9.

Intermediate tree. A tree with the relative height of between 0.5 and 0.8.

Understorey tree. A tree with the relative height of below 0.5.

List of symbols

C_W Crown width (maximum width)

dbh   Stem diameter at breast height 1.3 metres above ground, above bark

h   Tree height. Length of the stem from ground to top.

sp   Species. Pine means *Pinus sylvestris* L. Spruce means *Picea abies* (L.) H. Karst. Birch means *Betula pendula* Roth and *Betula pubescens* Ehrh.

v   Tree stem volume above bark, stump excluded

D_g Basal area weighted mean diameter of a set of trees

G Basal area of a set of trees, m^2 or m^2/ha.

H_g Basal area weighted mean height of a set of trees

H_{dom} Dominant height of a set of trees. The arithmetic mean of height of trees with 100 largest diameters per hectare.

Vtot   Total stem volume of a set of trees, m^3 or m^3/ha excluding the stump. Calculated by using taper curves.

Vs   Total saw wood volume of a set of trees, m^3 or m^3/ha. Determined by letting an algorithm grade stems.

Vp   Total pulp wood volume of a set of trees, m^3 or m^3/ha. Determined by letting an algorithm grade stems.

#D   #-dimensional

ALS   Airborne laser scanning (lidar)

AT   Aerial triangulation

CIR   Colour infrared (false-colour film)

COL   Colour (colour film)

DEM   Digital elevation model

GCP   Ground control point

LS   Least-squares

RGB   Red, green, blue

Δ   Difference between observed and estimated, or between observations of different type. E.g. Δ(Z), Δ(C_W))

Aerial images: Copyright FM-kartta International ltd., Helsinki. Used with permission.

1 Introduction

1.1 Framework

The thesis of this work is that in Finnish conditions individual trees can be recognised and measured in three dimensions (3D) by using multiple high spatial resolution digitised aerial photographs. Another assertion included in this work, is that forest inventory systems based on the photogrammetric observations for tree position, height, crown diameter, and tree species, can be established as illustrated in Fig. 1.

Vertical aerial photographs taken with metric or calibrated cameras under clear sky conditions, when trees are in full leaf and the sun elevation exceeds approximately 30 degrees, are required. There should be at least two photographs per target, and the geometry of the photographs must be established with high accuracy so that reliable 3D data capture is possible. The spatial resolution of the images must be high such that a crown of a single tree is represented by several image elements. An accurate digital elevation model (DEM) is required for the estimation of tree heights.

The system in Fig. 1 is founded on a semi-automatic method for positioning tree tops in 3D, which is illustrated in Fig. 2. The idea is that image-based measurements of the crown size and tree species can partly be based on this confining information (cf. Pinz 1999a), and that tree heights are obtained directly by using a digital elevation model.

1.2 Motivation and Aims

A description of the forest, in which trees are given estimates for 3D position, species, height, and breast height diameter (Fig. 1) is detailed and useful for many purposes. Pre-harvest inventories, planning of wood procurement, forest management, control of logging activities, conventional forest monitoring, and landscape planning can derive benefit from such data. The costs of data acquisition and maintenance, accuracy, precision, scale and purpose all need consideration (Nyyssönen 1979, Päivinen 1987, Ståhl 1994). It seems evident that for many applications, sole photogrammetric observations will not suffice, and field visits are needed (cf. Nyyssönen 1955). Field observations may also be needed for reasons of validation and calibration.

Aggregated forest variables, such as the total volume of stems refer to an area or a set of trees. A forest compartment, for example, can be measured by applying sampling or by the full mapping of trees. The ill-posed problem of delineating a compartment needs to be solved by force if sampling is applied and the results are needed for a stand. Forest data comprising of mapped and measured trees would facilitate the delineation of stands by making it a more objective process. This can be seen as a motivating factor. There are also technical motives for this study. Current forest management planning systems are in principle capable of treating individual trees as basic computational units (e.g. Jonsson et al. 1993). A detailed spatial description would possibly be of use in the preparation of forecasts for the development of the forest (e.g. Mitchell 1975, Pukkala and Kolström 1991).

Remote sensing based forest inventory systems have been developed mainly to improve the cost-efficiency of data acquisition. Different passive and active, analog and digital sensing techniques, with varying radiometric and geometric properties, have been available for the experimenters. Because of the fast development of digital technology, they are now becoming available for a larger audience, and used in practice. (e.g. Pope 1957, Poso 1972, Aldred and Hall 1975, Nelson et al. 1988, Leckie 1990, Tomppo 1992, Næsset 1997, Holopainen 1998, Hyyppä and Inkinen 1999, Poso et al. 1999, Næsset and Økland 2002).

In the scope of this work, the emergent field of
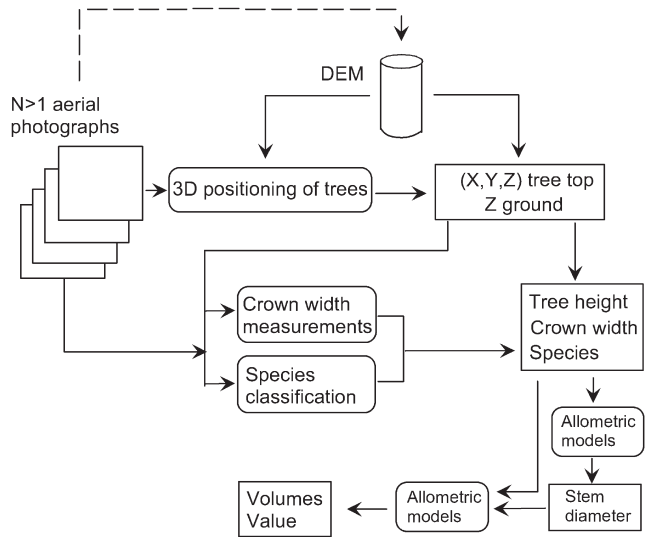
Fig. 1. Flowchart of a photogrammetric forest measurement system operating at the single tree level. Rounded rectangles represent measurements or indirect model estimation, and rectangles results.
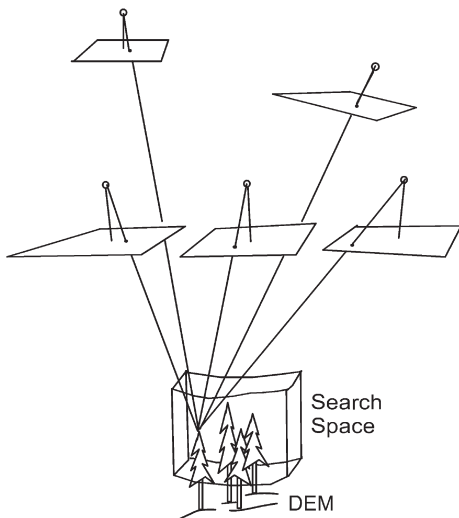
Fig. 2. The idea of positioning trees in the 3D with multiple aerial photographs (Korpela 2000). A search space is set with a priori information about the terrain elevation and height distribution of trees. A search space fills the canopy, and a finite set of candidate positions for tree tops is established there. The photographs give support to the correct positions. In subsequent steps, multiple photographs are available for the measurement of crown dimensions and tree species.

digital photogrammetry (Helava 1991, Cramer 1999, Schenk 1999) and the development of satellite positioning technology (Jiyu et al. 1996, Næsset 1999, Tötterström 2000, Bilker and Kaartinen 2001) are important. At present, computers and algorithms are replacing the high-cost, mechanic-optical, and analytical photogrammetric instruments, and the adoption of satellite positioning has caused a radical reduction in surveying costs. For the use of aerial photographs for forest inventory, this has opened new possibilities since the costs of acquiring and analysing high-accuracy digital images can be reduced.

The overall motivation of this work was to investigate the possibilities of establishing forest measurement systems utilising single tree photogrammetric measurements and indirect estimation as illustrated in Fig. 1. Any inventory schemes, which sprout from the framework, will be based on the measurements of individual trees, which need to be positioned in 3D.

1) To develop and test a semi-automatic method for 3D tree top positioning and tree height estimation was the primary objective of this study.

The basis for the tree top positioning method is from the work by Larsen and Rudemo (1998) and Korpela (2000). The objectives of the testing of

the 3D tree top positioning method were to study the effects of imaging geometry (image scale, film type, image number), the effects of target properties (stand structure) and the effects of different algorithm-parameters on the performance of the method. The costs of photography are affected by the requirements on the scale and the number of images. Film type, scale, and number of images were assumed to have an effect on the accuracy of tree top positioning. The method of positioning tree tops by using aerial photographs is semi-automatic, and based on the use of parameters that control the processes. It was considered essential to gain knowledge about the behaviour of the tree top positioning algorithm with respect to changes in the control parameters.

The forest measurement system that is based on photogrammetric observations of single trees (Fig. 1) is restricted to a small set of tree-variables on which the indirect estimation chain is based. Measurement errors in tree height, crown width, and species recognition are probable. Imperfect models are used for indirect estimation. It is likely that not all trees in a forest are discernible at all. Imperfect observations and models have an effect on the results of the forest inventory. To elaborate the possibilities of establishing a forest inventory system, information was needed about

2)   the discernibility of trees in aerial photographs,
3)   the attainable measurement accuracy of the photogrammetric tree variables (species, height and crown width), and
4)   their combined effect within the indirect estimation chain illustrated in Fig. 1.

1.3 Survey of the Use of Aerial Photographs for Forestry

Photogrammetric interpretation of qualitative and quantitative forest stand characteristics using manual methods of stereo photogrammetry is an area, which has been studied widely since the 1940s. Thus, the concept of utilising aerial photographs for forest inventory is not novel. Small-scale photographs have been used for forest mapping, assessment of insect, fire, or wind damage, estimation of stand attributes and estimation of tree species composition to mention some applications. The stratification of the forest

area into homogenous compartments or strata has been employed to improve the efficiency of field sampling in multi-stage sampling designs or in connection with the stand-wise forest inventory for forest planning. (e.g. Sarvas 1938, Bäckström and Walander 1948, Willingham 1957, Avery 1958, Spurr 1960, Nyyssönen 1962, Bickford et al. 1963, Nyyssönen et al. 1968, Poso and Kujala 1971, Axelsson 1972, Murtha 1972, Poso 1972, 1979, Ericsson 1984, Hall and Aldred 1992, Næsset 1992a, 1992b, 1993, 1998)

Visual interpretation of large-scale aerial photographs for single tree characteristics such as species, height, crown width and area, and breast height diameter has been tested in many experimental studies (Worley and Landis 1954, Nyyssönen 1955, Johnson 1958, Lyons 1961, Gerrard 1969, Aldred and Sayn-Wittgenstein 1972, Sayn-Wittgenstein and Aldred 1972, Aldred 1976, Talts 1977, Sayn-Wittegenstein 1978, Spencer and Hall 1988, Savioja 1991, Kovats 1997, Anttila 1998). Both twin-camera fixed-base and single-camera sequential photographic systems have been used in the experiments. Unlike small-scale photographs, large-scale aerial photographs have not been widely used in applications. Possible reasons are the higher costs and the requirement for expertise in photogrammetry.

Digital aerial photographs have been used in practice for forest management planning in Finland since the mid-1990s. The digital computing resources had to reach the required level for fluent handling of the image data. Tarp-Johanssen (2001) distinguishes the digital analysis of forest images in two sections: 2D and 3D methods. 2D methods operate in the image domain of individual images alone whereas the 3D methods combine information from several images to operate in the physical 3D-object domain. This statement could be refined here such that 3D methods combine auxiliary information, which can also be other views, about the scene to operate in the object space. For example in orthoimage production, the auxiliary information resides in an elevation model. Such geometric constraints and conditioning are widely used in photogrammetry so that 3D information can be obtained using single images (van den Heuvel 1998).

2D digital image analysis methods for the interpretation of aerial photographs for forestry have

been studied since the late 1980s. Automating the stand delineation task by image segmentation, estimation of forest variables using spectral and textural information (van Alphen 1994, Holopainen 1998, Poso et al.1999, Muinonen et al. 2001) as well as interpretation at the single tree level have been studied (Gougeon 1995, Dralle and Rudemo 1996, 1997, Pollock 1994, 1996, Larsen 1997, 1998, 1999a, 1999b, Larsen and Rudemo 1997, 1998, Brandtberg and Walther 1998, Brandtberg 1999, 2002, Wulder et al. 2000, Pitkänen 2001, Haara and Nevalainen 2002). Forest inventory systems are also being developed to incorporate automated or semi-automated aerial photo interpretation (Pinz 1999b).

3D automated methods for the interpretation of tree or stand information from aerial photographs are a new field of applications (Kiema 1990, Korpela 2000, Tarp-Johanssen 2001, Sheng et al. 2001, Gong et al. 2002). They have evolved with the development of digital photogrammetry which has its roots in computer technology, digital image analysis and analytical photogrammetry, and which is targeted at the automation of traditional, operator based, photogrammetric data-reduction (Helava 1991, Schenk 1999). Work on the general automation has continued since the late 1950s. This has mainly been within the branch of photogrammetry (Hobrough 1959, Helava 1978, 1991, Case 1980, Rosenholm 1980, Förstner 1982, Horn 1983), but also in the field of machine vision (Jain et al. 1995, Sonka et al. 1998).

1.3.1 Discernibility of Trees in Aerial Photographs

Individual tree based forest inventory is based on measurements of all trees in a given area. This is attainable only if all trees are observable and measurable for the needed variables.

In general, only trees that have a part of the crown in direct sunlight are detectable on an aerial photograph (Kiema 1990). This is the case especially with CIR film. Panchromatic film with proper filters is used for topographic mapping in which it is necessary to obtain information about the shaded ground. The choice of optimal film-filter combination is always a compromise targeted at meeting the needs of interpretation

(Lyytikäinen 1972). Despite the progress in sensor technology, it seems that it will be difficult, if not even impossible, to detect the smallest occluded and shaded trees in a stand. This is implied also by the findings obtained from the use of very high-resolution laser scanning (Persson et al. 2002). Because the small trees are undetectable on the photographs, the need for field visits or the use of indirect estimation (e.g. Maltamo et al. 2001) seems unavoidable.

Aggregated tree crowns, in which individual branches of several trees overlap, are difficult to discern (Ilvessalo 1950, Talts 1977, Anttila 1998, Pitkänen 2001, Persson et al. 2002). The number of manually or automatically detected stems will be an underestimate under such forest conditions.

Concerning the relative size of trees that are visible to aerial images and the effect of stand structure the findings of Persson et al. (2002) are interesting although the results were obtained by using low scanning angle laser. The overall detection rates were best for stands in which only one layer of trees occurred. Detection rates were lowest in stands with bi-modal or wide height distribution. Since the undetected trees (29%) were composed of small trees with relatively small volumes, their proportion of the total volume was low (10%). The undetected trees were characterised by two variables describing the relative size of the tree: (i) distance to the closest detected tree, and (ii) the vertical angle from the tree top between zenith and the tree top of the closest detected tree. In the two-dimensional space, outlined by the two variables, most of the undetected trees were found to be small trees close (low distance, low angle) to tall trees.

1.3.2 Tree Allometry

Only the upper parts of the crowns are typically visible in vertical aerial photographs, and the contrast is low for the shaded parts of the tree crowns hampering the exact measurement of crown dimensions. The trunk is invisible, and direct measurements on the stem diameters can not generally be taken (cf. Talts 1977), hence indirect estimation needs to be employed. The size of the crown has been shown to reflect the diameter

of the stem (Zieger 1928 in Spurr 1960 p. 383, Ilvessalo 1950, Jakobsons 1970, Kalliovirta and Tokola 2003). As early as in 1950, Ilvessalo motivated his study "On the correlation between the crown diameter and the stem of trees" with the requirement that such fundamental information is needed for estimating the growing stock from aerial photographs.

The allometric models drawn up by Kalliovirta and Tokola (2003) for Finnish conditions are important in the context of this work. Regression models for Scots pine (*Pinus sylvestris* L.), Norway spruce (*Picea abies* (L.) H. Karst.), and Birch (*Betula pendula* Roth and *Betula pubescens* Ehrh.) were derived using a large sample tree data set from the eighth and ninth Finnish National Forest Inventory. The models predict the diameter at breast height by three different sets of independent variables: {sp, h}, {sp, C_W}, and {sp, h, C_W}. The three-variable models had RMSEs from eight to ten per cent. In a separate test material consisting of 295 trees, the standard deviations of differences were from 20 to 23 mm for the {sp, h, C_W}-models without notable bias. The data for the models were not free from measurements errors, and the regression models tend to average. It is unlikely for the models to produce extreme values correctly (cf. Smith 1986). On the other hand, the material was representative and performed well in the test data.

Assuming that it is possible to recognise the tree species correctly, and to measure tree height and crown diameter with high accuracy from aerial photographs, the allometric models can be used to obtain an estimate for the dbh with 20–30 mm accuracy. Measuring dbh with a caliper leads to a five to seven millimetre standard error (Päivinen 1987), and the recently introduced laser dendrometer has eight-millimetre standard error (Kalliovirta 2003). Thus, the accuracy is inferior when indirect photogrammetric measurements and model estimation is applied. The dependencies between variables dbh, height, and crown width are on average such that a change of one metre in tree height results in the same change in dbh as a 0.2–0.35 metres' change in crown width (Kalliovirta and Tokola 2003).

1.3.3 Measurement Accuracy of Crown Width and Tree Height

Talts (1977) reports that crown diameters in Swedish conditions could be measured without notable bias with a RMS error of 0.37–1.05 m, except for a stand in which the canopy was closed and crowns interlaced. Talts used very large-scale (1:2500–1:4000) aerial photographs obtained with terrestrial wide-angle metric camera, and mature stands. Talts (1977) concluded that measurements of individual crown diameters would not be possible with images in a smaller scale and in dense stands, although he reports of no such tests.

Persson et al. (2002) obtained estimates for crown diameters and tree heights using airborne laser data in Swedish conditions. A RMSE of 0.61 m for crown width was achieved for trees with C_W varying between three and eight metres. Automated measurements by segmentation of laser data of low scanning angle and high resolution were used. Thus, the perspective effects were minimised in this study. Persson et al. (2002) used Jakobsons' (1970) models (cf. Talts 1977) to predict the dbh and obtained a RMSE of 3.8 cm, which corresponds to 10% of the mean in the data. Combined use of tree height and dbh estimates lead to 0.21 m^3 or 22% RMSE in the single tree volume estimates.

In a recent Canadian study (Pouliot et al. 2002) small coniferous trees with C_W varying from 0.1 to 1.4 metres were manually delineated with an 11% RMSE using digital aerial images of five centimetre pixel size. Correspondingly, using an automated delineation method, a RMSE from 17.9 to 39.0% was obtained for varying pixel sizes from 5 to 30 centimetres. In this study, the maximum nadir angle or the field of view of the image data was low – less than seven degrees – to minimise the perspective effects.

Besides the effects that are connected with stand density and vertical structure, it seems likely that perspective effects and the overall image-object-sun geometry (Section 1.4.2) affect crown diameter measurements on aerial photographs. However, no studies were found in which the effect of viewing geometry on tree crown diameter-measurements would have been investigated.

The accuracy of height measurements from aerial photographs has been studied in the context of visual stereo interpretation (Worley and Landis 1954, Nyyssönen 1955, Johnson 1958, Lyons 1961, Aldred and Sayn-Wittgenstein 1972, Talts 1977, Spencer and Hall 1988, Cagnon et al. 1993, Kovats 1997, Anttila 1998). In the context of this study, studies on the accuracy of non-stereo methods (multiple image-matching, see Section 1.4.4), manual or automatic, in which the measurements are done from two or more monocular photographs, would be interesting, but as such they are missing. Findings of the stereo-methods suggest that factors related to the photography (scale, film material, and timing) and to the target (crown geometry and radiometric properties, stand structure, stand density, species composition, topography) affect height measurements. The risk of underestimating heights is apparent since the very highest top shoots can not be detected (Worley and Landis 1954, Nyyssönen 1955, Talts 1977, Anttila 1998). The amount of underestimation is related to scale such that with higher scale the bias increases (Talts 1977). This relationship between scale and accuracy of height measurements has not always been observed (e.g. Pope 1957). In stereo interpretation of large-scale photographs, the relatively large horizontal parallax hampers the stereoscopic height measurements in such a way that the operator cannot view both the butt and the tree top at the same time (Pope 1957, Talts 1977). Talts (1977) recommends the use of narrow-angle cameras for a satisfactory solution for this problem. Also, the elevation of the ground is not always easily measurable from the photographs, and may hamper tree height estimation. Talts (1977) refers to the work of Kvarnbrink and Thunberg (1952) in which it was found that only 12% of the ground is visible, from the above, under normal Swedish forest conditions.

1.3.4 Tree Species Recognition Using Aerial Photographs

Species identification is crucial in forest inventory for technical, economic, and ecological reasons. In the boreal zone, the number of trees species is low, and in Finland, the main species Scots pine, Norway spruce, downy birch, and silver birch constitute 96.5% of the total stem volume (Tomppo et al. 2001).

In practical forestry, CIR photographs, with suitable enhancement, have been used successfully for delineating stands and separating between coniferous and deciduous stands. Visual interpretation is a slow and subjective process, which motivates for the use of numerical methods. Tree species recognition algorithms that operate at the individual tree level have been developed for high-resolution images and ranging data. They are mainly based on the spectral properties of the observed signal (e.g. Rohde and Olson 1972, Meyer et al. 1996, Gougeon et al. 1999, Pinz 1999a, Haara and Haarala 2002). Structure-based classification methods have also been developed (Brandtberg 1999, Brandtberg et al. 2003). Combined methods in which structural and spectral features are used have also been developed (Brandtberg 2002).

In customary determination of tree species, a forester would rely on a number of distinctive features with varying scale. Sometimes ecological factors are used to help species identification – impossible choices are ruled out and likely ones are stressed. If the species-specific features are distinct and well known to the interpreter, visual species identification on the ground can be very accurate. Species identification is challenging when the number of features is reduced or if the features are shared by several species. The latter holds often true for species in the same genus (cf. Brandtberg et al. 2003). Details such as leaves and branches become unusable when the scale of aerial photographs is higher than 1:5000–1:8000 (Talts 1977, Sayn-Wittgenstein 1978, Haara and Haarala 2002). Very large-scale photographs have been used successfully for species recognition (Lyons 1961, Talts 1977, Sayn-Wittgenstein 1978).

CIR and colour film represent the simplest form of multispectral sensing. Spectral resolution is better for multispectral scanners, which have also been tested for species identification (e.g. Rohde and Olson 1972, Gougeon et al. 1999). However, there seems to be a general trade-off between the geometric and radiometric properties of sensors (cf. Leckie 1990). This also implies that the use of hybrid methods and data for the different tasks of individual tree measurements

is advisable as suggested by Pinz (1999a). Identification accuracy results obtained for different classification methods and imagery are not always comparable. Studies have been carried out in different vegetation zones, which affects the number of species. In general, it has been found that the spectral signatures in most cases overlap between species, and varying amount confusion between species is inevitable, independent of the used classification method (e.g. Gougeon et al. 1999, Brandtberg 2002).

For digitised aerial photographs and spectral classification, there are specific problems related to the varying image-object-sun geometry within an image (e.g. Rohde and Olson 1972, Haara and Haarala 2002). For example, a delineated crown segment can be comprised of pixels originating from the sun-lit crown alone, or the segment is accompanied by a varying proportion of pixels representing the shaded part of the crown. The illumination, exposure, development, and scanning processes affect the radiometric properties of the images. Two images of the same forest taken on successive days can differ from each other if the above mentioned factors are not controlled.

Training sets on which the classification is based are generally required. They are sets of trees with a known 3D position and species. Field observations are accurate, but expensive. Visual interpretation using large-scale aerial photographs can be used alternatively or in combination with field data. However, very large-scale photographs add to the costs.

1.3.5 Individual Tree Detection and Positioning

For the 3D reconstruction of objects by using multiple images, the same corresponding objects or primitives need to be detected on the images. The objects in the images and in the object domain can be points such as tree tops, area features such as projections of crown surfaces, line features, curved edges, or even individual pixels (Schenk 1999). Traditionally, 3D correspondence algorithms are divided into two groups: area-based and feature-based methods (Sonka et al. 1998, Schenk 1999). In feature-based matching points, edges, and corners are automatically identified in the images before matching takes place. Area-based algorithms, on the other hand, are based on the general assumption that pixels in correspondence have similar intensities.

For the feature-based 3D positioning of tree tops, it is desirable to have an operator or an algorithm that extracts the point locations of tree tops in the images as proposed by Larsen and Rudemo (1998). For the measurements of crown dimensions, the general approach has been to attempt the delineation of the crown into a segment, which is then measured for dimensions and possibly further processed for tree species recognition, defoliation classification etc. (e.g. Gougeon 1995, Stoltze 2001, Anttila and Lehikoinen 2002, Haara and Nevalainen 2002, Haara and Haarala 2002). The segmentation approach has also been used for obtaining stem counts and positions (Uuttera et al. 1998, Pitkänen 2001). However, for the accurate 3D reconstruction of trees, segments of crowns are not suitable. This is because the segmentation usually only succeeds with nadir views, and because the segments obtained for different viewing angles do not represent the same object, i.e. partial crown surface. Area-based matching methods have been tested for the 3D-reconstruction of individual tree crown surfaces (Sheng et al. 2001), and for canopy surface modelling and for the subsequent derivation of stand mean height (Næsset 2002).

In the context of this study, the 3D methods are emphasised although the 2D image analysis methods are also essential for tree species classification and measurement of crown dimensions.

Dralle and Rudemo (1996, 1997) have developed semi-automated tools for estimating the number of stems and tree top image positions from digital aerial photographs. The basic idea is that for a single crown there exists a local brightness maximum in the image. A high-resolution image is at first suitably smoothed and then determined for local maxima. The method was tested for panchromatic images of a Norway spruce thinning experiment. Dralle concluded (1997) that for plots with a heavy or medium thinning, 95% of the tree tops were found with a displacement error of 65 cm in the object scale. The brightness maxima were systematically located off the true positions of tree tops on the images. For the dense plots, the method produced larger

omission, commission, and displacement errors. The results were best in the nadir views. For front-lighted views, the method was no longer applicable. In front-lighted views, the branches of the trees formed spurious local maxima in the tested images of the scale 1:4000.

The local-maxima method (Dralle and Rudemo 1996, 1997, Dralle 1997, Wulder et al. 2000) is not robust against the varying image-object-sun angular orientation, which causes the appearance of similar objects to vary greatly within an aerial photograph. Template matching based tree top detection takes this effect into account (Pollock 1994, 1996, Larsen 1997, 1999a, 1999b, 1999c, Larsen and Rudemo 1997, 1998, Olofsson 2002).

Pollock (1996) built geometric-optical models for the broad-leaved trees and conifers of Ontario, Canada to be used with high spatial resolution images. The geometric-optical models were used for rendering synthetic templates of tree tops in a given imaging geometry. The method was tested with multispectral MEIS II images with a 0.4-metre resolution. The field data consisted of uneven-aged forests with many species, variation in crown size and in growing conditions. The recognition results were successful also in cases where the tree crown image regions were not clearly delimited by a contrasting background region. Human interpretations were better in cases where the crowns had irregularities caused by high stocking. Omission errors – i.e. lost trees – were the main source of error in the automatic recognition. (Pollock 1996).

Larsen (1997, 1999a, 1999b, 1999c, Larsen and Rudemo 1997, 1998) modelled the crown shape and crown-light interaction to produce ray-traced (e.g. Hearn and Baker 1997) elliptic templates representing Norway spruce tops as seen by the aerial camera. The aerial images were operated with the template to produce a cross-correlation image in which local maxima correspond to tree tops. Larsen and Rudemo (1998) report that at best the standard errors for positioning were, excluding bias, 25–30 centimetres, and that 91–98% of the trees was recognised. The use of stereo-methods, which combine results from several images, was proposed as a possible way of improving the results (Larsen and Rudemo 1998). This study and an earlier work (Korpela 2000) were strongly motivated by the proposal.

In the work by Kiema (1990), the objective was to develop a method for creating a simplified synthetic aerial image in which individual pixels were classified as having reflected from (i) the sun-lit, (ii) the shadowed part of the tree crown, or (iii) from the background. Edges of this synthetic image could be superimposed on the aerial image for finding a set of field mapped trees from the aerial image. The synthetic image was rendered using Z-buffering (Hearn and Baker 1997). Trees were given a parabolic surface as their crown envelope form. Kiema (1990) reports that the orientation of the images suffered from a low geodetic quality of the ground control points and that the radiometric quality of the scanned images was poor. The trees of two out of four plots were located on the computer screen with the help of the crown edge map.

The method proposed by Korpela (2000) for positioning tree tops in 3D incorporates the 2D template matching approach used by Larsen and Rudemo (1997, 1998) for finding tree tops from individual images. Template matching transforms the aerial images into correlation images where local maxima are assumed to correspond to projections of tree tops. The forest canopy is discretised into a 3D-point grid using a priori information about the ground elevation and the height distribution of trees. Each 3D locus is mapped on the correlation images and aggregated for a 3D-correlation value. Local maxima in this volumetric correlation data were shown to correspond to tree top positions. The acquisition of templates was simplified. Rectangular templates representing tree tops on the images were simply cut from the real images. (Korpela 2000).

In a conventional image-matching scheme for 3D reconstruction from images, very little prior knowledge about the object is needed. The strategy used by Korpela (2000) and Tarp-Johanssen (2001) uses unavoidable geometric constraints in confining the search space. 3D-models representing the object to be recognised and reconstructed in 3D or 2D, are forms of prior geometric knowledge (e.g. Grün and Baltsavias 1988, Kiema 1990, St-Onge and Cavayas 1995, Pollock 1996, Larsen 1997, Strahler 1997, Tarp-Johanssen 2001, Sheng et al. 2001, Gong et al. 2002).

Tarp-Johanssen (2001) presented a method for positioning and measuring oak stems in 3D by

using very large-scale leaf-off aerial photographs. For positioning the stems in 3D, the base of the oak-tree is modelled as a vertical cylinder, which is rendered for image templates that are matched with the aerial images to transform them into correlation images (cf. Korpela 2000). A 3D search space is established in the forest floor as a regular grid of points. Each point in the grid is computed for an average 3D-correlation by mapping the points onto the correlation images. 3D positions are found by processing the 3D correlation data for local maxima. In the estimation of the size of the stem, the parameters for the position, size, and shape (tapering was included for size estimation) of the cylinder modelling the stem are optimised by using maximum likelihood estimation. The estimation was ensured to converge by a stepwise procedure in which the position is first solved for a good approximate value. A link is established between the parameters and the image pixels. The problem is turned into finding the optimal model tree parameters. For dbh, a standard deviation of 3.2 centimetres was obtained without notable bias. The planimetric accuracy was of the same order, but the accuracy of Z was lower. Tarp-Johanssen used panchromatic aerial photographs in the scale of 1:4000 with a 4-centimetre pixel size. The optimisation by means of likelihood estimation was computer intensive and resulted in long run-times, from six to 30 minutes per tree. Match-rates with zero omission errors varied from 85% to 98%.

Gong et al. (2002) present an interactive tree interpreter to be used with three large-scale images having large forward overlap. The approach resembles that of Kiema's (1990). Kiema (1990), used a parabola of revolution to represent crown envelope. Gong et al. (2002) report on the use of generalised hemi-ellipsoids (cf. Horn 1971, Pollock 1996, Larsen 1997, Sheng et al. 2001) with parameters characterising crown depth, radius, and curvature. The interpreter is interactive and is founded on the skill of the operator that first measures the tree for butt and top 3D coordinates. When the approximate parameters for the 3D geometric tree model are known, its silhouette can be superimposed on the images. The problem turns then into optimal tree model determination, which is solved manually or semi-automatically by adjustment of the parameters that determine

the crown shape (cf. Tarp-Johanssen 2001). An edge-indicator, which compares the projected silhouette curve and the pixel values, is used for the automatic selection of an optimal model tree.

1.3.6 Development of Photogrammetry

Conventional 3D aerial photo interpretation for forestry has involved the use of analogue, optically enlarged and manually normalised (for stereopsis) photograph pairs viewed by a stereo-operator. Lens and mirror stereoscopes and parallax bars have been typical low-cost viewing and measurement instruments. High precision topographic mapping instruments such as analog or analytic stereoplotters and comparators have also been tested and used to some degree, for example in Sweden and in Norway (Talts 1977, Åge 1983, Eriksson 1984, Savioja 1991, Jensen and Köhl 1992, Næsset et al. 1992, Næsset 1992a, 1992b, 1992c, 1993, 1998). The analytical instruments, which expand the instrument ranges and allow specific formulation of the geometry of the sensor, and in which the computations and registration of observations are performed by a computer, have been commonly available since the mid 1970's (Talts 1977, Schwidefsky and Ackermann 1978, Konecky 1981, Kamara 1989, Helava 1991).

The concept of digital or softcopy photogrammetry is quite old (Schwidefsky and Ackermann 1978, Konecky 1981, Sarjakoski 1981, 1989, Schenk and Toth 1992), but only recently has the price of powerful digital computing and digital storage made digital photogrammetric workstations (DPW) and digital 3D image analysis algorithms competitive. There are many benefits in digital photogrammetry that makes it favourable (Helava 1991, Schenk 1999). The high accuracy image measurements that require sophisticated and expensive optical-mechanic instruments are done only once when the image is scanned for with a photogrammetric scanner. In principle digital images are long lasting, if properly stored, and orientations are solved just once. Image processing capabilities are available for the operator, a photo laboratory is no longer required for the basic tasks, and DPWs are universal and flexible as they possess the functionality that resides in the algorithms. If DPWs are used in visual stereoscopic

interpretation of forest scenes, a DPW cannot be expected to provide any major improvement in the visual interpretation accuracy over analog instruments such as stereocomparators or stereoplotters. The analog-to-digital transformation of the photographs always degrades the geometric and radiometric properties of the images (Helava 1978, Jain 1989, Schenk 1999). The possible benefits come in the form of improved efficiency explained mostly by the equipment flexibility and lower price of DPWs and the automation of image processing and analysis (Schenk 1999).

1.4 Geometry of Aerial Photography and Photographs

1.4.1 Sensor Geometry and Perspective Mapping

To reconstruct the position and shape of objects from photographs, the geometric laws by which images were formed need to be known. Metric aerial cameras, used commonly in aerial photography, can be regarded with sufficient accuracy to produce central projections of the photographed spatial objects and the perspective, or, the pinhole camera model can be employed.

In central projection, the points P in the object space E are mapped on the plane Π through lines (homocentric ray pencil) that pass the projection center point K and intersect the plane at points P'

$$p: E \rightarrow \Pi, p(P) = KP \cap \Pi = P' \qquad (1)$$

A Cartesian 3D-coordinate system (x, y, z) may be established to represent the camera. The origin is at the projection center (K). The film plane (Π) is co-planar with the xy-plane. The principal distance c, is the distance between the film plane (at the principal point (x_0, y_0)) and the projection center along the optical axis. By this definition, all points in the film plane have constant values for $z = \pm c$ depending on the orientation of the camera z-axis.

True cameras are never perfect realisations of the pinhole camera and the physical imaging deviates from the mathematical model chosen to model the process. For a real camera, the theoreti-

cal location of the projection center, the principal distance (or the camera constant, c), the coordinates of the principal point, and possible corrections to lens imperfections, are mathematically defined in a process called camera calibration. The inner orientation of the camera is established in this process. (Schwidefsky and Ackermann 1978, Fryer 1989, McGlone 1989, Kraus 1993).

Interior orientation of the camera establishes the ray-pencil in the projection centre-centred camera coordinate system. To map points from the object space to the film plane, the camera needs to be given 3D-position and attitude in the object coordinate frame. The attitude of the camera is represented by an orthogonal 3×3 rotation matrix, $\mathbf{R}$ that describes the differences in attitude between the camera and the object coordinate systems. The elements of $\mathbf{R}$ are the direction cosines between the coordinate axes. The angular orientation of the camera can be defined in several ways, but all definitions aim at the same fundamental target, the $\mathbf{R}$-matrix. A common way to define the attitude of the camera is to give three rotation angles $(\omega, \varphi, \kappa)$, which define how the camera coordinate system is rotated in the space with respect to the X, Y, and Z-object coordinate axes. The location of the projection center K (X_0, Y_0, Z_0) and the attitude of the camera $\mathbf{R}(\omega, \varphi, \kappa)$ define the exterior orientation of the perspective camera in six parameters.

As stated, the perspective projection $P \rightarrow \Pi$ requires that the inner and exterior orientations be known. Collinear equations that map the object coordinates (X, Y, Z) to the camera coordinates (x, y), omitting any additional calibration or atmospheric corrections, are (cf. Salmenperä 1973, Methley 1986, McGlone 1989, Kraus 1993):

$$\begin{cases} f_x: \quad x - x_0 = \\ -c\dfrac{r_{11}(X-X_0)+r_{12}(Y-Y_0)+r_{13}(Z-Z_0)}{r_{31}(X-X_0)+r_{32}(Y-Y_0)+r_{33}(Z-Z_0)} \\ f_y: \quad y - y_0 = \\ -c\dfrac{r_{21}(X-X_0)+r_{22}(Y-Y_0)+r_{23}(Z-Z_0)}{r_{31}(X-X_0)+r_{32}(Y-Y_0)+r_{33}(Z-Z_0)} \end{cases} \qquad (2)$$

r_{ij} in (2) are elements of the rotation matrix $\mathbf{R}$.

From equations in (2) it can be seen that for every object point there is a corresponding photo point.

Collinear equations and their linearizations is the core of analytic photogrammetry (Salmenperä 1973).

The equations may be solved for the object coordinates (assuming that the camera coordinate system is centred at the principal point, i.e. $x_0 = y_0 = 0$) and the inverse collinear equations are obtained

$$\begin{cases} X = X_0 + (Z - Z_0)\dfrac{xr_{11} + yr_{21} - cr_{31}}{xr_{13} + yr_{23} - cr_{33}} \\[2mm] Y = Y_0 + (Z - Z_0)\dfrac{xr_{12} + yr_{22} - cr_{32}}{xr_{13} + yr_{23} - cr_{33}} \end{cases} \quad (3)$$

The individual equations in (3) represent planes in the 3D-object space. Any 3D point along the image ray that was projected to the point on the film plane can be anywhere in the intersection of these two planes forming the ray. Equations (3) may be used to solve the 3D path of the camera ray by fixing one of the unknown object coordinates.

The perspective camera model and the collinearity equations constitute a basis for the modelling of the image-object-relationship and the solving of the photogrammetric problems. The model is often extended to cover factors such as lens imperfections and the refraction of light in the intermediate substance (cf. Schwidefsky and Ackermann 1978, McGlone 1989, Kraus 1993).

The exterior orientation of aerial photographs may be solved in many ways. The overall aim is to determine for each image frame the location of the projection center and the attitude of the camera. Aerial triangulation (AT) is the traditional indirect method that employs a set of well-known ground control points (GCP), a number of conjugate tie points, and for these their corresponding image coordinates (Kraus 1993, 1997). Image observations are obtained either manually or automatically. AT can be extended to make use of observations such as polar points, spatial distances and directions measured in field (Kraus 1997), and satellite positioning estimates for the projection centres measured during the flight (Cramer 1999). Satellite positioning estimates reduce significantly the required number of GCPs, thus rationalising the process of AT (Cramer 1999).

Direct geo-referencing i.e. the direct measurement of the exterior orientation of an imaging sensor employing satellite positioning and inertial systems, has been stimulated in recent years by the development of airborne push-broom scanners (cf. laser-scanning), which require continuous orientation information. Direct geo-referencing of aerial cameras has been shown to fulfil high accuracy requirements, and is a potential economic substitute to the somewhat laborious AT-methods. (Cramer 1999, 2001, Cramer et al. 2000).

1.4.2 Image-Object-Sun Angular Orientation

The varying image-object-sun angular orientation of aerial photographs is described by four angles illustrated in Fig. 3. The appearance of tree tops, which can be described as sharp vertical peaks, changes along with variation in the image-object-sun angular orientation. In an attempt to automate the process of positioning tree tops from aerial photographs this must be considered.
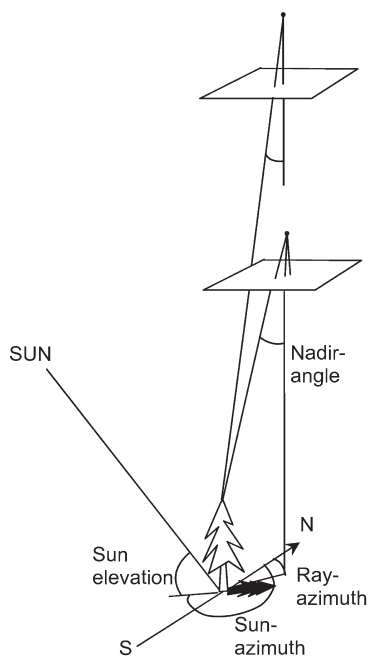

Fig. 3. Image-object-sun angular orientation. The example illustrates the back-lighted case and two cameras with different focal lengths.

Sun elevation gives the angle of the incoming sunrays to the horizon. For forest photographs, the acceptable range is usually defined to lie above ca. 30 degrees. In Southern Finland, aerial photography is possible from early April to the middle of September. Lengths of daily time-windows and phenology of flora need to be considered also. In Finland, aerial photographs are taken in the morning hours (Fig. 4) with the sun in East or Southeast.

Nadir angle (~ viewing angle) is the deviation of the camera ray from the camera nadir. For vertical photographs, it is almost the same as the image angle, the deviation of the camera ray from the optical axis. The radial displacement of vertical objects is determined by the amount of the nadir angle. Aerial cameras typically have a 23 × 23-cm film format and the focal lengths range from 9 to 30 cm. With 15-cm focal length, the maximum image angle is approximately 45 degrees in the corners of the photograph. Occlusion of objects is partly explained by the oblique viewing and the probability of occlusion increases for objects further away from the image nadir. The net area becomes small if near-nadir views are desired. Increase in the focal length reduces perspective distortion, decreases the field of view, and impairs the accuracy of Z-estimation (Fig. 3).

The azimuth angles for the camera ray and the sunrays may be used to describe image-object-sun geometry of an object on the photograph. The photograph can be classified into four sectors: front-lighted, back-lighted, back-side-lighted and front-side-lighted (cf. Dralle 1997, Larsen 1997). In the front-lighted region, sun is behind the camera, and the sunlit parts of the tree crowns are observed. In back-lighted views the shadowed sides of the crowns dominate.

1.4.3 Correspondence Problem

"One of the most fundamental processes in photogrammetry is to identify and to measure conjugate points in two or more overlapping photographs. Stereo photogrammetry relies entirely on conjugate points. In analogue and analytical photogrammetry the identification of conjugate points is performed by a human operator; in digital photogrammetry one attempts to solve the problem
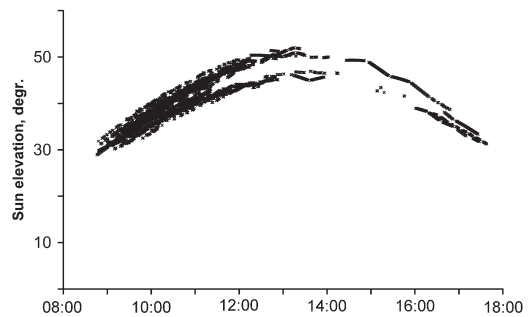
Fig. 4. Time of aerial photography in Finnish conditions during summer 2003 (CIR photography for forestry). 85% of photographs were taken before 1 p.m. local time. Nearly 10 000 exposures covering the whole country. In courtesy of FM-kartta International ltd., Helsinki, Finland.

automatically – a process known as image-matching" (Schenk 1999 p. 231). Image-matching is also known as the stereo correspondence problem in computer vision (Sonka et al. 1998).

3D measurements of objects are possible with two or more oriented photographs. The object must be seen from different perspectives i.e. the camera rays should intersect in the object space. The intersection of the camera rays gives the 3D coordinates of the object. The reliability of the 3D measurements relies on the accuracy of the image orientations, the accuracy and number of the image observations, and the imaging geometry. Here imaging geometry means the effects of camera optics, image overlap, and the flying height. (Kraus 1993).

The image observations must apply to the same, corresponding object on all images. It may be solved by stereoscopically viewing a normalised stereo pair, or by identifying the corresponding entities from multiple images monoscopically.

Schenk (1999 p. 234) provides a problem statement for image-matching:
1. Select a matching entity in one image
2. Find its conjugate (corresponding) entity in the other image(s)
3. Compute the 3D position of the matched entity in the object space
4. Assess the quality of the match.
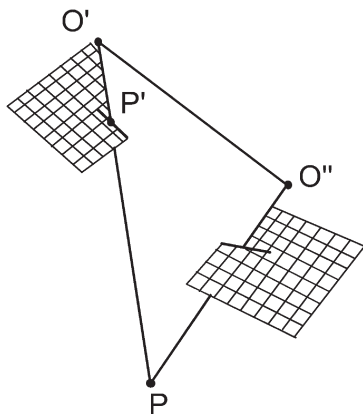
Fig. 5. Epipolar geometry of an image pair. The white triangle depicts the epipolar plane connecting the projections centers O' and O" and the object P. The search for object P pointed at image location P' is restricted to a line on the other image.

Fig. 6. Epipolar geometry of a set of three aerial photographs. The tree top at 3D-position B is pointed from image 1 at B'. The camera ray from B' to B, within the expected range in Z, [Zmin, Zmax], maps into line segments e1(B) on images 2 and 3. The dots on the images represent possible candidates (neighbouring trees) to be matched with B'. On image 2 there is only one which intersects e1(B). If that image point (camera-ray) is pointed, epipolar line segments e2(B) are defined on images 1 and 3. The intersection of epipolar lines in image 3 shows a likely candidate for the solution of correspondence problem if B really is restricted to [Zmin, Zmax], and the geometric accuracy of the images is high.

The fundamental problem of image-matching is that it is ill-posed. To be well-posed the solution should exist, be unique, and depend continuously on the data. Image-matching violates several, if not all, of the conditions above (Schenk 1999 p. 235). Ambiguity occurs in matching if the matching entities provided by step one above are not unique enough. In complex scenes with occlusion, the solution does not necessarily exist.

1.4.4 Multiple Image-Matching

Traditionally the 3D interpretation of aerial images for forestry has been done stereoscopically by using stereopairs. A good stereo operator can provide fast and accurate 3D reconstruction, and for many tasks, the human interpretation still surpasses automatic methods in efficiency (Helava 1991, Schenk 1999). Disadvantages of stereoscopic viewing and interpretation are in its subjective nature, and in the inability of the human spatial vision system to accommodate itself to an angular difference of more than 1.2 degrees (Kraus 1993, cf. Talts 1977), and in the fact that information of only two views may be used at a time.

With the presumption that the imaging geometry is accurate, the search for corresponding entities can rely on the epipolar geometry of the images (Fig. 5, Fig. 6). If an object is detected on one image at one point, the search for this object on other images is restricted to the central projections of the camera-ray of that image observation. These projections on the other images are epipolar lines, which are found on the intersections of the image planes and epipolar planes (Fig. 5). The epipolar line degenerates into a point on one image, but for the other images, lines are defined on the image planes.

The 3D path of a camera-ray may be solved with the inverse collinearity equations (3). Given an image observation and by fixing two Z-values, two 3D points along the camera-ray that produced that image observation are computed. This is ade-

quate for calculating the epipolar line segments in the other images. These two fixed Z-values may represent, for example, the extremes of the expected elevation of the object (a tree top is expected to lie within Zmin and Zmax in Fig. 6). The corresponding object point is located along the epipolar line segments, if the assumption of the expected elevation holds, and the geometry is accurate. A good approximation of the Z-coordinate reduces ambiguity of image-matching.

Computation of the 3D object coordinates of the point, which is observed on several images, calls for non-linear methods. If it is assumed that imperfect image observations were made, the problem is solved by using least-squares (LS) adjustment in which the norm of the 2D observation errors in the photographs is minimised. On the other hand, if it is assumed that perfect observations were made, but the exterior orientation of the photographs is erroneous, the 3D-point position is found by minimising the 3D errors in the object space. LS-adjustment is typically used in photogrammetry.

1.5 Qualitative Analysis of the Image Chain

1.5.1 Motivation for a Critical Examination of Task Complexity

An elaborate analysis of the image chain, or the flow of information, should be done when image interpretation is attempted. The analysis should consider all aspects affecting the feasibility of an image-based task. Recognizing the image chain includes critical examination of target properties and their variation, examination of the effects of imaging conditions, sensor geometry and radiometry, and the interpretation methods applied. (Lyytikäinen 1972).

"Image analysis is a process of discovering, identifying and understanding patterns that are relevant to the performance of an image based task" (Gonzalez and Woods 1993, p. 571). In the framework of this study, the patterns of interest are tree tops and the task is to give the tree tops a position in 3D and to measure other tree variables. The task is automated where possible. The automated recognition system should exhibit some degree of intelligence. It should be able to

extract pertinent information about the tree tops from a noisy background. It should be robust against changes in different circumstances such as the imaging geometry, and scale. In addition, the system should have some ability to make inferences from incomplete information. These characteristics can usually only be implemented in a very limited operational environment (Gonzalez and Woods 1993, Jain et al. 1995). Because of this, a single algorithm is most likely unable to solve the tasks of finding, isolating, measuring, and classifying individual trees (Pinz 1999a). Hybrid procedures are thus required.

Jain et al. (1995 p. 463) provide a qualitative method for analysing the complexity of model-based object recognition:

1. *Scene constancy*: Illumination, camera parameters, viewpoint, background, and forest characteristics. Variability is present in these factors in the case of aerial photographs and forests scenes.

2. *Image-model spaces*: For example in template matching the models of trees can be three-dimensional objects that are ray-traced for 2D templates (e.g. Pollock 1996, Larsen 1997). Perspective effects and 3-dimensionality increase the complexity of the recognition (Horn 1983).

3. *Number of objects in the model database*: Number of tree species, their varying shape, size and reflectance properties. Need for size invariance in feature detection and object description. The number of objects affects the amount of effort that needs to be spent in selecting appropriate features.

4. *Number of objects in an image and possibility of occlusion*: Occlusion is present and leads to the absence of expected features. The possibility of occlusion should be considered at the stage of hypothesis verification or quality assessment.

1.5.2 Spatial and Radiometric Properties of Analog Aerial Photographs

Aerial cameras are passive optical sensors that capture electromagnetic radiation during exposure. An object on the ground absorbs a part of the total incident light and remits by diffuse or specular reflectance the remainder. The incident light at an object point consists of direct and scattered diffuse light. Scattering occurs in the atmosphere as well as in the objects on the ground.
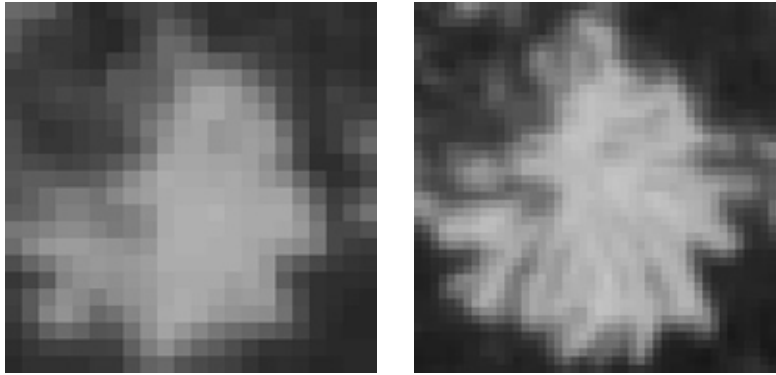
Fig. 7. 1:5000 and 1:10000 near-nadir views to a dominant spruce tree. Pixel sizes on ground are 12.5 and 25 centimetres respectively. The diameter of the crown is approximately 4.5 metres.

The irradiance on the film emulsion consists of a superimposition of the scattered radiation and of the radiation that reflected from the objects in the direction of the camera ray. The spectral sensitivity of the film depends upon the sensitivity of different chemicals in the film layers. Filters are used in connection with aerial photography to compensate for atmospheric and lens effects. The choice of the correct film-filter combination is a compromise targeted at meeting the needs of interpretation. (Lyytikäinen 1972, Lillesand and Kiefer 1979, Kraus 1993, Fent et al. 1995).

The finest details, which are visible in the aerial photographs are mainly dependent on the quality of the lens system, the film emulsion, and the immobility of the camera system during exposure (Lyytikäinen 1972, Kraus 1993). Aerial cameras are usually equipped with a forward motion compensator and a heavy-duty or stabilized camera mount (Lillesand and Kiefer 1979, Kraus 1993). The resolution of a photograph is measured in line pairs per millimetre. The interpretation of the resolution values should include a critical review of the test environment. The photographic resolution of modern aerial films and cameras, obtained in laboratory conditions, is approximately 40–105 lp/mm. The resolution is highest in the center parts of the focal plane and typical values of an average, area weighted average resolution, are 50–60 lp/mm (Kraus 1993, Schenk 1999). The optical properties of the target are also of great importance. For example, thin power lines can be

visible and blurred on aerial photographs when details of the same size are not seen in the underlying vegetation. Resolution is strongly dependent on contrast (Lyytikäinen 1972, Kraus 1993).

1.5.3 Digitized Aerial Photographs

Commercial, solid-state metric cameras that could provide the same spatial resolution as film-based aerial cameras have not yet entered the market (Schenk 1999, Petrie 2003). The data acquisition phase at the present includes the processes of selecting the film, and filters and exposing, developing and scanning the film. Scanners are usually linear sensors and the sampled and quantified signal obtained with a scanner is an approximation of the signal that was stored on the film. Scanners further introduce geometric and radiometric inaccuracy to the 2D-signal (Jain 1989, Gonzales and Woods 1993, Jain et al. 1995, Schenk 1999).

1.5.4 Scale

Humans perceive objects in the world as having structures both at coarse and at fine scales. A tree may appear as having a roughly round or cylindrical shape when seen from a distance, although it is built from a large number of branches. On a closer look individual leaves become visible, and

we can observe that the leaves in turn have texture at an even finer scale. The scale of observation has important implications when analyzing measured signals, such as images, with automatic methods (Woodcock and Strahler 1987, Lindeberg 1994). Fig. 7 illustrates the effect of scale. Individual branches contribute to the texture in the 1:5000 scale image.

Lindeberg (1994) emphasised that the problem of scale must be faced in any image situation. Two scales, the inner scale and the outer scale determine the extent of any real world object. The outer scale of an object or a feature may be said to correspond to the minimum size of a window that completely contains the object or the feature, while the inner scale may loosely be said to correspond to the scale at which substructures of the object begin to appear. In a given image, only structures over a certain range of scales can be observed. For a digital image, the inner scale is determined by the pixel size and for a photographic image by the grain size in the emulsion.

A too detailed image may even prove harmful in some situations. For example, an appropriate scale for tree crown detection and delineation may be one in which branches do not contribute to contrast and influence the behaviour of a segmentation algorithm. (Pouliot et al. 2002).

Multi-scale representations of signals such as image pyramids may be used to explicitly represent the multi-scale aspect of real world data (Lindeberg 1994, Jain et al. 1995). An image-processing algorithm may operate at first at a coarser level and continue further at a more detailed scale (Horn 1983, Zheng 1993, Brandtberg and Walter 1999, Pinz 1999a).

Scale has also significant implications on the costs of aerial photography. In general, it can be said that scale and costs are in quadratic ratio. An operational forest inventory system, which is a based on aerial photographs, needs to be cost-efficient. Thus, it is essential to study the effects of scale.

1.5.5 Objects to be Detected – Individual Trees

The many elements that absorb and reflect radiation in a tree include the foliage, flowers, cones, branches, epiphytes on the shoots, and the stem. The radiometric properties also vary during the growing season. For example, a spruce tree with an abundance of pistils and stamens and fresh shoots is easily mistaken for a deciduous tree when interpreted from an early-summer CIR photograph (cf. Brandtberg 2002). Timing of photography with respect to phenology has been shown important for tree species recognition (Sayn-Wittgenstein 1978, Key et al. 1999). The radiometric properties of needles and leaves change during the growing season (Gates 1980, Stenberg 1996). Temporal, between-year variation in the development and senescence of foliage is explained mainly by weather conditions. In a given area, the phenologic status of trees also varies between sites and tree species. In planning the timing of aerial photography, the phenology of trees and other forest flora need to be considered. However, there can be little room for fine adjustment in the timing if the season for photography is short, and appropriate weather conditions is scarce.

The crown shape, density and amount of foliage, and branching pattern vary between tree genera and species (Kujala 1958, 1965, Sarvas 1964, Horn 1971, Sayn-Wittgenstein 1978, Lillesand and Kiefer 1979). Needles of conifers are clumped in shoots (Oker-Blom 1986, Nilson and Ross 1996). Within a tree crown the density of needles is, on average, higher in the upper and outer parts of the crown. The amount of needles or foliage varies during the growing season. Crowns can be sparse. For example, crowns of pine trees growing on barren bogs are almost impossible to discern on CIR photographs because the trees have very sparse crowns, which, furthermore, have vital bog shrub and moss flora forming the background.

The branching of Scots pine is regular. There are whorls of primary shoots and no later secondary branching from lateral dormant buds. Alike most species in the Pinus-family Scots pine has a round-conical crown form. The density of needles is higher towards the surface of the crown envelope, since the spurs with needles are formed

only in new branchlets and the lifetime of needles is from two to five years. Old pines have round apexes. (Kujala 1958, Sarvas 1964). The crown shape of Norway spruce is often conical. It is a semi-shade-tolerant tree species with relatively deep crown. The branching pattern is not as regular as in the case of pine. The lifetime of needles is from five to twelve years. The pistils usually occupy the upper parts of the crowns, and there is strong variation in the flowering and cone production between growing seasons. There is also an element of between-tree variation in the flowering. (Kujala 1958, Sarvas 1964). The crown shape of silver and pubescent birch can be said to vary from conical to 'plum-shaped'. The top is not always a very distinct point feature. Birch usually has a single trunk, but occasionally has multiple stems due to stump sprouting. Birch is a light demanding, pioneering tree species. (Kujala 1965)

In Finland, aerial photographs for forestry are taken on sunny, cloudless middays. There are hardly any gale winds, but tree-sway may be assumed to take place. Any sway, or target motion, will affect the accuracy of 3D data capture from images (cf. Aldred 1964). Trees respond to variable forcing of the wind with an oscillating motion. For example, Flesch and Wilson (1999) measured angular displacements of white spruce stems and observed an average fundamental frequency of tree sway at 0.4 Hz. Secondary peaks at higher frequencies were assumed to be caused by the motion of shaking branches. Given the natural frequency of tree sway, the systematic layout of camera locations and the constant aircraft velocity, it is possible that the consecutive photographs are taken at a frequency that causes systematic errors in the reconstructed 3D-positions of the tree tops or even impedes image-matching. For example, during the field measurement campaign of this study, it was noticed that normal midday summer-wind impeded reliable height measurements from the ground. The tops of slender, 20-metre high birches swayed and bent outside the field-of-view of the hypsometer optics, even some metres away from the resting position.

1.5.6 Scene Constancy – Stand and Regional Level Aspects

Trees in a stand vary in stem and crown size, tree species, state of health, and many other qualitative and quantitative characteristics. There are stands in which the spatial pattern of trees is regular, clustered or inhomogeneous, random, or a non-stationary mixture of the preceding (Tomppo 1986). If such within-stand variation in tree-variables would not exist and trees would stand in rows on a plane, automation of photogrammetric stand cruising would be much easier.

Planted stands can have a very regular spatial pattern of trees. Birch and aspen reproduce from root and stump sprouts and often form clumps of stems with overlapping crowns. The stand structure of managed forests is altered in intermediate thinnings. In Finland, the thin-from-below-rule has been commonly practised. In addition to the effect of regeneration and intermediate fellings, soil conditions, wood harvesting tracks and ditches affect the spatial pattern of trees. Sun-lit blob-like patches on the forest floor caused by openings in the canopy are easily misinterpreted on monocular images as trees (e.g. Pitkänen 2001).

In unmanaged dense stands, the height distribution of trees is wider, spatial pattern of trees can be irregular, and the number of occluded and shaded trees is therefore likely higher. Unmanaged stands, in which the quality of the forest is decreased in regard to timber production, make up 18% of productive forest land in Finland (Tomppo et al. 2001). Only four or five species are favoured in silviculture, and pine, spruce, and birch constitute 96.5% of the total volume. Two-layer stand structure occurs in 8.4% of productive forestland, and uneven-aged forests constitute 0.8% of productive forest land. Stands in which the proportion of the main species is over 95% make 62.4% of the area of productive forest area. Mixed stands in which the percentage of main species is below 75% constitute 12.2% of productive forest. (Tomppo et al. 2001).

A 1:10000 scale photograph covers an area of approximately 2.3 by 2.3 kilometres. In Finnish conditions, an area of such size can contain almost all of the variation in forest characteristics for the region (e.g. Kangas 1994, Fish 2000).

Table 1. Examples of outlined inventory schemes (models) utilising photogrammetric individual tree measurements.

Work phase	A No field visits	B Systematic sample of field plots	C Field visits in stands of interest
I	Image (and laser data) acquisition, preparatory work.		
II Field	–	{Position, sp, dbh, h, C_W} – field observations e.g. from systematic layout of field plots. Satellite positioning + laser-relascope	{Position, sp, dbh, h, C_W} – field observations in every stand. Satellite positioning + laser-relascope
III Image	Semi-automatic measurement of tree top position and height.		
IV Image	–	Training sets for image based species classification	Training sets for image based species classification
V Image	Interpretation of tree species and measurement of crown width.		
VI	Indirect estimation of dbh and derivation of volumes. (Calibration/validation procedures in B and C).		
VII	The estimation of forest variables for the non-discernible tree stratum.		
VIII	Computation of the aggregated results, density maps etc.		

1.6 Outlines for Inventory Procedures

In this study, the task of forest data acquisition for which methodology is proposed is highly restricted. We confine ourselves to the basic quantitative tree and forest variables related closely to the commercial value of the forest. Forest management problems are secondary in the chosen context.

The thesis is that by applying photogrammetric measurements and indirect estimation with models, the following tree variables can be assessed (cf. Fig. 1, p. 8):

The set of independent variables of the allometric models f_1 that predict the dbh from photo-measurable quantities can differ. Calibration and validation of the models as well as photo-measurements is also possible for the control of gross systematic errors. Allometric models f_2 represent tree-level volume and taper curve functions. Forest variables are aggregated from the single tree data. Field visits may be needed to assess the role of small undetectable trees since the photogrammetric estimates are by nature underestimates. In the context of this study, several alternative inventory models can be considered. Three models are

– Tree top position in 3D
– Tree top position in 3D + DEM $\Rightarrow$ height
– Tree top position in 3D + Images + field data $\Rightarrow$ species
– Tree top position in 3D + Images $\Rightarrow C_W$
– f_1 (height, C_W, species) $\Rightarrow$ dbh
– f_2 (height, dbh, species) $\Rightarrow$ tree volume, sortiments, value

outlined in Table 1. The list is far from complete and the outlined models can be varied for different sampling designs.

Model A describes an inventory model without any field visits (Table 1). Results obtained by type A inventory are most susceptible to systematic errors since the tree species identification relies on photogrammetric observations only, and there is no field control for the tree and forest estimates. Models B and C require fieldwork for mapped tree-data that can be linked together on a one-to-one basis with the trees found from the aerial images. This is a fair assumption considering the recent development in the field equipment. Satellite positioning under forest canopy provides positioning accuracy in the metre level (Næsset and Jonmeister 2002). Laser-relascope, which is equipped with a ranging laser, electronic compass, angle gauge and a dendrometer, can be used for fast mapping of trees and measurement of dbh and height (Kalliovirta 2003). The measurement of crown width in the field can be time-consuming and inaccurate. It is therefore more tempting to calibrate the indirect estimation chain for the estimated dbh (phase VI) instead of the photogrammetric crown width measurement (phase V). In model B, the field data is collected from a systematic sample of field plots. This approach is intended to be used with a large area forest inventory. In model C stands are delineated. Model C represents stratified sampling and is comparable with traditional stand-wise inventory for management planning or pre-harvest stand cruising. In an inventory, which applies model C, the results are not necessarily wanted for the whole forest area. In B and C, model-calibration and validation of results is possible within the limits of the field data.

2 Material and Methods

2.1 Data

2.1.1 Field Data

The forest data consists of 24 plots from Hyytiälä in Southern Finland, 61º50' N, 24º20' E (Table 2). The study area is on state owned land. The field data has been collected in 1995–1997, 2000, and 2002–2003. Some field plots have been measured twice. There are square-shaped, rectangular, and circular plots with varying size, and three of the plots are actually fully mapped stands. Tree butts were mapped in 3D with a tacheometer in a local Cartesian coordinate system. Living and dead trees with dbh above a threshold, which varied between plots from 25 to 90 millimetres, were recognised as trees that make up the forest. All trees were recorded for species, dbh, height, and the state of health. Other tree variables such as crown width, crown length, six-meter stem diameter, stump diameter, and stump height were collected for a sub-set of trees. On each plot, basic tree measurements were repeated for a sub-set of trees in order to control measurement errors.

The field plots were named such that the main species and development class can be determined from the name. The letters P, S and B denote tree species for pine, spruce and birch respectively. Fifteen plots belong to a thinning experiment (Räsänen et al. 1992). These are plots P1–P4, P6, B1–B4, and S1–S6. Plots PS1 and PS2 are also thinning stands in which both pine and spruce occur. Mature stands are marked with a prefix Ma. The species mixtures in proportion of stem volume are given in Table 2.

The chosen object coordinate system was the Finnish coordinate system KKJ. KKJ is not a true Cartesian coordinate frame, which is required in a photogrammetric project, but it serves as a good approximation in a small area (cf. Kraus 1997). KKJ was re-defined as right-handed. Seven geodetic points surrounding the study area had coordinates in KKJ. For AT fifteen complemen-tary ground control points were measured and marked in the study area with a kinematic GPS in August 2000. The estimated measurement accu-racy for these points was four centimetres for the planimetric coordinates and five centimetres for Z-coordinate.

The elevation of each field plot was measured by levelling. Nine levelled points were marked with a signal and used as tie points in AT. The differences in Z-coordinates for these points had a –0.02 metre mean and a 0.11 metre standard deviation. From this, it can be assumed that the plot elevations are within ±25 cm (95% confi-dence) from their true values (or rather the differ-ence between the chosen local photogrammetric datum).

The XY-coordinates for the trees were obtained by measuring the tree tops using four to six CIR photographs (see Sections 2.3, 3.1.1). In order to transform the local coordinates into the object coordinate frame, a rotation angle in XY-plane, and shift parameters in X and Y, were estimated by using the photogrammetric observations and field data.

The accuracy of the tree butt locations inside the plot coordinate system was evaluated by re-meas-urements on plots B1, B2, MaPS3 and MaPS4. The results implied that within each plot the XY-coordinates for the butts should be within ±40 cm (95% confidence) from the true values. The data can be assumed heterogeneous as it has been collected over several years and by many people. There are blunders in the data. Plots B1 and B2 were re-mapped with a tacheometer because the tree tops (XYZ-points) did not match well with the patterns on the aerial images. It was found that on both plots the Z-coordinates for the tree butts had a systematic 40-centimetre error with respect to the plot origin. This was most likely due to incorrectly set prism height during the first mapping. In addition, the planimetric coordinates had an element of systematic error. When the tacheometer measurements were taken, the prism

Table 2. Stand attributes of the field plots.

Plot	Size, m	Forest regen. method	Site type variation	Age yr.	N ha⁻¹	Min dbh cm	G m²ha⁻¹	Dg cm	Hg m	Hdom m	Vtot m²ha⁻¹	Vs m²ha⁻¹	Vp m²ha⁻¹	VPine %	VSpruce %	VBirch %	VOther %
B1	40×40	Planted	OMT-MT	32	600	2.5	15.0	18.5	20.3	21.7	141	16	121	–	–	100	0
B2	40×40	”	OMT-MT	32	1250	2.5	21.7	15.5	19.5	21.8	196	1	185	–	–	100	–
B3	40×40	”	MT	32	519	2.5	14.6	19.7	20.0	21.3	135	25	106	–	–	100	–
B4	40×40	”	MT	32	519	2.5	15.1	19.8	20.2	21.4	141	22	116	–	0	100	–
P1	50×50	Planted	VT, paludified, rocky	50	1276	2.5	20.9	17.9	15.8	18.7	164	49	107	92	6	2	0
P2	50×50	”	VT	50	1672	2.5	24.7	18.6	15.9	18.9	193	74	109	95	2	2	1
P3	50×50	”	VT, paludified, rocky	50	1380	2.5	21.9	18.9	16.0	19.2	171	69	94	87	4	8	1
P4	50×50	”	VT	50	1796	2.5	29.9	17.2	17.2	20.0	253	55	187	97	0	3	0
P6	50×50	”	VT	50	1412	2.5	21.5	18.8	15.3	18.7	162	62	91	83	11	5	1
S1	50×50	Natural	MT	55	864	2.5	25.4	24.0	18.5	22.5	226	129	92	–	92	8	0
S2	50×50	”	MT	55	1124	2.5	20.9	21.4	17.4	20.8	175	97	71	–	87	13	0
S3	50×50	”	MT	55	2056	2.5	40.0	19.9	18.3	22.5	362	167	181	0	83	15	1
S4	50×50	”	MT	55	1544	2.5	29.3	19.9	17.4	22.0	250	111	130	–	91	8	1
S5	50×50	”	MT	60	1776	2.5	33.2	17.3	15.8	19.0	264	60	193	0	98	2	0
S6	50×50	”	MT	55	984	2.5	25.2	20.6	17.4	20.7	215	103	107	–	98	1	1
PS1	r 20 m	Planted	MT	40	975	4.0	20.7	17.9	15.2	17.4	155	32	118	48	47	5	–
PS2	r 20 m	Planted	VT	40	833	4.0	18.6	18.2	16.0	18.1	148	40	103	70	26	4	–
MaP1	50×50	Natural	CT	95	340	4.0	16.1	25.5	20.2	21.9	152	117	34	100	–	–	–
MaP2	47×50	Natural	CT	95	468	4.0	20.4	24.6	20.4	22.3	196	138	55	100	–	–	–
MaPS1	1.08 ha	Natural	Bog-MT-VT-rocky	115	536	5.0	18.1	23.7	20.8	24.0	177	114	59	73	20	7	0
MaPS3	1.68 ha	Natural	VT	120	470	9.0	23.1	28.0	22.6	24.9	239	188	48	77	21	2	–
MaS1	0.49 ha	Planted	OMT	70	545	4.0	36.7	32.0	25.8	28.1	441	385	53	–	89	1	10
MaPS2	1.03 ha	Natural	OMT-MT	130	494	5.0	31.8	31.4	27.5	31.5	403	349	51	15	80	5	0
MaPS4	1.39 ha	Natural	VT-MT	130	486	9.0	33.2	36.7	25.7	28.8	376	330	45	40	58	2	–

Table 3. Image parameters.

Scale	Film	N images	Overlap forward/ side %	Date ddmmyy	Local time	Sun azim. degr.	Sun elev. degr.
1:6000	CIR	22	60/60	270502	0945	113	35.2
1:6000	COL	22	60/60	100702	1054	128	42.5
1:12000	CIR	18	70/60	270502	1000	117	36.7
1:16000	CIR	10	60/60	270502	1015	121	38.2

Film: Kodak Aerochrome 1443 (CIR), Agfa Aviphot Chrome 200 PE3 (COL)
Exposure: Aperture stop 4, speed 150 (CIR), 300 (COL). Filters: 520AV+80% (CIR), 420AV (COL)

that reflects the laser back to the apparatus was placed in front of the trunk at the height of 1.3 metres. The position in XYZ obtained this way should be corrected by using the measured dbh, since the correct position for the prism should be 'inside the trunk'. This correction was not done for a part of the data (1995–1997 mapped stands) and could not be done afterwards, since necessary data was lacking. The error pattern is such that the trees are shifted towards the tacheometer positions in these stands.

The tree top positions in the 3D object coordinate frame were obtained by using the 3D position of the butt (after a transformation consisting of shift and rotation) and the tree height. Thus, the inaccuracy of height measurements affects the accuracy of Z of the tree top positions. On each field plot, a subset of trees was double-measured for height. No systematic errors were encountered, and the precision (standard error, assuming equal precision for both measurements) of the measurements varied from 0.35 to 0.6 metres between plots. Single large errors up to ±3 metres were observed. The measurement imprecision was largest in the dense unmanaged stands and in the mature stands with high trees.

Given a single tree top in the data set, its position accuracy (95% of cases) in the object coordinate frame was assessed to be 50 centimetres in XY, and ±80–100 centimetres in the Z-direction. However, the accuracy most likely varies significantly between plots.

Local, raster-DEMs with a one-metre spatial resolution were computed for each plot by using the local coordinate data for tree butts. A k-nearest-neighbour, inverse-distance interpolation was applied. These DEMs were used in the tests of the semi-automatic 3D tree top positioning method.

2.1.2 Image Data

Including images in different scales and of different film material was the main objective in the planning of the aerial photography. The images were intended to exhibit variation in the image-object-sun geometry. The budget limited the total number of images to 72, and these were then divided to provide a satisfactory experimental design. Unfortunately, images taken with a normal angle camera (effect of lesser perspective distortion) could not be included in the experiment.

The CIR photography took place in the morning of May 27, 2002 and the colour photography on July 10, 2002. May 27 is exceptionally early. Two wide-angle Wild RC 20 cameras, with a 15-cm focal length were used with antivignetting low-pass filters. The 23 by 23 centimetre films were developed on the following week and scanned in July–August 2002 with a photogrammetric scanner at 14-micrometer resolution. (Table 3). The photography was initially planned for 2001, but was cancelled that year because of poor weather for aerial photography. Only some three to four days were suitable for photography in 2001.

For the development of the methods used in this study, a set of 42 photographs taken between 1995–1999 was available. These include CIR, colour, and black-and-white images from the study area in scales of 1:5000–1:20000. In solving the exterior orientation, the older images and a set of 1:30000 CIR images taken in 2002 were included in the image block (N = 114) in order to have them all in one datum. The tests for this study are all done by using the 2002 photographs in scales of 1:6000–1:16000 (Table 3).

The parameters for affine fiducial mark transformation were solved by using least-squares

Table 4. Standard errors of exterior orientation parameters for the 2002 images (N=72) in scales 1:6000–1:16000 (images used in the experiments) and standard errors of tie point coordinates in metres.

| | Projection center position, m | | | Rotation angles, radians | | | Tie point coordinates, m | | |
	X_0	Y_0	Z_0	omega	phi	kappa	X	Y	Z
Mean	0.22	0.23	0.09	0.000161	0.000152	0.000050	0.08	0.07	0.17
Min	0.11	0.11	0.03	0.000072	0.000076	0.000028	0.02	0.02	0.04
Max	0.46	0.67	0.30	0.000430	0.000317	0.000085	0.52	0.45	0.98

Table 5. Differences in triangulated and field measured coordinates for the GCPs (N=22) in metres.

	X	Y	Z
Mean	0.01	0.01	0.03
s	0.06	0.07	0.11
Min	–0.19	–0.10	–0.08
Max	0.14	0.25	0.47

estimation. RMSEs had an average of 6.7 microns and ranged from 2.6 to 11.3 microns.

AT was carried out by using bundle block adjustment (Kraus 1993). Image observations were collected monoscopically with sub-pixel accuracy. Twenty-two GCPs and one hundred tie points were used. The images were fastened to the block with the help of tie points which were mostly stones or corners of buildings. The use of natural tie points reduces the costs without affecting the accuracy (Gruen 1982). Altogether there were 1187 image observations (9.7 per field point). At solution, the RMSE of weight unit was 9.3 microns and the residuals ranged from –46 to +42 microns. The standard errors for the unknowns are given in Table 4. All image observations independent of scale, film or point type had the same weight in the adjustment.

The work was done in phases by including individual images in the block and then by re-calculating the results (cf. El-Hakim and Ziemann 1982). Small observation errors were difficult to trace because adjustment effectively spreads the errors among the elements of the residual vector.

The largest standard errors for tie points (Table 4) and differences for GCPs (Table 5) were obtained for detached single points in the borders of the block coverage.

Image decimation by a factor of two was performed for the 1:6000 images after AT because of the computational complexity of cross-correlation. The non-decimated versions were used in all other experiments but those involving the use of cross-correlation for template matching (see section 2.4.2). With a decimation factor set at two, 25% of the pixels are retained, but the run-times of template matching, when using cross-correlation, are reduced by a factor of 1/16. There is a trade-off between the computational burden and the precision of the images and subsequent image-matching results. The image decimation was done uniformly in the row and column directions, and in two phases. First, the images were operated with a 3×3 binomial low-pass filter (Schenk 1999, p. 119) that reduced the bandwidth of the signal by reducing the high frequency spectrum. The actual decimation followed as the second step, and in it, the unwanted samples were removed. The parameters of the affine fiducial mark transformation were recomputed for the decimated image versions by simply multiplying the parameters with the reciprocal of the decimation factor. The effect resulting from odd image dimensions was accounted for.

The majority of computer analysis of the image data, the statistical analysis, and the simulations were performed by a program written in Visual Basic and C. A part of the statistical analysis was carried out with Statistix.

2.2 Models for Indirect Estimation of dbh and Stem Volume

The allometric models by Kalliovirta and Tokola (2003) were used for deriving dbh for a tree with estimates on species, height, and maximum crown width. General models that apply for the whole of Finland were chosen. The form of the models is

$$\sqrt{dbh} = a_0 + a_1\sqrt{h} + a_2\sqrt{C_w} + \varepsilon \qquad (4)$$

Coefficients for the model are given in Table 6.

Pine has the largest dbh given the tree height and crown width. The difference between pine and spruce is not large, between –15 mm and 25 mm for trees with a height ranging from 5 to 25 metres. If species identification fails for birch, larger systematic errors could be expected, something in the order of 10 to 80 mm in dbh. Birch has wider crowns than pine and spruce for a given height × dbh combination.

Stem volumes of individual trees and sortiments were calculated with polynomial taper curves (Laasasenaho 1982). The volumes exclude the stump. Certain log-lengths and minimum log-top diameters define the sortiments. These were defined separately for each species, the saw-wood, and the pulpwood in order to follow average definitions on the wood market. Division into sortiments (grading, bucking) was optimised for the maximum saw-wood proportion.

2.3 Tree Discernibility and Manual Tree Top Positioning in 3D

2.3.1 Manual Image-Matching Using Multiple Images

When the correspondence problem for tree tops is to be solved manually, the operator can point the tree top in many cases unambiguously and the corresponding tree top on other images is found along the epipolar lines (Fig. 6, p. 19). Other constraints are used as well to solve the correspondence problem. The relative size of the tree top with respect to neighbouring trees, crown shape, the topology (spatial pattern) of the trees partially distorted by the central projection, and the apparent differences in tree species among the neighbouring trees are used in solving the correspondence problem. With these constraints the operator can rule out impossible choices and gradually solve the ill-posed image-matching.

A tree top is not always a clear point feature. The shape of the crown, image scale, and contrast all have an effect on how accurately the point location of the tree apex may be determined on an image. For example, tree tops are well detected if

Table 6. Coefficients for allometric models (4). (Kallio-virta and Tokola 2003).

Species	a0	a1	a2
Pine	–3.140	0.691	1.400
Spruce	–3.224	0.819	1.092
Birch	–3.076	0.622	1.246
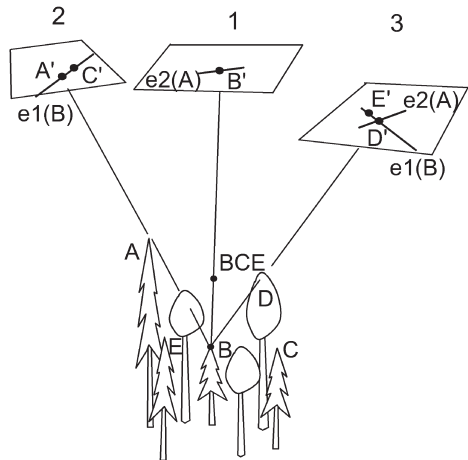
Fig. 8. Occlusion is the cause of omission and commission errors. Tree top B is first pointed from image 1 at B'. Epipolar lines e1(B) are defined in images 2 and 3. If tree A in image 2 at A' is thought to be the corresponding tree top, epipolar lines e2(A) are defined on images 1 and 3. The operator would, perhaps, then notice that the tree top at the intersection of epipolar lines in image 3 is not a conifer (as B is), and 3D solution at point B would be rejected. Point BCE is a possible commission error. For point BCE, there is a crown of a conifer in every image (B→image 1, C→2, E→3).

they are in direct sunlight but against a shadowed dark background. Correspondingly, in front-lit parts of the images tree top detection may be difficult because of the low contrast.

A tree top may not visible in all views. If the correspondence problem is solved for multitemporal images, the set of tree tops in direct sunlight can differ between the images. This may further hamper or facilitate the problem, depending on whether the operator or algorithm is aware of the

fact that the images are multitemporal. Occlusion, shadowing, and the varying image-object-sun angular orientation between images all cause ambiguity in image-matching that result in omission and commission errors (Fig. 8). An operator can try to take into account these factors. For example, a tree with a small crown that is visible in a near-nadir view may be missing in an oblique view. The operator stops the search of the conjugate tree top in oblique views where occlusion of a relatively small tree is likely.

2.3.2 Test Set-up for the Experiment of Tree Discernibility

All 7708 living trees in the field data were tried for a photogrammetric measurement for the tree top position by using manual multiple image-matching. The positions were computed by using least-squares ray-intersection (e.g. Korpela 2000).

Non-decimated CIR images, 4–6 per plot, in scale 1:6000 were used. Plots MaS1, PS2, MaPS1, MaPS3 and MAPS4 were not covered by a complete set of images in 1:6000. For these plots, substitute 1:12000 CIR photographs, exposed 15 minutes later, were used.

The operator knew where to look for the trees, because the 3D points representing the field-measured tree tops could be superimposed on the images. The work was organised such that the operator first measured the dominant and co-dominant trees. These were visible in all four views and easily measurable without auxiliary information. For the suppressed trees, field data was used to assist the work. Tree tops, which could be subjectively recognised on at least two images, were measured for their 3D position. While pointing the tree tops monoscopically, the operator did not have the superimposed points on the image. A short training period in multiple image-matching preceded the work.

2.4 Proposed Method for Semi-Automated 3D Positioning of Tree Tops

2.4.1 Choice of Strategy for Method Development

When a human operator does image-matching, the operator selects the matching entities, finds the conjugate entities in the other images and assesses the quality of the match. The computation of the 3D position is the only problem the operator escapes. Full automation of photogrammetric tasks is considered very difficult (Horn 1983, Helava 1991, Schenk 1999, Gong et al. 2002) and therefore the semi-automatic approach, with human intervention, was chosen. The complexity-analysis, the findings of previous studies, the experience gained during method development, and the overall objective of solvability of research problems confirmed the choice of strategy.

2.4.2 Extraction of Tree Tops from Individual Images by Template Matching

Tree crowns in an image are area features. A tree top on the other hand may be considered to be a point feature both in the image and object domains. Here the tree top is defined to be the highest point of a tree.

The extraction of tree tops from aerial image is based on a image processing and object recognition technique called template matching. Template matching has been used for tree top extraction (e.g. Pollock 1996, Larsen 1997, Olofsson 2002). Tree stems have also been recognised (Tarp-Johanssen 2001). As such, template matching does not provide tree top image locations to be matched for 3D positions. The correlation image, ρ needs to be processed for local maxima to provide a list of tree top locations or stem count (Pollock 1996, Larsen 1997).

A template is a sub-image, which models the appearance of the object to be recognised from the image. The presence of the object in the scene is detected by searching for the location of a good match between the template and the scene. The measure of match energy may be defined in different ways. (Secilla et al. 1987, Jain 1989, Jain et al. 1995, Schenk 1999). Normalised cross-

correlation ρ (Eq. 5) was used. It is scaled in the interval $\rho \in [-1,1]$. If there is no similarity at all between the template and the image at a given image location (i, j), then the cross-correlation has value zero. If $\rho = -1$, the correlation is inverse. Such is a case with a positive and a negative of the same image.

$$\rho(i,j) = \frac{\sum_{k=1}^{m}\sum_{l=1}^{n}\left[g(k,l)-\overline{g}\right]\cdot\left[f(k,l)-\overline{f}\right]}{\sqrt{\sum_{k=1}^{m}\sum_{l=1}^{n}\left[g(k,l)-\overline{g}\right]^2\cdot\sum_{k=1}^{m}\sum_{l=1}^{n}\left[f(k,l)-\overline{f}\right]^2}} \quad (5)$$

In (5) the size of the template, g is $m \times n$. It intersects the image f. $\overline{g}$ and $\overline{f}$ denote the mean of pixel values of the template and the image. $\overline{g}$ is constant and $\overline{f}$ varies. Cross-correlation is computed for the point (i, j) on the image.

Template matching, which uses cross-correlation as a measure of match-energy is computer intensive. With an increased image scale, the number of pixels grows in quadratic ratio, and the computational complexity increases to the fourth power. Unlike in some other measures, it cannot be halted in the middle of computations at a given image location if intermediate results imply a low match. Computations can be speeded if other measures are used, and the computations are done in the frequency domain using Fourier-transformations (Secilla et al. 1987, Tarp-Johanssen 2001). For a multispectral image, the cross-correlation may be computed separately for all channels or a transformation into a single channel precedes the computations. Here the three-channel CIR and colour images were transformed into intensity images by calculating the average of the three channels or by selecting the red (infrared, IR) channel only. A transformation (RGB → Intensity) that improves the contrast of the image such as the Hotelling transformation (Gonzalez and Woods 1993) could also be used.

Template matching-based object recognition is not invariant to varying object properties. In a complex scene with trees of varying size and species, a single template will most likely not perform effectively (Fig. 11, Fig. 12, Fig. 13). The image-object-sun geometry changes continuously in an aerial photograph. A template that takes into account the illumination and perspective effects is
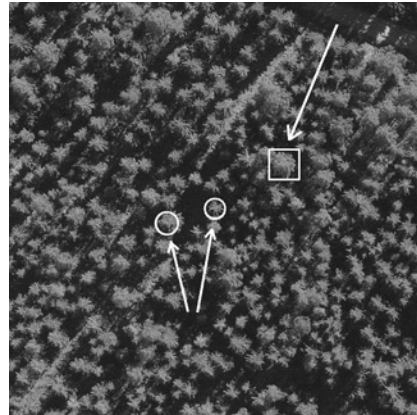
Fig. 9. A near-nadir panchromatic 1:5000 view of an unmanaged spruce-birch thinning stand. The white circles outline two crowns of spruce enlarged in Fig. 10 below. The square points out a relatively large crown of a birch.
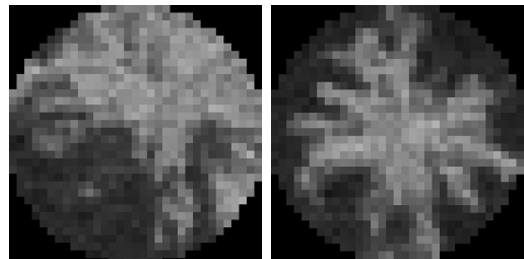
Fig. 10. Two enlarged elliptic templates capturing spruce trees in the near-nadir view of Fig. 9. The template on the left represents a larger dominant tree g_{large}, and the template on the right contains a smaller co-dominant spruce g_{small}.

therefore local. Occlusion is present and crowns are viewed against a changing background.

Figures 10–12 illustrate how template matching is not invariant to scale. The two cross-correlation functions appear quite different. The responses (Fig. 11) of the two templates representing trees of different size (Fig. 10) differ. There is a large crown of a birch outlined by a white square in the upper right part of the aerial image in Fig. 9. The local maxima for this birch crown in the cross-correlation images of Fig. 11 are, by visual examination, quite different. The local peak in correlation is not very distinct or high when a template representing a relatively small spruce crown
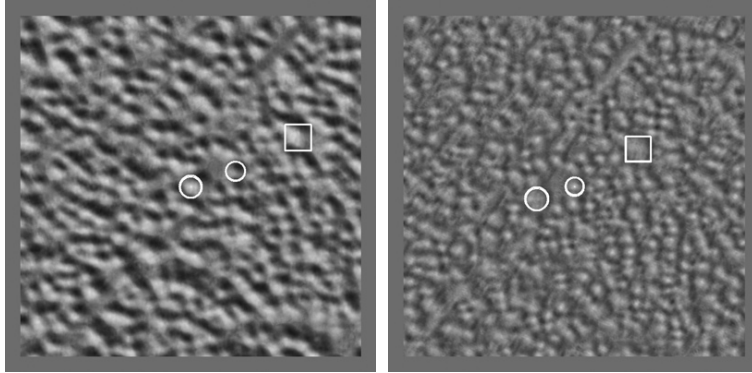
Fig. 11. Cross-correlation functions ρ for the image in Fig. 9 obtained by using templates of Fig. 10. Left: $\rho = f \circ g_{large}$, right: $\rho = f \circ g_{small}$. The circles and the squares depict the same trees (image position) as in Fig. 9.
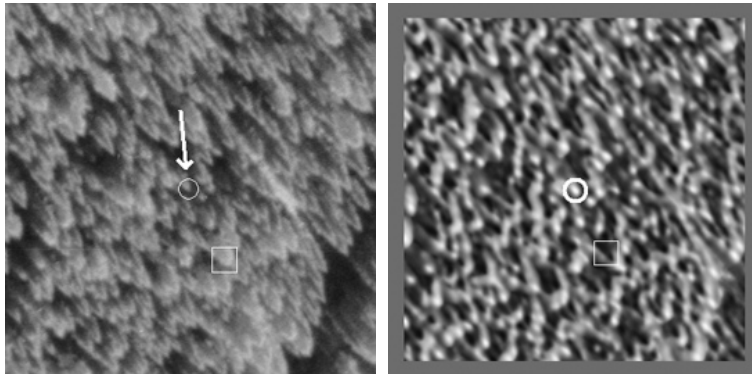
Fig. 12. Left: an oblique back-lighted view of a spruce-birch stand. Right: Cross-correlation function ρ computed with the template pointed out by an arrow and a circle in the aerial image. The squares depict the image location of the same birch as in Fig. 9.
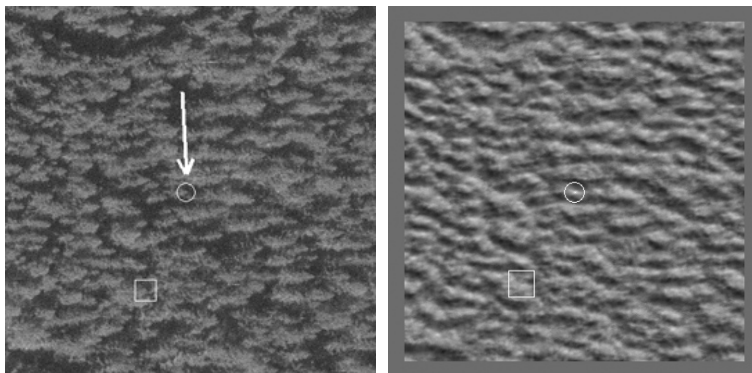
Fig. 13. Left: an oblique front-side-lighted view of a spruce-birch stand. Right: Cross-correlation function ρ computed with the template pointed out by the arrow and the circle in the aerial image. The squares depict the same birch as in Fig. 9.

is applied. The response seems better for the template representing a bigger spruce crown.

In some cases, the local peak in the correlation image is shifted from the correct location because of the variation in the background. Overlapping crowns can produce this effect. The local peaks found in non-nadir, oblique views are not as circular-symmetric as in nadir views. Fig. 12 and Fig. 13 illustrate the effect. Often, the local peaks in the cross-correlation images are elongated and oriented with the direction of the radial displacement. In addition, for oblique views the variation in the background of a tree top increases with the nadir-angle. It has been shown that template matching, at least in the case of spruce stands, does not produce the same accuracy as when applied in a different image-object-sun orientation (Larsen 1997). In nadir views, the lower parts of the crowns and the ground form the background. In dense forests, the background is mostly shaded and dark, and thus the sun-lit crowns are easily discernible from nadir-views.

The image-matching algorithm for 3D positioning of tree tops, which follows template matching, relies on the quality of the cross-correlation images. Template matching is the feature detector in the algorithm (Section 2.4.5). A good feature detector is robust against changes in different circumstances such as imaging geometry, scale and background noise. A good feature detector works also with incomplete information (Gonzalez and Woods 1993 p. 572, Jain et al. 1995 p. 462). An ideal response of a tree top detector would be a complete set, without any omission or commission errors, of accurate image coordinates for the tree tops to be matched in 3D. Attached with the image coordinate information, the ideal feature detector would also provide accurate information of the type of the detected feature such as tree species and crown size information. This would support the solving of the remaining ill-posed correspondence problem. These characteristics of the ideal feature detector are hardly ever realised even if we consider the superb capabilities of the human perception. Occlusion inevitably results in an uncompleted set of detections, and the accurate image observations are further impaired by camera lens and orientation-errors.

Templates of tree crowns in a given viewing geometry can be generated by using methods of computer graphics and geometric-optical modelling (cf. Kiema 1990, Pollock 1996, Larsen 1997). In the method proposed in this study, instead of rendering an image of the tree top with a computer-graphics method, the templates are copied from real images by using a single subjectively selected model tree. The coordinates of the tree top are manually solved, and the template is captured for each image by using parameters that define the position, size, and shape of the template on the image (Section 2.4.5). Geometric-optical modelling was not used since geometric-optical models of pine and birch were lacking.

2.4.3 Search for Tree Tops in the Object Space

Corresponding entities are located in the intersection of the camera-rays. A local peak in the cross-correlation image does not define one distinct camera-ray. The peak maps into a geometric object (loosely defined as a ray-pencil with associated probability) that occupies a space around the true camera ray that came from the 3D point object (Fig. 14). If the peak in the correlation image is circular-symmetric, the camera ray turns into a cone. As explained earlier, corresponding entities are found on the images from the intersections of epipolar lines. With the uncertainty of cross-correlation, the camera-rays are volumetric, as well as the epipolar planes. The intersection of epipolar lines in the images is therefore represented by a high summed cross-correlation, $\rho 3D$ for a point in 3D, $\Sigma \rho_i \rightarrow \rho 3D(X, Y, Z)$. The 3D space below the cameras' is full of these 3D maxima (cf. Fig. 14). They are mainly false solutions to the correspondence problem. Correct solutions are amongst them, and may be selected if an approximation for the range in Z can be specified. This is called the search space. A too deep search space produces false solutions. Inevitably, there will be false solutions even if the depth of the search space is optimal due to the height variation of trees (Fig. 8, p. 30). Also, false solutions as well as omission errors are inevitably produced due to the imperfect response of template matching.

It is clear from Fig. 14 that the response of template matching, the cross-correlation image,
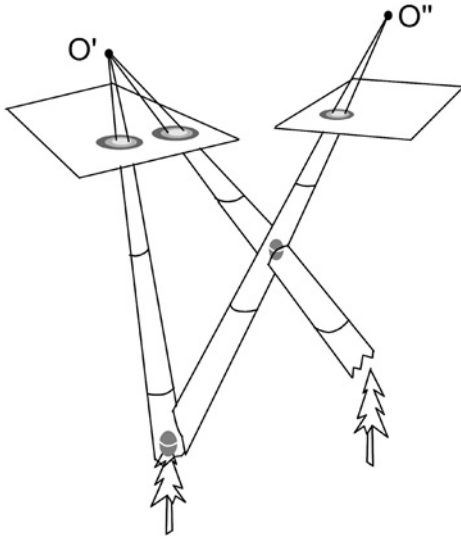
Fig. 14. Illustration of 3D 'intersecting epipolar volume', which is in the intersection of the camera-rays (cones) passing through local 2D maxima in cross-correlation images. Due to the inaccuracy of template matching (images with projection centres O' and O" are cross-correlation images) camera rays are volumetric. Grey ellipsoids depict two 3D maxima of cross-correlation one of which is a correct solution to the correspondence problem. The 3D⇔2D mapping is used to retrieve an aggregate cross-correlation for 3D points in the object space below cameras.

should exhibit sharp peaks at the correct image locations to make the conical 'intersecting epipolar volume' as thin as possible. This would improve 3D accuracy, and would restrict the ambiguity of image-matching by making the local maxima of correlation in 3D more compact.

Near-nadir views have proven best in many 2D applications for tree crown delineation or tree top detection. A requirement of several near-nadir views in image-matching is not, however, practicable. Costs would be high and the accuracy of Z-estimation would be inferior to that of the planimetric coordinates. It can be expected that an increase in the number of images in matching improves results, provided that template matching works for that added view (image-object-sun geometry, scale, time of photography). If template

matching fails, an added image can even impair image-matching.

As stated earlier, it would be desirable if the step in which tree tops are detected would produce information on tree species, crown size and shape. Thereby more constraints, consisting of features and symbols could be used in solving the ill-posed correspondence problem. In this respect, template matching cannot be valued very high as a feature detector. However, the image-matching approach, which will be represented in more detail in Section 2.4.5, relies on geometric constraints only and on the use of template matching.

2.4.4 Quality Assessment

A good quality assessment procedure provides a feedback loop to the previous stages of image-matching: (i) the tree top detection (selection of conjugate entities) routine and (ii) the correspondence problem solver. The feedback 'guides' the previous stages of image-matching so that eventually the matching results are optimal. Optimality needs to be defined separately. In the case of finding tree tops from aerial photographs there are several criteria that can be used. An optimal image-matching could be the one that maximises the number of correct hits (correct 3D tree top positions produced by image-matching) while allowing no commission errors. Alternatively, a matching that provides the best estimates for the number of trees, regardless of the 3D-accuracy, can be considered optimal. Maximising the number of accurate hits without any false solutions may be optimal, if the automatic matching is to be made complete with additional manual measurements, and the manual rejection of false solutions is considered expensive.

The assesment of quality operates autonomously in the sense that it does not usually posses the information about the correct hits. Such information may be available. For example, the number of planted trees in an area may be known, or the total number of trees in an area could be estimated from a manually pre-measured sub-sample.

In the 3D tree top positioning method presented in the next section, the assessment of the quality of the matching is left to the operator. Feedback is provided in the form of changes in the para-

meters that control the algorithm. The assessment is based on visual evaluation of the agreement of the algorithm-found tree tops, which are superimposed on the aerial images. Alternatively, as stated above, the assessment can be based on the comparison of the expected and estimated number of trees.

2.4.5 Algorithm

Only geometric constraints are used in the proposed semiautomatic image-matching method for 3D tree top positioning. It relies on epipolar geometry and a restricted, properly set search space. There are parameters (Table 7, p. 42), which need to be given values.

The semi-automatic positioning of tree tops in 3D consists of steps 1–9:

Step 1. Manual delineation of the forest area to be measured, in 3D, by using monoscopic or stereoscopic interpretation

For an aerial photo-plot the map coordinates are known, and delineation is not needed.

Step 2. Acquisition of a priori coarse-level information about the height-profile of the trees to be mapped

This can be done alternatively by stereoscopic viewing (Anttila 1998), by area-based image-matching (DEM algorithms, Næsset 2002), by analysing high-resolution lidar-data (Hyyppä and Inkinen 1999), or from a forest database.

Step 3. Selecting and measuring a *Model Tree* and capturing templates representing it on all images

The operator selects a *Model Tree* and measures the 3D tree top position, point 4 in Fig. 15 with coordinates (X_t, Y_t, Z_t). The size of the area to be mapped limits the applicability of the model tree in terms of the varying image-object-sun geometry. Elliptic templates (Fig. 15, Fig. 16) are
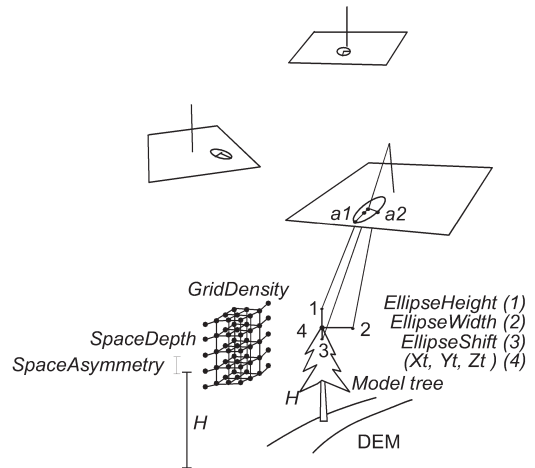
Fig. 15. Illustration of metric parameters of 3D tree top positioning. See text below (step 3 and step 5) for further explanation.

captured from the images. Three metric parameters, defined in the object space, determine the location, size and shape of the ellipses. On each image, the major axis of the ellipse is aligned with the direction of the radial displacement.

Parameter *EllipseShift* shifts the center of the template in the direction of the radial displacement, i.e. in Z-direction. At value zero, the template is centred at the tree top position. A negative value produces a template centred below the tree top (point 3 in Fig. 15). The size and shape of the template are determined by parameters *Ellipse-Height* and *EllipseWidth*. The length of the major ellipse axis a_1 parallel to the direction of the radial displacement, is determined by calculating the photo-distance between points (X_t, Y_t, Z_t) and $(X_t, Y_t, Z_t + EllipseHeight)$. Similarly the length of the axis a_2 perpendicular to the direction of radial displacement is computed from projections of points (X_t, Y_t, Z_t) and $(X_t + EllipseWidth/2, Y_t, Z_t)$. The shape is conditioned: *if* $|a_1| < |a_2|$ *then* $|a_1| = |a_2|$. Thus, the templates are only allowed to be elliptic for oblique views with a large value of *EllipseHeight* and only in the direction of the radial displacement. Parameters are common in all images. (Fig. 15, Fig. 16).

Templates are rectangular sub-image copies of the aerial images. Pixels outside the ellipse are masked out. The location of the tree top within
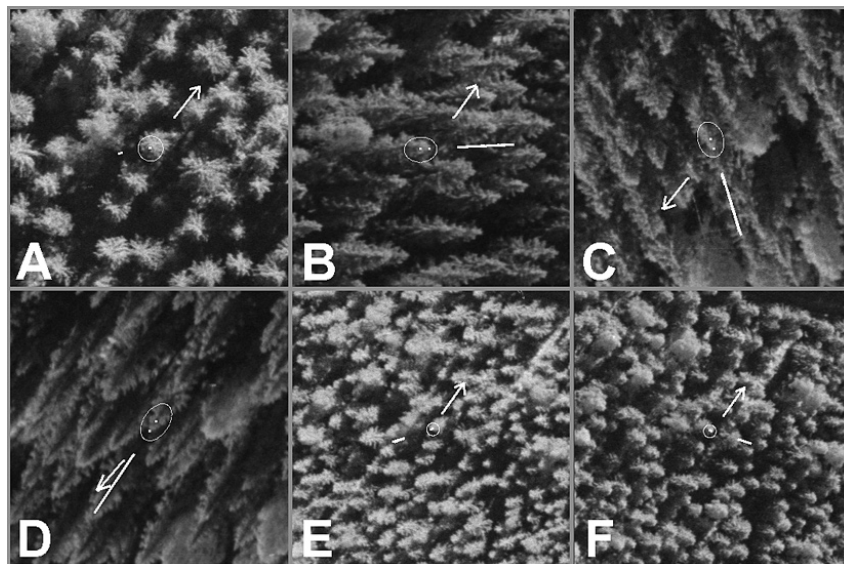
Fig. 16. Template acquisition for a model spruce tree. Parameter values: EllipseHeight = 3 m, EllipseWidth = 2.6 m, and EllipseShift = –1.7 m. Positions of the tree tops (hot-spot) and template centers are marked by a point. The arrows mark the direction to the sun. Ellipses are outlined as well as the direction and length of radial displacement corresponding to a change of 10 metres in Z. The illumination-class and nadir angle in degrees for the sub-images are: A front-lighted 3, B back-side lighted 29, C back-side 32, D back 35, E front 14, and F back-side 14. Images are in scales 1:6000 and 1:12 000.

the template extent, the so-called hot-spot, is stored for each template, and is accounted for in cross-correlation computations.

Step 4. Template matching

The image areas that will cover the search space need to be determined so that cross-correlation is not computed for excessive areas. Image decimation may precede the cross-correlation computations for very high-resolution images for time-saving reasons.

Step 5. Setting the vertical position and extent of the search space above the DEM – Setting up sample points within the 3D search space

The information on the height (tree top elevation) profile of the forest is provided by step 2. The

quality of the information can vary. Here it is assumed that the 3D tree top positioning is tried over a homogeneous stand or plot in which the height of dominant trees does not vary spatially to a large degree. This leads to the assumption that the depth and the vertical position of the search space is constant. If more detailed spatial information is available, the depth and vertical position of the search space could vary in space.

The height of the model tree, H is computed with the help of a DEM. H serves as an approximation for the mean height of trees. The operator sets the depth of the search space by giving a value to the parameter *SpaceDepth*. Asymmetry of the search space with respect to H, in the direction of the Z-axis, is defined by parameter S*paceAsymmetry*. *SpaceAsymmetry* is set at zero if the model tree is assessed to represent the mean height of discernible trees. A negative value is given for a dominant, relatively tall tree in order to lower the search space to better occupy the

canopy of discernible trees. (Fig. 15).

The search space is filled with points. *Grid-Density* gives the spacing. At each XY-position, the DEM is consulted for ground *Elevation*. A particular XY-position is established with points at *GridDensity*-distances starting from

Elevation + *H* + *SpaceAsymmetry* – *SpaceDepth/2*

up to

Elevation + *H* + *SpaceAsymmetry* + *SpaceDepth/2*.

Step 6. Mapping of each point in the 3D grid to the cross-correlation images

Each 3D point in the search space is computed $\rho 3D$, which is a measure of correspondence:

$$\rho 3D(X,Y,Z) = \frac{\sum_{i=1,N} w_i \rho_i \left(A_{x(i)} \left[f_{x(i)}(X,Y,Z) \right], A_{y(i)} \left[f_{y(i)}(X,Y,Z) \right] \right)}{\sum w_i} \quad (6)$$

In Eq. 6 ρ_i are the 2D-correlation images, and collinear equations f_x, f_y for each image i map the 3D-points in the search space to the corresponding camera coordinates. A_x and A_y are the functions of the (affine) fiducial mark-transformation, which map the camera coordinates to pixel coordinates. Weights w_i may be given for example to reflect the scale, imaging geometry, and film format of the images. In this study, equal weigths were applied. For sub-pixel accuracy, the cross-correlation images can be interpolated.

Step 7. Clustering of $\rho 3D$-data into tree top candidate positions

Volumetric $\rho 3D$ data is clustered (Fig. 17). Clusters are candidate tree top positions. Clustering is performed by first sorting the $\rho 3D$ data. Clusters are formed from points in the 3D point set with $\rho 3D$ above a lower limit, *Rlimit*. Points are merged into existing clusters during the processing of the sorted list. This is controlled by a planimetric distance parameter, *XYthin*. Points closer than the set value are merged and do not form a new cluster.

The position of the cluster is the mean of the 3D points that belong to the cluster and $\rho 3D$ is used in linear weighting of the coordinates. The list search is stopped when the first point with $\rho 3D$ below *Rlimit* is found. At that point there are M clusters, i.e. candidate tree tops. The computational complexity of the search is $O(N^2)$, where N is the number of 3D points in the search space, since for each 3D point (Max N), the minimum distance between existing M (Max N) clusters and the 3D point is computed.

Rlimit is a parameter, which can be used for controlling the quality of the clusters. Only the best clusters are accepted as candidate tree tops, if *Rlimit* is set to a high value. In such a case, commission errors are few if the search space is set correctly. Lowering the value of *Rlimit* brings about new clusters, but at the cost of commission errors.
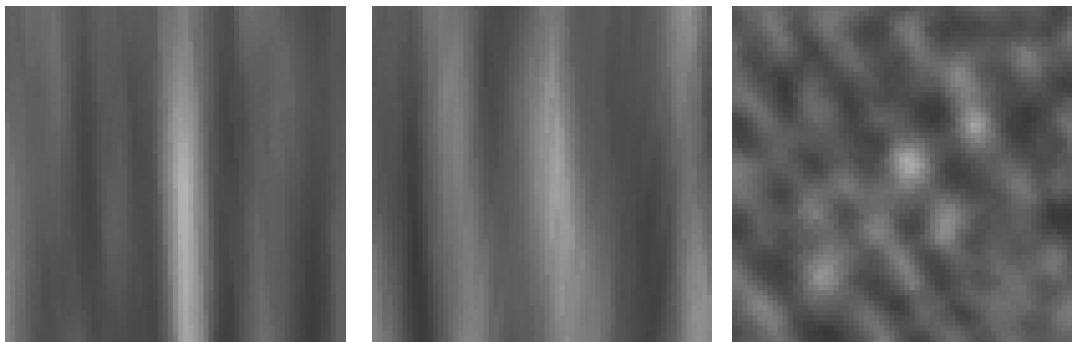
Fig. 17. Illustration of the 3D volumetric correspondence data, $\rho 3D$. Left: Vertical slice along YZ-plane. Middle: XZ-plane. Right: XY-plane at Z=192 m a.s.l. The images represent an area of 30 metres in X and Y, and 10 meters in Z. Data is from a spruce stand and obtained using three panchromatic 1:10 000 images. The bright pixels depict high value of correspondence ($\rho 3D$).
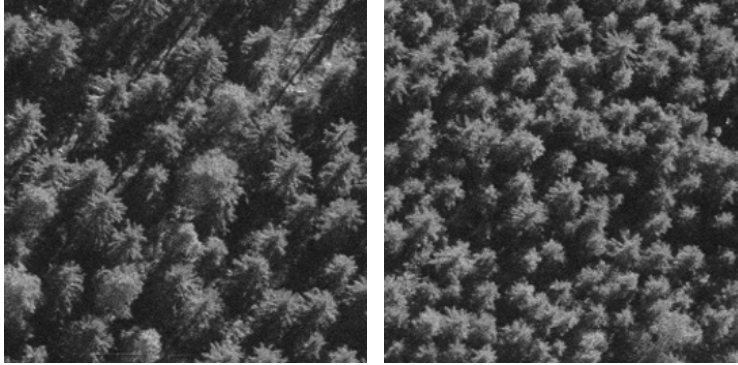
Fig. 18. Left: A near-nadir, back-lighted view to a mature spruce stand, right: A near-nadir view to a young dense thinning stand of spruce. Photograph scale 1:5000, pixel size 10 centimetres on ground, 256×256 pixels.
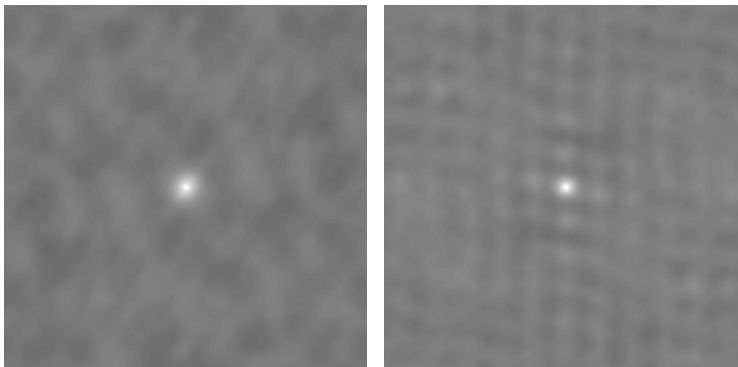
Fig. 19. Autocorrelation functions of the aerial images in Fig. 18. Images are shifted to zero-lag in the center, and contrast enhancement is performed for visualisation purposes.

The merge-parameter *XYthin* controls the density of the clusters. A value, which is too large, causes neighbouring trees to be merged. Similarly, a value set too low can result in several clusters originating from the *ρ3D*-response of a single tree.

The parameters *Rlimit* and *XYthin* are subjectively set and adjusted by the operator. An optional method for acquiring an approximate value for *XYthin* by spectrum analysis of the aerial images is presented below.

The determination of the parameter *XYthin* can be based on the analysis of the spatial structure of the images (Ripley 1981 p. 78–87, Jupp et al. 1988, Cohen et al. 1990, St-Onge and Cavayas 1995, Hyppänen 1996). Near-nadir views are preferred as they preserve the XY-topology of tree tops better. Lag-distance-correlation plots (correlograms), which are derived from the 2D-autocorrelation functions are used to analyse the spatial structure of the stand. Correlograms calculated from aerial images characterise tree size and density. Fig. 18 and Fig. 19 show an example of two image functions and their corresponding autocorrelation functions, which have been computed in the Fourier-domain (Gonzalez and Woods 1993). The lag-distance-correlation data in Fig. 20 is computed from the autocorrelation images by calculating the lag-distance of each pixel.
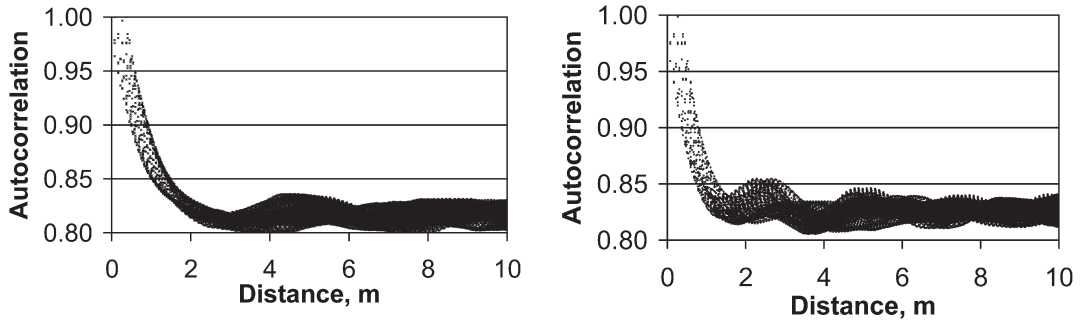
Fig. 20. Autocorrelation vs. lag-distance (correlograms) in the object scale computed from the autocorrelation functions in Fig. 19.

Approximate start-up values for the parameter *XYthin* may be determined by visually analysing the correlation lag-distance plots. The relatively regular pattern of trees of the young stand shows in the correlation data. There is a relatively distinct peak at a lag-distance of 2.3 metres followed by a secondary peak at approximately 4.6 metres (Fig. 20). The spatial structure of the mature stand seems to be less regular judging by visual examination of Fig. 18 and Fig. 19. In addition, the crowns in the mature stand seem to show larger variation in crown size in comparison to the young stand. This is possibly related with the slower relative rate of decline in autocorrelation at a small lag-distance.

Approximate values for the *XYthin* parameter could be found by visually examining autocorrelation-lag-distance plots instead of determining them by visual examination of the aerial images. This is, however, a time-consuming process and it can be disputed whether anything is gained from it. Empirical models that link the texture measures, e.g. autocorrelation or variogram-features with optimal values of *XYthin,* can be estimated as data accumulates. Models could be used for automatic, faster, and more objective determination of the parameter.

Step 8. Quality assessment of image-matching

The evaluation of the matching results is based on visual examination. The clusters i.e. candidate tree top positions are superimposed on the aerial photographs.

If necessary, the clustering algorithm is re-run with new values for *XYthin* and *Rlimit*. It is possible that the matching is repeated by selecting a new model tree (step 3), by re-specifying the search space (2 or 5), or by recapturing the template with new parameters. All subsequent steps need to re-computed, so it can become time-consuming if, for example, the process needs to be repeated from the beginning. It is therefore important to have good approximate values for the many parameters involved to avoid iteration.

Step 9. A manual correction to the automatic matching results (optional)

The matching results are examined and bad positions are removed. The measurements of the unrecognised trees are completed manually.

2.4.6 Measuring the Performance

A photogrammetric forest inventory, which utilises single tree photo-measurements, is practicable only if the share of manual work can be kept small. This is in part attained if the number of high-quality, automatic 3D tree top positions is high. In most cases, some editing of the positioning results will be needed. Editing consists of completion of the missed trees and deletion of the commission errors, i.e. the false tree tops produced by the algorithm. Thus, the number of commission errors should be kept minimal. In addition, amendment of some positionings can

be a part of the editing phase. 3D positioning accuracy is essential if the species-recognition process and the measurement of crown width rely on the top positionings.

For height estimation and subsequent estimation of dbh, it is desirable that the tree heights are obtained accurately and without bias. Accurate height measurements yield the height distribution of a forest, which together with accurate C_W-measurements give the dbh-distribution. An unbiased but averaged height distribution produced by 3D positioning in which the extreme height values are lacking, will result in a distorted dbh-distribution that similarly lacks the extreme values. For the estimation of timber sortiments, the correct estimation of the joint dbh-height distribution is essential. In addition, unbiased but inaccurate height and dbh estimates can cause bias in the different tree volume estimates due to non-linear relationships between variables.

From above it is clear that the performance measures should take into account several features, and that the evaluation of the performance is a complex procedure also linked with the end-use of the data.

Rules are needed for separating between found tree tops, herein called hits, and false candidates, i.e. commission errors. If the positioning algorithm produces a candidate close to the field-mapped tree top it can be considered a hit. One candidate can only hit one tree; other candidates are hits for neighbouring trees or commission errors. A tree top that has no candidates in its vicinity is missed. Uncertainty in tree mapping and height measurements in the field, phenomena such as tree sway and slant, as well as the uncertainty of image orientations, should be accounted for in setting the rules for a hit-or-miss test. For example, given the field and image data at hand, it would be unreasonable to require centimetre-level positioning accuracy for a hit.

A hit-cylinder was defined for the tests. It is centred on each field-measured tree top and each candidate produced by the algorithm. It was defined to be 2.4 metres in width and six metres in height. The candidate can be 1.2 metres aside the tree top, with a three metre erroneous Z-coordinate and still produce a hit. It is clear that the size of the hit-cylinder has an effect on the measures of performance. A small hit-cylinder will produce fewer hits with a better, observed positioning-accuracy. In a dense stand, large hit-cylinders can have plenty of overlapping volume, which complicates the hit-or-miss testing.

The performance of image-matching-based 3D tree top positioning, manual or automatic, is tested against a set of field measured tree tops. The set of field trees can be confined with respect to tree size. In the field data for this study, lower bounds for dbh were defined, and small trees were left out already in the field measurement phase. Thus, the stem number estimates obtained from the field vary in accuracy. The stem number estimate is a function of the lower bound and thus a poor reference value. For the hit-or-miss testing, the set of field trees was further confined to the set of discernible trees (Sections 2.3, 3.1). It was assumed that non-discernible trees would not be detected by automated methods either. An estimate for the need of manual editing of the 3D positionings can be obtained, if the discernible trees form the ground truth.

The set of field trees comes from a restricted area, the field plot. There are always trees, which are located near the border. The 3D positioning algorithm can produce a candidate that falls just outside the XY-extent of the plot, but is still a hit for a tree inside. Similarly, there can be candidates, which are inside the field plot extent but hit trees outside and should not be accounted for as commission errors. To take into consideration this border-effect, the hit-or-miss testing was always performed for circular plots with a buffer of mapped trees surrounding them.

The number of hits is the total number of trees inside the plot that have a unique candidate within the extent of the hit-cylinder, including trees that are hit by a candidate from the buffer zone. Hit-rate is the ratio between the number of hits and the total number of trees, both inside the plot. Hit-rate in total volume is the ratio of total stem volume between the hit trees and all trees. The number of commission errors is the total number of candidates inside the plot extent that do not hit any tree inside the plot or in the border zone. Commission error rate is the ratio between commission errors and the total number of trees inside the plot. The number of omission errors is the total number of trees, belonging to the plot, without a hit.

Table 7. Parameters of 3D tree top positioning algorithm.

Parameter description	Symbols
1) Selection of model tree and measurement of the top location. (errors *dX, dY, dZ*)	X_t, Y_t, Z_t
2) Parameters defining the size, shape and location of the elliptic templates.	*EllipseHeight*, (*EH*) *EllipseWidth*, (*EW*) *EllipseShift*, (*ES*)
3) Parameters defining the vertical extent and density of the search space in the canopy.	*SpaceDepth*, (*SD*) *SpaceAsymmetry*, (*SA*) *GridDensity*, (*GD*)
4) Parameters controlling the clustering of ρ3D.	*Rlimit, XYthin*

The 3D-positioning accuracy of the trees with a hit is evaluated with RMSE. It is computed separately for the planimetric (ΔXY) and elevation error-components (ΔZ). The positioning error-vector [ΔX, ΔY, ΔZ] is defined as **field position–candidate position** in the object coordinate frame. For example, an error vector [–0.2, 0.5, –0.8] means that the candidate is 0.2 metres East, 0.5 metres South and 0.8 metres above the field measured tree top position.

Mean differences, i.e. the means of ΔX, ΔY and ΔZ, are also used as error measures. In order to evaluate the averaging of Z, a regression line was fitted in the $\Delta Z \times$tree height data and the slope coefficient [m/m] was computed.

2.4.7 Set-up for the Performance Testing Experiment

It is practically impossible to optimise the 3D tree top positioning given a forest, the image data, and the large number of parameters. In practice, an operator needs to find an optimal parameter combination quickly, but does not necessarily have much field data to support the work. It was decided to let the computers try a large number of different parameter combinations, store the results, and analyse the data for best cases. It was assumed that the best cases would imply on the effects that imaging geometry and forest conditions have on the performance of 3D tree top positioning.

The semi-automatic 3D positioning algorithm relies on several parameters, which are set manu-

ally. These are, in the course of the algorithm, given in Table 7, and illustrated in Fig 15, p. 36.

The height of the model tree (*H* in Fig. 15) was used for defining the vertical position of the search space (step 2 in section 2.4.5)**.**

The dimension of the parameter-space is nine, if the selection of the model tree is included as a single parameter. However, the measurement of the model tree top position is susceptible to errors (*dX, dY, dZ*). This further adds to the dimension of the parameter space.

Ten plots were selected for extensive testing of the 3D tree top positioning algorithm. These plots were B1, B2, B3, P3, P4, S3, S6, PS1, PS2, and MaS1. Plot MaS1 is a mature spruce stand and all of the other plots represent thinning stands. Plots B2, S3 and P4 have all escaped thinnings and have a high density in terms of stem number and basal area. Plot B1, B3, S6 and P3 represent normally managed stands. Plots PS1 and PS2 represent young recently thinned mixed stands.

Different sets of aerial images were selected for each plot to examine the effect of imaging geometry (Table 8). Sets LNAD, MNAD and WNAD represent theoretical image combinations, but were included in the tests to study the effect of nadir angle. The hypothesis is that the image sets with low nadir angle images only, the LNAD sets, would produce higher hit-rates than sets MNAD and WNAD. Sets 6COL, 6CIR, 12CIR and 16CIR all contain images in one scale only. Sets 6COL and 6CIR compare well since the camera locations are nearly the same. Sets 612CIR and 616CIR consist of an image pair in 1:6000 and a quadruplet in the smaller scale. For

Table 8. Description of the image sets used in the performance tests.

Set name	Description
LNAD	CIR images (1:6000, 1:12000, 1:16000) that view the stand with low nadir angle. 6–8 images.
MNAD	CIR images (1:6000, 1:12000, 1:16000) with variation in nadir angle. 6–8 images
WNAD	CIR images (1:6000, 1:12000, 1:16000) with large nadir angle. 6–8 images
6COL	1:6000 colour images. 4 images. 60 / 60% overlaps
6CIR	1:6000 CIR images. 4 images. 60 / 60% overlaps
12CIR	1:12000 CIR images. 6 images. 70 / 60% overlaps
16CIR	1:16000 CIR images. 4 images. 60 / 60% overlaps
612CIR	Pairs of CIR images in 1:6000 and four 1:12000 CIR images
616CIR	Pairs of CIR images in 1:6000 and four 1:16000 CIR images
P6CIR	Different pairs of CIR images in 1:6000, 60% overlap
P12CIR	Different pairs of CIR images in 1:12000, 60 and 70% overlaps
P16CIR	Different pairs of CIR images in 1:16000, 60% overlap

Table 9. Dimension of the grid of parameters per Plot×image set×model tree combination used in the perform-ance tests. See also Table 7 and Section 2.4.5 for explanation about the parameters.

Model tree	dX	dY	dZ	EH	EW	ES	SD	SA	GD	Rlimit	XYthin
10	1–3	1–3	3–5	3	3–4	3	6–8	3–5	1	10–15	6–10

different sets of 612CIR and 616CIR, the pair of images in scale 1:6000 is changed. All images in scale 1:6000 were downsampled by a factor of two for 28-micrometer pixel size. This means that the images in scale 1:6000 and 1:12000 had the same nominal resolution on ground.

Ten (eleven in plot S6) model trees were selected in each plot by using systematic sampling and by following the every Nth rule. All other parameters except for *GridDensity* were allowed to take multiple values in a multidimensional grid (Table 9). *GridDensity* was kept constant at 0.5 metres.

The runs were carried out with a cluster of 24–40 computers, which run the performance tests during night-time and over the weekends. If a run was terminated abruptly due to lack of time, the simulation was repeated with a new, less dense grid of parameter values until the simulation could be finished for that model tree×image set combination. This unfortunately resulted in variation in the density of the parameter grid between trials. Primarily, the density of parameters *Rlimit* and *XYthin* was altered for the adjustment of the run-times. The number of trials, i.e the number of times tree top positioning was tried and performance measures computed for a plot×image

set×model tree combination, varied from about 40.000 to over 1.5 million. The number of trials was larger for the 'weekend-runs' that had longer run-times.

The interval of parameters was selected separately for each plot, based on tests with a few subjectively measured model trees, and experience gained with them. Hence, it cannot be guaranteed that the grid captures the global optimum, i.e. the best case in performance. The 3D positions for the model trees' tops were obtained by manual image-matching in the discernibility analysis (Sections 2.3, 3.1). The top position was allowed to vary at maximum ±0.3 metres in the X and Y-directions and ±0.5 metres in Z-direction by altering parameters *dX*, *dY* and *dZ* (Table 9). In the discernibility analysis, four CIR images in 1:6000 were used for measuring the tree top positions manually. In a real situation, the position of the model tree is measured from the image material, which is available. In this respect, the top positions of the model trees are too optimistic especially for the image sets lacking any 1:6000 scale images. This affects the analysis of the effect of scale on the performance.

The set of photo-discernible trees formed the

ground truth trees for the performance tests (see rules for hits and errors in Section 2.4.6). Thus, the results do not directly apply to the whole set of field measured trees. Also, circular plots with a two-meter wide buffer, centred within the field plots were used in the tests. Circular plots were used because of the simplicity of inclusion testing.

2.5 Measurement of Crown Width

In nadir views, tree tops are seen from straight above. The longest branches are visible provided the contrast is good and image resolution high. In very large-scale aerial photographs, say 1:2000 in scale, details such as individual leaves contribute to the texture. With such image material, it is possible to measure the crown width perhaps even more accurately than in the field with a plumb and tape.

Tree crowns vary in shape. The maximum crown width, typically used in allometric and growth models, may occur at different relative crown height. That part of the crown may not be visible at all on the photograph. Similarly, an irregular, non-symmetric crown may be observed from a direction that prevents observing the maximum width. Only the very tops of suppressed trees are visible.

A simple manual method for measuring crown widths was applied in this study. First, the tree top is located in 3D by manual image-matching (see Section 1.4.4). The elevation of the butt is obtained from a DEM. With this information, the trunk of the tree can be superimposed on the images. A line segment represents it. The operator makes two point observations on each image for the maximum width of the crown. A line connecting the observed points is superimposed on the image, and the operator checks that the line is perpendicular to the trunk line segment for oblique views with considerable radial displacement. This assures that the observations are made approximately horizontally in the object space. The observed crown edge points are solved for 3D positions assuming they were made at the elevation of the tree top. The crown width is the distance between the 3D solutions.

The experiment was carried out such that the operator had the photogrammetrically obtained tree top position superimposed on the images. Images, maximum nine at a time, were centred on the computer screen for that position, and the stem of the tree, represented by a line segment was superimposed on the image. The operator measured the maximum width of the crown and classified the observation. In cases where it was difficult to discern both crown edges, symmetry-assumption was used, or, if measurement was considered impossible, it was not made, and classified accordingly. The images were placed in the order of camera-ray's azimuth angle on the computer screen so that the viewing angle changed as little as possible when switching over to a new image. The crown widths of a field plot were measured first from a set of COL and CIR images in the scale of 1:6000 followed by another set of images in the scales 1:12 000 and 1:16 000. In order to avoid correlation between consecutive observations, a random order of trees, plots, and images had perhaps been better.

754 sample trees were measured for C_W in the field. Systematic sampling using the every Nth tree rule, and basal area weighting were applied in selecting the trees. In the discernibility analysis, 715 of these trees were defined as discernible. These 715 trees were manually measured for C_W on all images in scales 1:6000 (non-decimated), 1:12 000, and 1:16 000.

2.6 Tree Species Recognition

2.6.1 Spectral Classification Using Multiple Images

In this study, the use of new spectral signatures for tree species detection is demonstrated. With the tree top exactly mapped in 3D, it can be sampled for pixel values from several images, and most importantly, from various parts of the crown, the sunlit and the shaded side (Fig. 21).

It is assumed that the tree tops are accurately mapped in 3D. An estimate for the crown width is possibly available. The image-object-sun geometry is known. Those images in which the sunlit and shaded sides of the crowns are seen are selected. It is assumed that there are field observations to support species classification. These are

Table 10. Image data and classification variables.

Plot / Image	Scale	Image-object-sun geometry	Nadir angle, degrees	Channels in the pattern vector, SH = shaded, SL = sun-lit
MaPS2 / 22044592	1:6000	Back-side	13	RED-SH, GREEN-SH
MaPS2 / 22054598	1:12000	Front-side	17	RED-SL
PS2 / 22044588	1:6000	Front	19	RED-SL, GREEN-SL
PS2 / 22054608	1:12000	Back	6	BLUE-SH
PS1 / 22044581	1:6000	Back-side	29	GREEN-SH
PS1 / 22054599	1:12000	Front	29	RED-SL, GREEN-SL
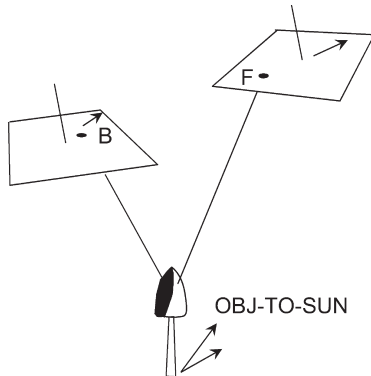
Fig. 21. Simultaneous use of two images for species recognition. The crown is sampled for the sun-lit (F = Front-lighted image region) crown and the shaded (B = Back-lighted) crown for pixel values. Extinction of light is related to foliage/needle mass density and may provide the basis for species discrimination. Arrows depict the direction of sunlight.

field mapped trees which are one-to-one linkable with the 3D positioned trees. Mapped tree data can be collected with a laser-relascope (Kalliovirta 2003). Satellite positioning should provide good approximate values for the linking between photo-measured and field-measured trees.

Training data, i.e. sets of pixel values, is collected by using the trees with known species. Crowns are sampled for pixels in a window. The features for classification are channels of the CIR images as suggested by Haara and Haarala (2002).

2.6.2 Set-up for the Species Recognition Experiment

The suggested method for species classification was tested for demonstrative purposes with the data from plots MaPS2, PS1, and PS2. These plots represent mixed stands in which pine, spruce, and birch occur.

Discernible trees formed the trees, the test sets, for which species classification was tried. On each plot, a training set consisting of 10 trees per species was selected randomly. The small number of birch on plots PS1 and PS2 resulted in a smaller training set, and the same birches were re-measured for the test set. Trees not belonging to the training set formed the test set of plots PS1 and PS2. On plot MaPS2 all pines and birches not belonging to the training set formed the test set together with a systematic sample of spruces.

For each field plot, two CIR images were selected such that the sun-lit sides of the crowns would show on the one image, and the shaded sides of the crowns would be seen on the other (Fig. 21). The image pairs consisted of an image in scale 1:6000 and another in scale 1:12 000 (Table 10). The crowns were manually sampled for RGB-values in a 3×3 pixel window, corresponding to 25×25 and 50×50 centimetres on the ground. A sample was taken manually from the sun-lit and shaded part of the crown. The images were centred automatically to the 3D position of the tree top, a sunray (direction of sunlight) and trunk (vector giving the image direction of radial displacement) were superimposed on the images to assist the work.

RGB-values from two images formed the set of six classification variables from which to select the features for the minimum distance and Bayesian classifiers (Gonzalez and Woods 1993,

45

p. 588–590). 3D-feature space was chosen because of simplicity. The selection of variables was done subjectively by simply comparing the differences between the means of the six channels between the three tree species in the training set. This is not optimal. The selected variables are shown in Table 10. Minimum distance classifier was employed on all plots, and for plot MaPS2, classification was computed with a Bayesian classifier for comparison.

2.7 Simulation of Photogrammetric Stand Cruising

2.7.1 Motivation

The accuracy of a forest inventory is explained largely by three error sources: (i) errors due to imperfect observations and measurements, (ii) sampling errors and (iii) errors due to imperfect models of indirect estimation. An estimate of the combined effect may be obtained by numerical simulation. Assumptions are made about the magnitude and quality of the individual error-sources. Errors travel through the system, and the total effect may be difficult, in some cases impossible to assess without numerical calculations. Non-linearity and inter-dependencies are difficult to describe analytically. Simulations can be used to provide information about systematic errors arising from erroneous observations and about the necessary sample sizes or measurement accuracy for a wanted end-level accuracy.

Tree discernibility, accuracy of tree top positioning and crown width measurements, DEM-accuracy, species recognition accuracy, and accuracy of the allometric and tree-volume functions all set fundamental limits for individual tree-based forest inventory. These are tried to account for, as realistically as possible in the simulations.

It should be noted here that the cost-efficiency of an inventory is essential. In this respect, the degree of automation of both field work and image analysis is important. The cost-efficiency was not evaluated in the simulations since the needed information was lacking.

Monte-Carlo-simulation was used in the simulations. In it, the inventory chain (stand cruising with full mapping of trees, scheme C in Table 1,
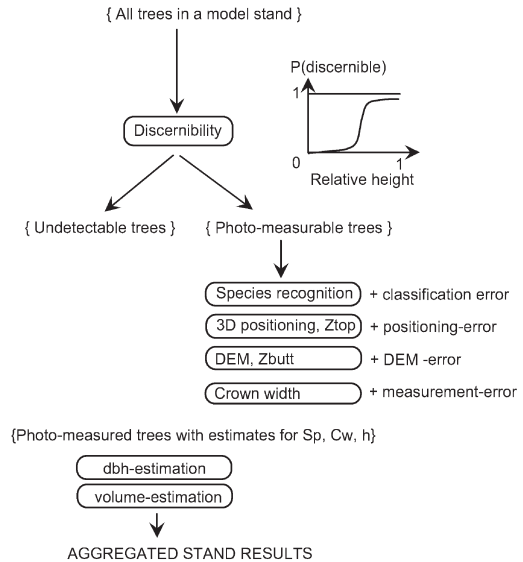
Fig. 22. Flowchart of simulation. Simulated sub-processes are depicted with rounded rectangles.

Fig. 22) is repeated several times for two model stands and results are computed for variables of interest. Measurements, observations, and model estimates are affected by errors drawn from statistical distributions. The fluctuation and systematic deviation of the variables of interest was studied. Simplifying assumption on the error distributions were made.

2.7.2 On Restrictions and Assumptions

The realisation of a forest inventory, which utilises the model presented in Fig. 1, was simulated (Fig. 22) by computer. However, plenty of simplifying assumptions were made, and they need to be considered when interpreting the results.

Nothing explicit is said about the image material. It is assumed that single tree photo-measurements are possible, and that changes in the image material are reflected by the changing magnitude of the observation errors. Field data is expected to be available for species recognition. It is assumed that an accurate digital elevation model is available for height estimation and that DEM-errors are included in the positioning-errors (cf. Fig. 22).
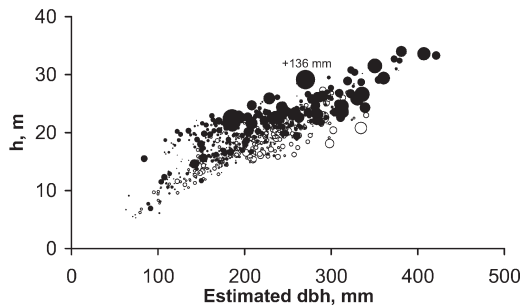
Fig. 23. Differences between 753 field-measured and model-predicted (Eq. 4) breast-height diameters (circles) plotted in the estimated dbh-field measured height-space. Underestimates are marked in black and overestimates in white. The width of the circle represents the absolute value of dbh-difference (in mm, scale 1:5 with respect to dbh-axis).

The errors drawn from statistical distributions are thought to model the observation error processes. Dependencies between processes are not considered. This is an assumption that most likely violates any real situation. For example, an error in the positioning of a tree top will most likely affect both crown width measurement and species recognition, if these processes use the 3D-position estimate as confining information. Similarly, an error in which two trees with overlapping crowns is detected and positioned as a single tree, will lead to a considerable overestimation in crown width and dbh.

The allometric models (Eq. 4) which predict dbh with estimates on species, crown width and height are assumed to produce unbiased estimates for unbiased measurements. This may require that the inventory chain includes a calibration phase in which the predicted dbh-values are corrected for systematic errors. For example, in a validation test for 753 field-measured trees from the study area, the models underestimated dbh by 6.7 mm (Fig. 23). The differences between field-measured and model-estimated dbh had a standard deviation of 26.6 mm. Mean differences of field-measured and model-estimated dbh were 22.5 and 19.1 mm for plots MaPS3 and MaPS2, respectively. These plots represent stands in which exceptionally old pine and spruce occur. It is possible that the allo-

metric relationships of old trees are not properly described by the allometric models.

For the simulations, two model stands were generated by using the field data from plots S2 and MaPS3. Stand S2 represents a thinning stand and plot MaPS3 represents a mature stand. Model stands consist of tree-records with true values for species, dbh, height, and C_W. Pine, spruce and birch were recognised as species and the small number of other broad-leaved species were treated as birches in all phases. Field-measured C_W was not available for all trees. It was estimated by inverting the regression models (4) dbh = f (sp, C_W, h). These estimates were not in accordance with the field measurements especially in the case of Model stand MaPS3. Inverted regression functions cannot be expected to yield a correct functional form unless the correlation between X- and Y-variables is very high. To add variation to the estimates of C_W, a Gaussian error term with 40-centimetre standard deviation was added to the model inverted values. This was derived by subtracting the estimated measurement error of C_W (0.6 m) from the average mean square errors of local regression models $C_W = f$ (sp, dbh, h), which were estimated by using the 753 sample trees.

Single tree volume models $v_i = f$ (sp, dbh, h) for the total, the saw wood, and the pulp wood volume were assumed to yield the true values. However, the stem form of trees can vary within a stand and between stands. The models can, thus, give biased volume estimates with respect to the real values, which are only attainable by measuring the trees for a large number of variables. Description of the forest is far from perfect even if every tree is known for species, dbh, and height. This element of model errors in tree-level volume models is not accounted for in the simulations. In a real situation, it adds to the error.

Only saw wood and pulpwood sortiments were recognised. In a real situation, a single stem can be graded for logs representing up to three or four sortiments. The quality of the stem is affected by several qualitative and quantitative factors (e.g. Uusitalo 1995) that were not available for the simulation. In a real inventory, this information needs to be collected in the field, since it is likely that sole interpretation of aerial photographs will not provide it. In the simulation each tree is graded into logs of stump-residue, saw wood,

47
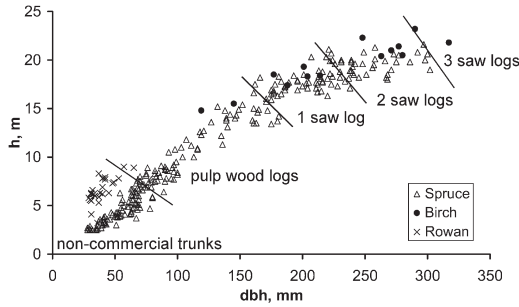
Fig. 24. Dbh-height distribution of model stand S2. An approximate division of the dbh-height plane into classes of trunk's commercial potential. For example, trunks with 21 cm dbh and 18 metre height can be cut to yield one saw log of allowable dimensions whereas a trunk with seven centimetre dbh and 6 metre height is classified as a non-commercial trunk yielding no pulp wood or saw wood logs.

Fig. 25. Empirical discernibility data and modelled discernibility-functions (7) for model stands MaPS3 and S2. Two sigmoids are drawn for Model stand MaPS3. For the curve 'v-weighted', the residuals are weighted with third power of relative height.

pulpwood, and tree-top residue. The algorithm utilises polynomial taper curves (Laasasenaho 1982), which give the stem diameter from the butt to the top. The saw wood volume of a single tree increases in a stepwise manner with increasing stem dimensions. For a single tree even a small deviation in dbh or height can cause gross changes in the saw wood or pulp wood volumes as the number and type of logs in changed (cf. Fig. 24). This is especially the case at the threshold, where the tree turns from a pulp-wood-only trunk into a stem that can potentially be cut for a saw log.

2.7.3 Flow of Simulation

1. Discernibility of trees

The first process selects the trees that are discernible, i.e. measurable in 3D using multiple images. In it, a sigmoid (Eq. 7) representing the probability of discernibility for a tree of given relative height (h_{rel}) is used (Fig. 25). The sigmoids were estimated from the empirical data obtained in the discernibility analysis (Section 2.3). Thus, they represent the situation in which four views in scales 1:6000 and/or 1:12 000 were available. For a smaller number of images, or images in smaller scale, the curves are probably too optimistic.

$$P(discernible) = (1 - e^{ah_{rel}^b}) \qquad (7)$$

The sigmoid produces values between zero and one for relative height in the same interval. Parameters a and b are estimated using non-linear estimation by least-squares adjustment. For model stand MaPS3, the parameters were obtained by weighting the residuals to the third power of relative height. This corresponds to weighting with stem volume, and the sigmoid has a locally better fit for the dominant trees (Fig. 25).

The discernibility-sigmoid is assumed to model omission errors in 3D tree top positioning. These are omission due to occlusion, shading, and overlapping crowns. A random deviate, with uniform distribution between zero and one, is generated and compared against the value from the sigmoid given the tree's relative height. If the random deviate has a smaller value than the sigmoid, then the tree is considered discernible in 3D, and is added to the set of photo-measurable trees.

Table 11. Error matrix consisting of conditional probabilities for species recognition. See text below for more explanation.

| True species | Pine | Probability to be classified as | | Total |
		Spruce	Birch	
Pine	$A + \varepsilon_1$	$D \times \lambda_1$	$E \times \lambda_1$	1
Spruce	$D \times \lambda_2$	$B + \varepsilon_2$	$F \times \lambda_2$	1
Birch	$E \times \lambda_3$	$F \times \lambda_3$	$C + \varepsilon_3$	1

2. Species recognition

All discernible trees are given an estimate for the species. This is based on conditional probabilities P_{ij}, which give the probability of a tree with true species i to be classified as species j. The species recognition process is not allowed to produce new species, which do not already occur in the stand. The errors in species recognition cause random effects in dbh and stem volume estimation, which is performed by using the species-specific allometric models (4) (cf. Fig. 26).

The conditional probabilities are put in a symmetric matrix (Table 11). The dimension is determined by the number of species. For each simulation at the stand level, the matrix is updated for new diagonal elements representing the probabilities for correct recognition. In Table 11 they are elements A, B and C, which are allowed to fluctuate ± 0.1 units as a result of adding uniform random variates ε_1, ε_2, and ε_3 to the diagonal elements. Coefficients λ_1, λ_2, and λ_3 assure that the row-totals equal one. A random uniform deviate between zero and one is generated for each tree, and it is compared with the values of the error matrix to determine the result of species recognition.

3. Measurement of crown width

The photo-measurement of C_W is simulated for the discernible trees by adding a Gaussian error term to the true value, with expectance EC_W and variance $\sigma^2(C_W)$:

$$C_W = C_W + \varepsilon \sim N(EC_W, \sigma^2(C_W)) \tag{8}$$

In the simulations $\sigma^2(C_W)$ was 0.36 m^2, while EC_W was varied.
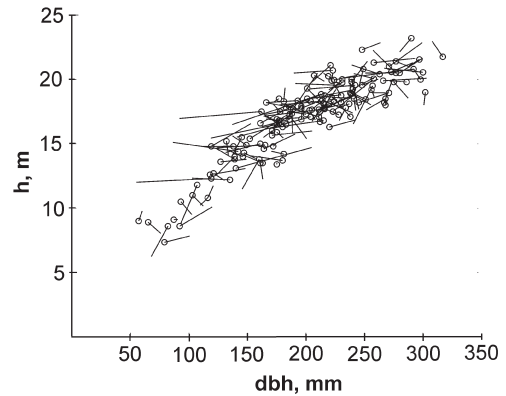
Fig. 26. One realisation of error-simulation of model stand S2. The line segments represent the simulated measurement and estimation errors in dbh and height for the discernible trees. $\sigma(h)$ = 1.0 m, $\sigma(C_W)$ = 0.6 m. Species recognition accuracy 85%.

4. Height measurement

Height estimates are affected by an additive Gaussian error term, with expectance Eh and variance $\sigma^2(h)$:

$$h = h + \varepsilon \sim N(Eh, \sigma^2(h)) \tag{9}$$

This error process is assumed to model both errors in tree top positioning and in the digital elevation model. In the simulations, $\sigma^2(h)$ was 1 m^2, while Eh was varied.

5. Dbh-estimation with allometric models

Discernible trees are estimated dbh given the photogrammetric estimates for species, crown width, and height using the allometric equations (4).

As a result of the measurement and model error processes, the dbh-height distribution is changed as illustrated in Fig. 26.

6. Computation of stand attributes

When all photo-measurable trees in the stand have estimates for species, dbh, and height; the

total volume, saw wood volume, and pulp wood volume for each tree is computed by using taper curves and a grading algorithm as described in Section 2.7.2. The results are summed up to stand level variables of total volume by species, saw wood volume, pulp wood volume, basal area weighted mean diameter, and basal area weighted mean height.

7. Simulation

Processes 1–6 above are repeated 200 times for each combination of error distribution parameters EC_W and Eh until they are allowed to change to a new set of values. $\sigma^2(h)$ and $\sigma^2(C_W)$ are kept constant at the chosen values. The mean and standard deviation of the stand variables from 200 repetitions are stored for analysis.

3 Results of the Experiments

3.1 Tree Discernibility and Manual Image-Matching of Tree Tops

3.1.1 Positioning Accuracy of Manual Image-Matching

For analysing the positioning accuracy a 3D error vector $[\Delta X, \Delta Y, \Delta Z]$ was defined as **field position–photogrammetric position**. The bias of planimetric accuracy cannot be analysed since the field plots were not oriented in the field by surveying (Section 2.1.1). The precision of X and Y coordinates varied from 0.16 to 0.43 m measured by standard deviation of ΔX and ΔY per plot. Observed imprecision was the largest in the birch plots B1 and B2 and in the mature stands MaPS1, MaPS2, MaPS3, and MaPS4. For example, in plot MaPS4, the standard deviations of ΔX and ΔY were 0.59 m and 0.50 m for pine and 0.32 m and 0.32 m for spruce. The tops of the old pine trees, which are from 130 to 215 years of age in plot MaPS4, appeared round on the photographs. It is clear that the shape of the tree-apex influences the 3D positioning accuracy (cf. Kraus 1993).

The means of ΔZ per plot varied from –0.6 m to 0.56 m. The mean ΔZ of 5675 discernible trees was –0.02 m with a standard deviation of 0.72 m. The CIR photography took place on May 27, 2002 at the beginning of the growing season, and the height measurements were made between May 22, 2002 and April 2003. The height growth of summer 2002 is missing in the images but present, in varying degree, in the field observations. It was estimated that the average missing height growth was 0.20 m. With this correction, the positionings were made, on average, 0.22 m above the tree tops. The plot elevations were assumed to be known with ± 0.25 m accuracy (95% of cases). The photogrammetric positionings can therefore be claimed unbiased in Z. The standard deviations of ΔZ per plot varied from 0.31 to 1.01 metres.

The largest values were obtained for the dense plots B2 and S3, and mature stands MaS1, and MaPS1, MaPS2, MaPS3, and MaPS4. The imprecision of height measurements and imprecision of tree butt Z-coordinates constitute a portion of the observed differences as well as the inaccuracies in the determination of the plot elevation by levelling. If it is assumed that the height measurements were done with a 0.5-m standard error, the precision of Z-coordinate of photogrammetric measurements was approximately 0.5 m.

It should be noted that the operator who measured the tree tops could learn from the field data where, on the image, to point out the tree top. Thereby the results of positioning accuracy are tentative.

3.1.2 Tree Discernibility

The number of discernible trees, their total volume, volume of saw wood, and volume of pulp wood are given for each plot relative to the total tree set (Table 12, Table 14). The number of discernible trees and the total number of trees by classes of relative height are tabulated for each plot (Table 13, Table 15). These proportions are also illustrated in Fig. 27.

Considerable underestimation in the total stem number was observed in spruce stands S1–S6. The discernibility-functions (Fig. 27) of the densest plots S3 and S5 differ from the others. On all spruce plots, almost all of the dominant trees were discernible except for trees, which had overlapping crowns. This shows in the proportion of measurable saw timber that varied from 97.8 to 100%. Of the total volume, 92% or more was discernible in the managed stands. On plot S3, which has escaped thinnings, only 88% of the total volume and 82% of pulp wood volume was discernible. (Fig. 27, Table 12, Table 13).
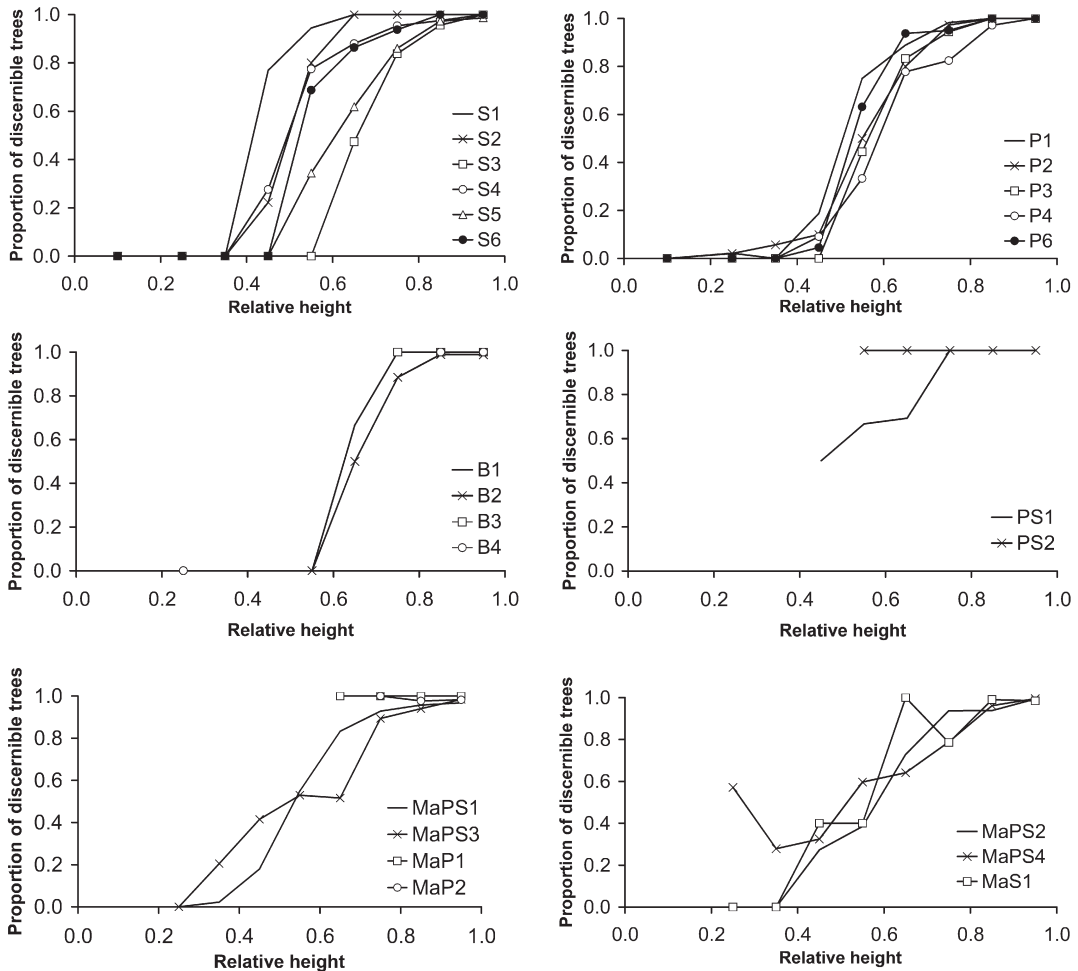
Fig. 27. Proportion of discernible trees as a function of relative height.

Pine plots P1–P6 have understorey consisting of spruce and pubescent birch. Because these small trees were mainly not visible on the photographs, the stem number of the set of discernible trees underestimated the true stem number considerably. The dominant, co-dominant, and intermediate trees are almost all discernible. Thus, the proportion of measurable total volume is high, from 95% to 98%. The dense unthinned plot P4 has a less dense understorey, which is probably due to high stocking of the dominant layer. This explains the low underestimation of stem number in plot P4. (Fig. 27, Table 12, Table 13).

The birch stands B1–B4 had no understorey

trees in 2002. A very dense understorey of spruce was cleared in the early 1990's (Räsänen et al. 1992). There are mainly dominant and co-dominant trees. 96.4% or more of the trees were discernible. On the non-thinned plot B2, there were some non-discernible dominant trees, which had overlapping or defoliated crowns. (Fig. 27, Table 12, Table 13).

Stands PS1 and PS2 have been recently thinned. Plot PS2 was thinned in spring 2002 and plot PS1 in autumn 2000. On plot PS1, 48% (D_g 15.2 cm for removed trees) and on plot PS2, 62% (12.2 cm) of the stems was removed in the intermediate felling. The thin-from-below strategy was

followed. There is a harvesting track, four to five metres in width, which runs through each plot. All trees were discernible on plot PS2. On plot PS1, six intermediate trees were not measurable. (Fig. 27, Table 12, Table 13).

Table 12. Stem number (N), total volume (Vtot), saw wood volume (Vs) and pulp wood volume (Vp) of the discernible tree set relative (%) to the total tree set. Thinning stands. Basal area (G) is given as a measure of stand density.

Plot	G m²/ha	N	Vtot	Vs %	Vp
S1	25.4	83.8	99.2	100.0	98.9
S2	20.9	49.4	96.1	100.0	96.4
S3	40.0	50.2	87.8	97.8	81.8
S4	29.3	64.5	94.2	99.2	92.4
S5	33.2	75.7	92.3	100.0	91.2
S6	25.2	79.2	96.9	100.0	95.0
P1	20.9	66.4	97.8	100.0	98.9
P2	24.7	51.2	96.5	100.0	98.7
P3	21.9	50.4	95.1	100.0	96.2
P4	29.9	72.4	94.8	100.0	94.8
P6	21.5	51.8	95.4	100.0	96.9
B1	15.0	98.0	99.4	100.0	99.4
B2	21.7	96.5	98.2	100.0	98.3
B3	14.6	100.0	100.0	100.0	100.0
B4	15.1	96.4	99.8	100.0	100.0
PS1	20.7	95.6	98.4	100.0	98.2
PS2	18.6	100.0	100.0	100.0	100.0

Plot MaPS1 represents a heterogeneous plot. The plot is 60 m wide and extends 180 m in south-north direction. In the south, it covers a drained bog dominated by pines with an understorey of pubescent birch. Two-thirds of the plot is on mineral soil. The site type there varies a lot and there are even openings caused by rocky soil conditions. Both pine and spruce occur in the dominant layer and understorey is missing. In the discernibility analysis, the plot was considered as a whole. There were many non-discernible intermediate trees resulting in low proportion of discernible pulp wood volume, 90.2%. (Fig. 27, Table 14, Table 15).

Plot MaPS3 is a stand, which was clear-cut in April 2003. The dominant trees consist of pines and spruces that grew in patches. In the pine-dominated parts, there was a dense understorey of small spruce, which was mostly excluded from the data because of the 90-mm lower bound for dbh. 90 mm in dbh corresponds to approximately seven to nine metres in height, which is from 28% to 36% in relative height. If the small spruces had been tallied, the underestimation in stem number would have been much higher than the observed 13.7%. Trees with a dbh lower than 90 mm are not harvested for commercial timber and their share of the total volume is small. This means that the estimates for discernible saw-wood and

Table 13. Number of discernible trees and total tree number of trees in relative height classes. Thinning stands.

Plot	Understorey −2	23	34	45	Intermediate 56	67	78	Co-dom 89	Dom 9–
S1	0/3	0/18	0/10	10/13	17/18	38/38	40/40	43/43	33/33
S2	0/38	0/41	0/47	4/18	8/10	15/15	19/19	48/48	45/45
S3	0/59	0/47	0/41	0/29	0/43	18/38	62/74	109/114	69/69
S4	0/29	0/37	0/28	8/29	31/40	66/75	62/65	39/40	43/43
S5	0/3	0/14	0/12	0/20	11/32	34/55	74/86	142/146	75/76
S6	0/16	0/7	0/9	0/7	11/16	19/22	60/64	52/52	53/53
P1	0/10	1/46	0/36	3/16	4/4	16/18	56/57	71/71	61/61
P2	0/33	2/97	3/53	2/20	5/10	8/10	35/36	75/75	84/84
P3	0/15	0/79	0/49	0/19	4/9	10/12	34/36	65/65	61/61
P4	0/31	0/31	0/25	1/11	2/6	21/27	61/74	137/141	103/103
P6	0/17	0/74	0/48	1/22	12/19	15/16	38/40	75/75	42/42
B1	–	–	–	–	0/1	2/3	3/3	21/21	68/68
B2	–	–	–	–	0/1	1/2	23/26	89/90	80/81
B3	–	–	–	–	–	–	6/6	18/18	59/59
B4	–	0/3	–	–	–	–	–	13/13	67/67
PS1	–	–	–	1/2	2/3	9/13	30/30	51/51	36/36
PS2	–	–	–	–	1/1	3/3	27/27	60/60	34/34

pulp wood volume would not have changed significantly even if the small trees had been tallied. (Fig. 27, Table 14, Table 15).

Plots MaP1 and MaP2 are located on barren mineral soil, on poor and dry CT forest type, where spruce is restricted to the understorey and pine dominates. Plot MaP1 has been thinned heavily and has only 340 stems per hectare. All trees were discernible on this plot. On plot MaP2 two trees, which were partly occluded by close neighbouring trees, were not seen by the operator. (Fig. 27, Table 14, Table 15).

Plot MaS1 represents a planted spruce stand, which was extended somewhat to include some large aspens with interlaced crowns. These aspens formed mainly the non-discernible total and saw wood volume. Initially the trees of MaS1 were

planted in rows. Although the density is high, 94% of the trees and 96.6% of the total volume was discernible. (Fig. 27, Table 14, Table 15).

Plot MaPS2 consists of spruce and pine, which are from 110 to 145 years old and between 20 and 34 metres high. The two species grow mixed. There is only a scarce understorey tree-layer. 13% of the stems and five per cent of the total volume was non-discernible. Pulpwood in stand MaPS2 was underestimated by 13%. This was mainly due to the non-discernible intermediate trees. (Fig. 27, Table 14, Table 15).

The clear-cut area represented by plot MaPS4 could be delineated in two stands. The northern part of the plot, 30% of the area, consisted of 215-year old pines and 40-year old spruce understorey. The rest of the plot was made up of a 130-year old spruce-pine forest with no understorey. Since the plot was an actual clear-cut, it was treated as a whole in the analysis. On plot MaPS4, understorey spruces below the old pines were mostly non-discernible. If an understorey tree was visible, it was only seen on two or three views, whereas the dominant trees could be seen in all four views. It should be noted here that a portion of the understorey spruce was not mapped in the field since the lower bound for dbh on this plot was 90 mm. It corresponds to approximately 8.5 metres (30% of H_{dom}) in height. Pulpwood was underestimated by 23% because a large portion of the intermediate spruce trees, with relative height between 0.3 and 0.7, were non-discernible. 97% of the saw wood volume was discernible (Fig. 27, Table 14, Table 15).

Table 14. Stem number (N), total volume (Vtot), saw wood volume (Vs) and pulp wood volume (Vp) of the discernible tree set relative (%) to the total tree set. Mature stands. Basal area (G) is given as a measure of stand density.

Plot	G m²/ha	N	Vtot %	Vs	Vp
Pine dominated stands					
MaPS1	18.1	78.2	94.0	96.8	90.2
MaPS3	23.1	86.3	96.0	97.8	89.6
MaP1	16.1	100.0	100.0	100.0	100.0
MaP2	20.4	98.2	98.3	98.8	97.3
Spruce dominated stands					
MaS1	36.7	94.0	96.6	96.7	96.1
MaPS2	33.2	87.2	95.0	96.2	87.6
MaPS4	31.8	76.5	94.5	97.0	76.8

Table 15. Number of discernible trees and total tree number of trees in relative height classes. Mature stands.

Plot	–2	Understorey 23	34	45	56	Intermediate 67	78	Co-dom 89	Dom 9–
Pine dominated									
MaPS1	–	0/13	1/45	7/39	11/20	45/54	104/112	134/140	151/156
MaPS3	–	0/1	8/39	22/53	9/17	16/31	42/47	157/167	427/434
MaP1	–	–	–	–	–	4/4	11/11	19/19	51/51
MaP2	–	–	–	–	–	–	11/11	42/43	55/56
Spruce dominated									
MaS1	–	0/3	0/4	2/5	2/5	1/1	11/14	106/107	131/133
MaPS4	–	4/7	17/61	24/74	37/62	34/53	41/52	150/156	210/211
MaPS2	–	0/14	0/2	3/11	5/13	43/59	135/144	106/113	152/153

3.2 Performance of Semi-Automated 3D Tree Top Positioning

3.2.1 Hit-rate Best-Cases

The best case was defined as the one with the maximum hit-rate with the commission error rate below five per cent, and the RMSE of Z below one metre. It was assumed that a five per cent of commission error-rate represents an acceptable amount of erroneous positions to be removed manually after an automated search for tops.

The best case in hit-rate was searched for each Plot×Image Set×Model tree-combination. The total number of such combinations was 1608 and, it equals the number of 'computer nights' that were used for the computations of performance testing.

Pine plots P3 and P4

Pine plots P4 and P3 (Fig. 28) form a pair for testing the effect of stand density on the performance of 3D tree top positioning. P4 has never been thinned, and has a basal area of 30 m²/ha. There is mortality due to overstocking. Plot P3 was last thinned in 1989 and had 22 m²/ha of basal area in 2002. Differences in the treatment history show in the dbh-distribution. The mean diameter of trees in plot P3 is two centimetres larger than in plot P4. In the discernibility analysis, approximately 95% of the volume was discernible in both plots. 50.2% of the stems were discernible in plot P3 and 72.4% in plot P4. These trees constituted the ground truth for the performance testing of the 3D tree top positioning algorithm.
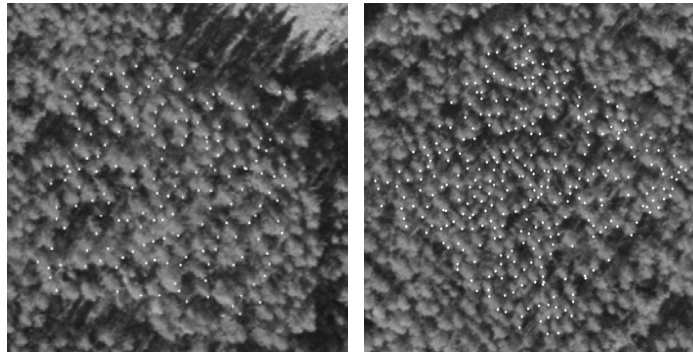
Fig. 28. Plots P3 and P4 in the aerial image 22054607 with tree tops of discernible trees. Scale 1:12000, nadir angles 17 and 16 degrees.

Table 16. Statistics of best cases in hit-rate (%) by image sets (Table 8). Pine plots P3 and P4. Ten model trees per plot. An asterisk marks the overall best case and N is the number of image set × model tree combinations.

Image Set	N	Plot P3 (thinned) Mean	s	Min	Max	Image Set	N	Plot P4 (unthinned) Mean	s	Min	Max
MNAD	10	91.3	4.3	81.5	95.8*	12CIR	10	70.8	15.5	38.2	83.0
6CIR	10	88.6	4.0	80.7	93.3	612CIR	19	70.7	18.6	11.3	84.0
612CIR	20	88.1	6.9	71.4	95.0	MNAD	10	69.9	24.5	15.6	86.8*
12CIR	10	87.5	4.7	80.7	93.3	6CIR	10	67.1	21.2	12.3	80.2
LNAD	10	87.4	8.5	68.9	93.3	6COL	10	65.7	14.4	35.9	78.8
WNAD	10	86.3	6.6	71.4	93.3	LNAD	10	65.4	21.4	17.5	80.2
616CIR	20	85.5	9.0	54.6	94.1	WNAD	10	64.3	20.0	10.4	80.7
16CIR	10	84.3	5.6	73.1	91.6	616CIR	20	63.8	21.1	7.1	80.7
P6CIR	20	73.8	11.4	44.5	85.7	16CIR	10	58.3	23.8	15.1	82.6
P12CIR	20	68.2	19.2	12.6	85.7	P12CIR	20	52.2	24.6	0.9	73.1
6COL	10	67.3	23.8	20.2	89.1	P6CIR	20	47.5	21.8	1.9	71.2
P16CIR	20	62.9	18.4	19.3	86.6	P16CIR	20	46.9	18.4	6.6	72.6
	170	72 077 064 trials					169	51 283 739 trials			

The best cases in hit-rate were 95.8% and 86.8% for plots P3 and P4 respectively. These were both obtained with the MNAD image set, which consisted of four images in scale 1:6000 and three images in scale 1:12000. Since plots P3 and P4 are located next to each other in the field, all image sets are identical. The best case hit-rates correspond to 98.3% and 92.6% hit-rate in total discernible stem volume. There is a clear difference in the mean hit-rates between the two plots. This is likely due to the differences in stand density and structure. However, it is also possible that the parameter space was incorrectly set. For example, the parameter EllipseWidth was allowed to take values 2, 2.3, 2.6, and 2.9 metres on plot P4. The mean of the 169 best cases was 2.10 m. Perhaps better results had been obtained by allowing the parameter to take lower values. The image set LNAD did not produce best hit-rates against expectations, and it is possible that the condition set on maximum RMSE in Z-coordinate caused this. The LNAD set with images viewing the trees from near-nadir directions is not able to produce the same Z-accuracy as the sets with images having variation in nadir angle. The image-pair sets produced on average poorer results on both plots and the variation in hit-rate between model trees was the largest for these sets. The differences due to image scale were not significant. Set 612CIR was superior to set 616CIR in both

plots, and set 16CIR produced lower hit-rates than sets 6CIR and 12CIR. Colour images in set 6COL produced on average lower hit-rates in comparison to CIR images in the set 6CIR. One model tree on plot P4 turned out very poor in all sets, and had an effect on the results. This tree had a small crown and was visible against the sun-lit forest floor in some of the images. For example, the mean hit-rate for image set MNAD would have been 74.0% instead of 69.9%, had that model tree been omitted. (Table 16).

Spruce plots S3 and S6

S3 has escaped all thinnings and S6 is a managed stand (Fig 29). The proportion of birch is 15% of total volume on plot S3, and plot S6 represents an almost pure spruce stand. Birches of plot S3 belong to the dominant layer, and grow in clusters with partially overlapping crowns.

The best cases in hit-rate were 98.4% and 77.3% corresponding to 99.2% and 82.6% of total discernible volume. In the discernibility tests 79.2% and 50.2% of trees and 96.9% and 87.8% of total volume was discernible on plots S6 and S3. It appears that the stand structure and density has an effect upon the performance of 3D tree top positioning. For the dense plot S3, the hit-rates are lower. Image set 612CIR produced the best

Table 17. Statistics of best cases in hit-rate (%) by image sets (Table 8). Spruce plots S6 and S3. Eleven and ten model trees. An asterisk marks the overall best case and N is the number of image set × model tree combinations.

Image Set	N	Plot S6 (thinned) Mean	s	Min	Max	Image Set	N	Plot S3 (unthinned) Mean	s	Min	Max
612CIR	22	92.4	8.1	66.1	98.4*	612CIR	19	63.3	8.7	49.4	77.3*
12CIR	11	84.2	17.8	34.7	96.9	616CIR	20	61.6	6.3	50.6	72.1
LNAD	11	84.0	13.8	48.0	93.7	LNAD	10	61.2	9.9	45.9	75.6
MNAD	11	82.2	16.3	45.7	96.1	12CIR	10	58.7	8.7	42.4	70.4
6CIR	11	78.7	15.7	37.8	90.6	MNAD	10	56.3	8.4	43.6	67.4
616CIR	22	77.4	21.7	15.8	93.7	16CIR	10	54.6	8.4	41.3	64.0
6COL	11	70.7	20.5	20.5	89.0	6CIR	10	51.2	13.9	25.0	64.0
16CIR	11	69.4	22.3	10.2	87.4	6COL	10	50.9	15.9	19.8	70.9
WNAD	11	61.8	23.4	22.8	85.8	WNAD	10	36.7	15.4	7.6	58.1
P6CIR	22	55.2	27.8	0.0	86.6	P6CIR	20	34.9	16.6	7.6	66.3
P12CIR	44	47.2	26.7	2.4	89.0	P16CIR	20	34.6	13.2	4.7	52.3
P16CIR	22	41.2	24.8	1.6	78.0	P12CIR	40	34.2	13.3	12.2	70.9
	209		100 239 430 trials				189		61 971 025 trials		
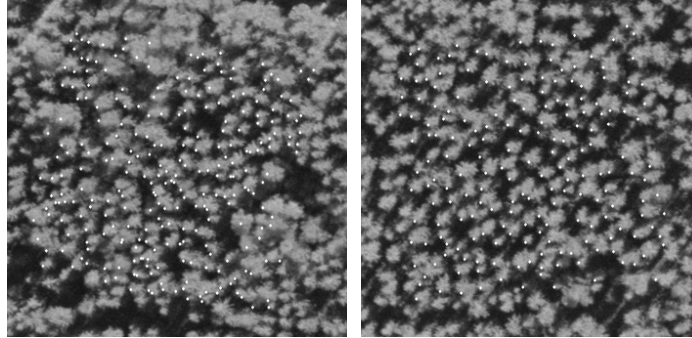
Fig. 29. Plots S3 and S6 in the aerial image 22054599 with tree tops of discernible trees. Scale 1:12000, front-lighted, nadir angles 13 and 10 degrees.

cases on both plots. Sets 12CIR consisting of six images in the scale of 1:12000 yielded higher average hit-rates than the sets 6CIR, which had four decimated images in the scale of 1:6000. By comparing sets 6CIR and 16CIR, it can be seen that the possible effect of scale is not consistent. Set 16CIR was better than set 6CIR on plot S3. Image pairs produced poorest results with large variation in the hit-rate between model trees. This is in line with the findings on pine plots P3 and P4. The expected order of the image sets LNAD, MNAD, and WNAD was fulfilled. Oblique views in the sets WNAD have more occluded trees, which lead to lower hit-rates. CIR images in the sets 6CIR proved better in comparison to colour images in the sets 6COL. (Table 17).

Birch plots B1, B2, and B3

Intermediate fellings have taken place in plots B1 and B3 whereas plot B2 is unthinned (Fig. 30). Plot B1 was thinned from 981 to 600 stems per hectare in winter 2000–2001, and plot B3 to 520 stems per hectare in 1992. Stem diameters and crowns on plot B3 are larger than on plot B1 possibly due to the thinning effect which has lasted 10 years longer on plot B3 than on plot B1. Plot B2 consists of slender trees with relatively short crowns. Mortality due to overstocking has taken place on plot B2. The weather was windy on May 27, 2002, when the CIR photography took place. At weather station 1.5 kilometres away from the birch plots, average wind velocity of 4.2 metres

per second was measured between 09:45 and 10:30 a.m. The maximum values, up to seven metres per second, occurred at 09:50–09:54. The CIR photography in scale 1:6000 took place between 09:46–09:55. In July 2002, it was verified that such wind causes considerable tree sway and bend in plots B1 and B2 where the trees are slender. Superimposed 3D points of field measured tree tops did not match the crown patterns on the images. This was observed in parts of the plots in two consecutive CIR images in scale 1:6000. Plot B2 is situated on a slope, and the tree tops not matching the patterns in the images were located at the hilltop. For plot B2, these two CIR images in scale 1:6000 were rejected and replaced with colour images in a set 6C_6CIR.

In the managed stands B1 and B3, there were cases in which all trees were hit. Hit-rates of 100% were observed even in some image-pair sets. For the dense plot B2, image set LNAD produced the overall best case of 97%. On plot B3, one model tree produced low hit-rates if a particular CIR image in the scale 1:6000 was included in an image set. This co-dominant model tree had an interlaced crown with a taller dominant tree located close by. Possibly this model tree×image combination produced a poor-quality, cross-correlation image, in which the correlation maxima were low and shifted. This image was included in sets 612CIR, 616CIR, 6CIR and P6CIR. (Table 18, Table 19).

The anticipated effect of nadir angle was observed in all plots. Set WNAD, consisting of oblique views, produced lowest hit-rates in com-

Fig. 30. Plots B1 and B2 in the aerial image 22054602 and plot B3 in image 22054608 with tree tops of discernible trees. Scale 1:12000, nadir angles 13, 12, and 14 degrees.

Table 18. Statistics of best cases in hit-rate (%) by image sets (Table 8). Birch plots B1 and B2. Ten model trees. An asterisk marks the overall best case and N is the number of image set × model tree combinations.

Image Set	N	Plot B1 (thinned in 2000) Mean	s	Min	Max	Image Set	N	Plot B2 (unthinned) Mean	s	Min	Max
MNAD	10	92.2	9.9	69.5	100.0*	LNAD	10	93.5	2.2	89.6	97.0*
LNAD	10	90.7	12.8	61.0	100.0	612CIR	10	93.0	2.0	88.9	95.6
612CIR	10	90.3	12.9	55.9	100.0	12CIR	10	90.6	3.4	84.4	94.1
WNAD	10	89.3	5.3	83.1	96.6	MNAD	10	89.2	3.4	83.7	94.1
12CIR	10	88.0	8.9	71.2	98.3	616CIR	10	86.4	7.0	71.9	94.8
616CIR	10	83.4	18.4	33.9	96.6	WNAD	10	85.0	6.8	66.7	90.4
16CIR	10	79.0	22.6	18.6	94.9	P6CIR	10	80.1	18.5	30.4	94.1
6CIR	10	78.5	16.0	39.0	93.2	6C_6CIR	10	79.8	13.7	48.2	95.6
P6CIR	10	73.9	15.0	40.7	94.9	16CIR	10	70.6	21.7	20.7	87.4
6COL	10	71.9	30.3	11.9	96.6	P12CIR	20	69.9	20.1	19.3	89.6
P12CIR	20	47.2	23.3	8.5	83.1	6COL	10	65.0	18.1	36.3	85.2
P16CIR	20	33.5	20.7	0.0	62.7	P16CIR	20	39.1	22.8	6.7	83.0
	140	58 337 141 trials					140	53 762 743 trials			

Table 19. Statistics of best cases in hit-rate (%) by image sets (Table 8). Birch plot B3. Ten model trees. An asterisk marks the overall best case and N is the number of image set × model tree combinations.

Image Set	N	Plot B3 (thinned in 1992) Mean	s	Min	Max
LNAD	10	98.7	3.6	88.7	100.0*
12CIR	10	94.5	12.9	58.5	100.0
MNAD	10	94.5	10.1	69.8	100.0
612CIR	20	93.6	15.8	43.4	100.0
616CIR	20	93.5	9.5	71.7	100.0
16CIR	10	90.8	15.5	49.1	100.0
6COL	10	87.9	11.6	66.0	100.0
6CIR	10	81.9	30.2	24.5	100.0
WNAD	10	79.6	26.2	17.0	100.0
P12CIR	20	78.0	25.4	15.1	100.0
P6CIR	20	71.8	27.8	11.3	100.0
P16CIR	20	64.3	30.2	9.4	98.1
Total	170	80 757 188 trials			

parison to sets LNAD and MNAD. CIR images in scale 1:6000 were better than colour images on plots B1 and B2. On plot B3, reverse order was observed. The effect of scale shows in the inner order of sets {612CIR, 616CIR}, {P6CIR, P12CIR, P16CIR} and {12CIR, 16CIR}. However, this is not only due the effect of scale since the sets 12CIR have six images with 70% forward overlap. In addition, sets 6CIR with images in scale 1:6000 produced on average lower hit rates than sets 12CIR and 16CIR. The observed effect of scale was therefore not consistent. The hit-rates for image pairs were considerably lower than for sets with four or more images. Sets P12CIR and P16CIR on plot B1 and set P16CIR on plot B2 produced clearly lower hit-rates. No likely reasons for this could be found. (Table 18, Table 19).

It seems also that in the case of pure birch stands, in which quite little variation in tree height occurs, the density of the stands plays only a minor role. The mean of best cases for the ten model trees produced by image set LNAD on the dense unmanaged plot B2 was 93.5%. This is more than in the best case for the neighbouring thinned plot B1. Plot B3 is on flat terrain, and the spacing of trees is quite even. In such conditions, the 3D tree top positioning gave high best-case hit-rates. (Table 18, Table 19).

Recently thinned, young pine-spruce stands PS1 and PS2

The maximum observed hit-rate for plot PS1 was 89.5% corresponding to a 95.5% hit-rate in volume. Image set LNAD, which consists of low nadir-angle images, produced the best average results in hit-rate, 83.2%. As expected, the set WNAD was inferior to sets MNAD and LNAD. The effects of scale and image number were unexpected. Image set 12CIR with six images in scale 1:12000 produced slightly higher hit-rates than scale-combination sets 612CIR and 616CIR. In addition, set 16CIR produced higher hit-rates than set 6CIR, and image pair set P6CIR was inferior to sets P12CIR and P16CIR. CIR images surpassed colour images also on plot PS1. (Table 20).

One model tree in plot PS1 was a 17.2-metre high birch. It produced the overall best case of 89.5% in set LNAD and the best case in four other sets with a mean hit-rate of 71.6%. The other best cases were obtained by using pines as model trees (mean hit-rate 67.7%) and the three tested spruce model trees with heights 13.8, 15.0, and 16.3 metres, produced an average best-case hit-rate of 59.9%.

On plot PS2, the maximum hit-rates were observed for the scale-combination set 612CIR. The best observed hit-rate was 93.5% corresponding to 92.6% in volume. This means that large trees were missed and a larger portion of the

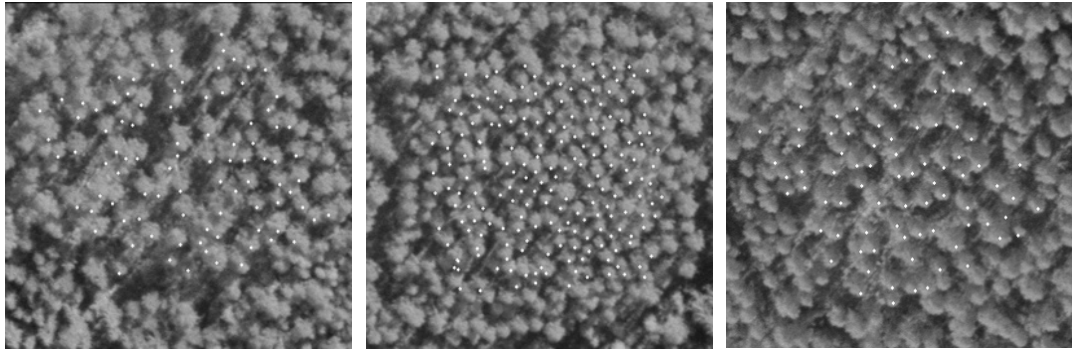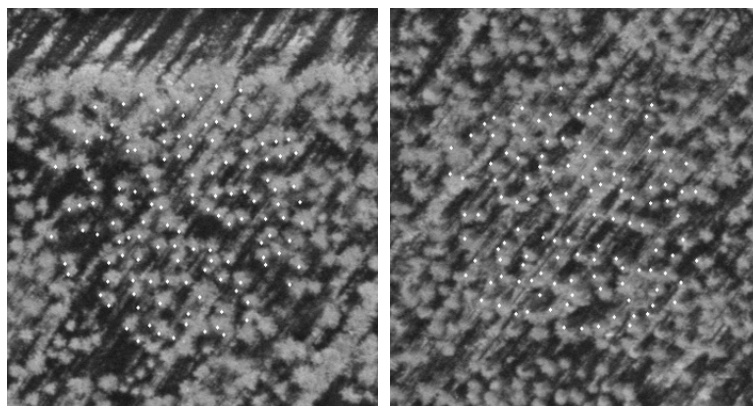**Fig. 31.** Plots PS1 and PS2 in the aerial images 22054600 and 22054608 with tree tops of discernible trees. Scale 1:12000, nadir angles 8 and 6 degrees.

Table 20. Statistics of best case in hit-rate (%) by image sets (Table 8). Plots PS1 and PS2. Ten model trees. An asterisk marks the overall best case and N is the number of image set × model tree combinations.

		Plot PS1						Plot PS2			
Image Set	N	Mean	s	Min	Max	Image Set	N	Mean	s	Min	Max
LNAD	10	83.2	4.0	77.9	89.5*	612CIR #	10	84.6	9.4	64.1	93.5*
MNAD	10	81.7	3.9	74.7	86.3	616CIR #	10	73.6	17.0	43.5	90.2
12CIR	10	80.6	4.7	71.6	86.3	MNAD #	10	69.2	20.4	39.1	91.3
612CIR	20	79.8	5.4	67.4	88.4	12CIR	10	62.9	23.9	17.4	84.8
616CIR	20	76.3	4.3	67.4	84.2	LNAD #	10	61.6	27.1	19.6	91.3
16CIR	10	75.5	7.9	55.8	82.1	WNAD #	10	57.7	16.6	19.6	81.5
6CIR	10	70.6	9.9	49.5	79.0	P6CIR #	10	52.9	14.5	32.6	73.9
WNAD	10	65.8	16.6	20.0	76.8	16CIR	10	46.4	22.3	13.0	68.5
P12CIR	20	55.2	18.6	20.0	83.2	6COL #	10	40.4	21.8	4.4	72.8
6COL	10	49.2	9.6	28.4	61.1	P12CIR	20	39.8	20.0	9.8	77.2
P16CIR	20	47.6	14.7	11.6	65.3	P16CIR	20	25.2	13.6	5.4	51.1
P6CIR	20	44.6	18.3	12.6	71.6	–	–	–	–	–	–
	170		92 216 321 trials				130		69 447 029 trials		
						# Plot PS2 is covered by only one strip in scale 1:6000					

small trees hit. The expected effect of scale was observed in the inner order of sets {612CIR, 616CIR}, {12CIR, 16CIR}, and {P6CIR, P12CIR, P16CIR}. Images in small scale produced lowest average best-case hit-rates. Comparison of CIR and colour images could not be made since full sets 6COL and 6CIR could not be formed due to deficits in image material. (Table 20).

There were three spruce model trees in plot PS2. The best case in five image sets was obtained with a 17.6-metre high spruce tree. The mean best case hit-rates for spruce and pine were 49.6 and 53.3%, respectively.

Mature, planted spruce stand MaS1

Plot MaS1 is a managed stand, in which trees were planted in rows in 1932 (Fig. 32). The rows still show in the spatial pattern although a large number of the planted trees have been removed in intermediate fellings. Height variation of trees on plot MaS1 is quite moderate. One co-dominant model tree, which had close and higher neighbouring trees, produced poor hit-rates in all sets. This model tree, when later checked, was barely discernible in the images. If it were rejected, the mean best-case hit-rate for the set 612CIR would be 98% with a minimum of 88%. For the set LNAD, corresponding values would be 98.3 and 95.4%. It should be noted that the set

Table 21. Statistics of best cases in hit-rate (%) by image sets (Table 8). Plot MaS1. An asterisk marks the overall best case and N is the number of image set × model tree combinations.

Image Set	N	Mean	s	Min	Max
612CIR #	10	90.9	22.5	27.7	100.0
LNAD #	10	89.5	27.7	10.8	100.0
MNAD #	10	89.1	27.0	12.3	100.0
616CIR #	10	86.6	28.0	7.7	100.0
16CIR	10	84.8	29.6	1.5	100.0
WNAD #	10	83.2	23.4	20.0	100.0
P12CIR #	20	78.9	29.0	6.2	100.0
P16CIR	20	58.7	34.9	0.0	96.9
P6 #	10	51.4	21.2	15.4	76.9
6COL #	10	45.7	17.0	16.9	67.7
Total	120		52 183 383 trials		

Plot MaS1 is covered by one strip of 1:6000 and 1:12000 images. Set 6COL consists of 3 images.

612CIR consists of two images in scale 1:6000 and two in 1:12000 since only one strip covers the plot extent in both scales. Similarly, the sets LNAD, MNAD, and WNAD have four, five, and five images respectively. Images in scale 1:6000 view the stand at oblique angles. This in its part explains why the results for image pairs in scale 1:6000 are inferior to pairs in the smaller scales. The effect of nadir angle is seen in the hit-rates of sets LNAD, MNAD, and WNAD. Set WNAD,
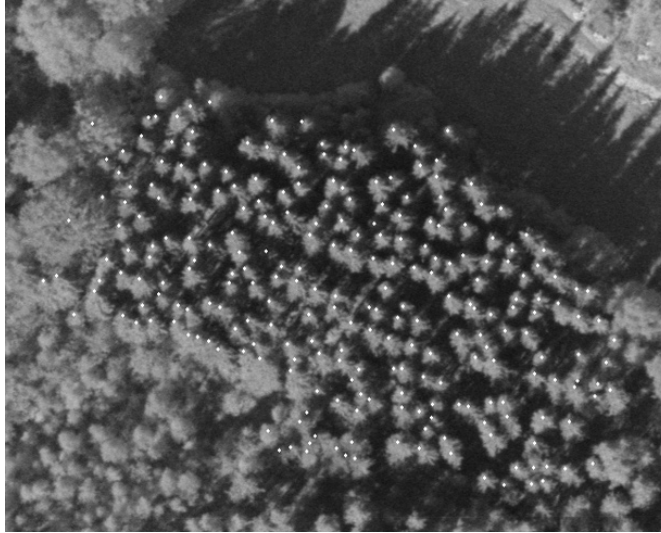
Fig. 32. Plot MaS1 in the aerial image 22054608 with tree tops of discern-
ible trees. Scale 1:12000, nadir angle 10 degrees, 110 × 88 metres.

with images of large nadir angle, produced lowest
hit-rates. A hit-rate of 100% was achieved in
fourteen model tree × image set-combinations.
It seems that the positioning algorithm performs
reasonably well even with a small number of
images in a stand such as MaS1. (Table 21).

3.2.2 Sensitivity to Changes in Parameters

Best-case results were analysed for their sen-
sitivity to changes in the parameters. This was
assumed to give an idea of the robustness of the
3D tree top positioning method, and the analysis
demonstrates the functioning and behaviour of
the algorithm. The best case from plot S6 was
selected for the analysis. The best case in hit-rate,
98.4% was obtained with tree 88 as the model
tree. One parameter at a time was allowed to
take values around its best-case optimum (Table
22) while the other parameter values were kept
constant.

RGB to greyscale transformation

In the performance tests, the templates and aerial
images were transformed into one-channel images

Table 22. The parameter values used in the sensitivity
tests for plot S6 and image set 612CIR. Optimal
values for model tree 88.

Parameter	Value at optimum
Model tree	88
dX	0.3 m
dY	0.3 m
dZ	–0.5 m
EllipseWidth	2.4 m
EllipseHeight	3.15 m
EllipseShift	–1.5 m
SpaceDepth	10 m
SpaceAsymmetry	0 m
GridDensity	0.5 m
Rlimit	0.34
XYthin	1.7 m

by calculating the average of RGB-values for each
pixel. By keeping all other parameters constant
(Table 22), and by using the red channel only
for template matching, the hit-rate changed from
98.4 to 94.5%. At the same time, RMSE of Z
changed from 0.81 to 0.79 metres indicating a
minor improvement in Z-accuracy. In this single
case, the two transformations produced compa-
rable results.

Table 23. Performance of the 3D tree top positioning algorithm between eleven model trees of plot S6. Optimal set of parameter values for tree 88. Image set 612CIR.

Tree No	Height photogr./ DEM, m	Height field, m	C_W photo,m	Hit-rate, %	Comm. error rate, %	Mean ΔX, m	Mean ΔY, m	RMSE (XY), m	Mean ΔZ, m	RMSE (Z), m
164	21.1	21.3	3.0	50.4	38.6	0.28	–0.14	0.72	0.09	1.19
173	20.7	20.6	2.6	81.9	33.9	–0.09	–0.57	0.82	–0.81	1.20
149	19.8	19.5	3.9	82.7	11.0	–0.02	–0.10	0.58	0.32	0.82
248	19.4	19.2	2.9	89.8	18.9	0.09	–0.13	0.63	–0.47	0.96
181	18.6	18.9	2.7	87.4	14.2	–0.29	–0.26	0.72	–0.33	0.86
8	18.2	18.5	3.1	92.1	17.3	0.27	0.03	0.65	–0.31	0.91
236	18.0	17.8	2.9	82.7	12.6	–0.04	–0.16	0.65	–0.14	0.85
156	17.7	17.4	2.8	93.7	10.2	0.07	–0.16	0.59	–0.25	0.65
*88	17.4	18.0	2.6	98.4	3.1	–0.10	–0.15	0.59	0.12	0.81
193	17.4	17.1	2.0	81.1	26.0	0.16	0.47	0.77	0.58	1.10
162	16.8	16.6	1.2	79.5	30.7	–0.22	–0.31	0.73	0.90	1.23

Table 24. Characteristics of model trees, optimal parameter values, and best cases of performance of 3D tree top positioning algorithm for the eleven model trees of plot S6. Image set 612CIR.

Tree No	Height in field, m	C_W photo, m	EW, m	ES, m	EH, m	SD, m	SA, m	Rlimit, ρ3D	XYthin, m	Hit-rate, %	Comm. error rate, %
164	21.3	3.0	2.4	–1.50	2.40	10	–3	0.40	2.0	85.0	4.7
173	20.6	2.6	2.7	–0.75	2.40	7	–3	0.34	1.8	95.3	4.7
149	19.5	3.9	2.7	–1.50	2.40	6	–3	0.34	1.4	95.3	3.1
248	19.2	2.9	2.4	0.00	3.15	9	–1.5	0.40	1.6	98.4	4.7
181	18.9	2.7	2.4	–1.50	3.15	7	–1.5	0.32	1.8	97.6	4.7
8	18.5	3.1	2.4	–0.75	3.15	9	–1.5	0.36	1.8	98.4	4.7
88	18.0	2.9	2.4	–1.50	3.15	10	0	0.34	1.7	98.4	3.1
236	17.8	2.8	2.7	–1.50	2.40	8	–1.5	0.32	1.8	98.4	3.9
156	17.4	2.6	2.4	–0.75	2.40	7	–1.5	0.40	1.4	97.6	4.7
193	17.1	2.0	2.4	–0.75	2.40	7	1.5	0.34	2.0	89.8	3.9
162	16.6	1.2	2.4	–0.75	2.40	10	0	0.38	1.6	96.1	4.7

Model tree selection

Table 23 gives the results of a test in which different model trees were used for 3D tree top positioning with the optimal parameter set of tree 88 (Table 22). Exceptions were the shift parameters *dX*, *dY,* and *dZ* which were set to zero value, i.e. the original photogrammetric positions obtained by manual image-matching were used. The results imply that the parameters are strongly dependent on the properties of the model tree. These properties possibly include relative height, crown width, and local neighbourhood, all factors which have an effect on how the tree is seen in an aerial image. For example, tree 162 is an intermediate tree, which had only the very top of the tree visible in the images. This model tree

produced poor results with the optimal parameter combination of tree 88. Tree 88 is a co-dominant (locally dominant) tree, which is clearly visibly in the images and does not have nearby neighbour-trees to cause crown overlap in the images of the set 612CIR. The crown patch of tree 162 in the images is relatively small, and the values for parameters *EllipseHeight* and *EllipseShift* at 3.15 and –1.5 metres, are likely too large. The optimal values for tree 162 were 2.4 and –0.75 m, and with these it produced a 96.1% best case hit-rate (Table 24).

To further clarify the role of the model tree, the best cases for plot S6 obtained with image sets 612CIR were analysed (Table 24). The tallest, 21.3-metre high model tree number 164 produced the lowest best-case hit-rate. It is possible that

Table 25. Performance of 3D tree top positioning algorithm for different vertical positions of model tree top. Plot S6, model tree 88, and image set 612CIR.

dZ, m	Hit-rate, %	Comm. error rate, %	Mean ΔX, m	Mean ΔY, m	RMSE (XY), m	Mean ΔZ, m	RMSE (Z), m
–0.5	94.5	5.5	–0.05	–0.24	0.63	0.61	1.08
–0.4	95.3	5.5	–0.06	–0.22	0.62	0.43	1.01
–0.3	96.1	3.9	–0.08	–0.22	0.62	0.35	0.97
–0.2	95.3	3.9	–0.05	–0.18	0.6	0.35	0.87
–0.1	95.3	4.7	–0.07	–0.17	0.6	0.38	0.9
0	98.4	3.1	–0.1	–0.15	0.59	0.12	0.81
0.1	96.1	3.1	–0.09	–0.21	0.62	0.04	0.85
0.2	96.9	3.9	–0.02	–0.19	0.6	–0.09	0.77
0.3	97.6	3.9	–0.02	–0.18	0.6	–0.09	0.75
0.4	95.3	6.3	–0.06	–0.18	0.6	–0.2	0.72
0.5	94.5	10.2	–0.08	–0.19	0.6	–0.24	0.69

the range in parameter *SpaceAsymmetry* was too narrow in the multidimensional grid, which was used in performance testing. The mean height of discernible trees on plot S6 is 16.9 metres. The maximum shift downwards (*SpaceAsymmetry*) was –3 metres, which centres the search space vertically at 18.3 metres above ground. Perhaps with a larger negative value for the parameter *SpaceAsymmetry* an even better best case would have been found for tree 164. (In a separate test, an improved hit-rate of 86.6% was obtained for *SpaceAsymmetry* at –5 metres). Highest best case hit-rates were obtained for mean-sized trees 156, 236, 88, 8, 181, and 248. This is possibly due to the inability of template matching to take into account size variation. Mean-sized model trees therefore performed the best. It is also possible that deficits in the multidimensional grid of parameters (Table 9, p. 43) are the cause for this effect. (Table 24).

Error in model tree top position

The Z-coordinate for the model tree top was allowed to vary in Z-direction by ± 0.5 metres. A new, better hit-rate maximum was not found. Hit-rates varied from 94.5% to 98.4% and the commission error-rate from 3.1% to 10.2%. The commission error-rate was at its minimum when the tree top was not shifted. Lowest RMSE in Z was obtained for the maximum commission error-rate. No likely reason for this was found. Mean ΔZ varied from 0.61 metres to –0.24 metres, a total

of 0.85 metres, as the position of the model tree top changed a metre. This implies that the error of the manual photogrammetric measurement of the model tree will be reflected in the positionings produced by the algorithm. It is close to a one-to-one relationship in terms of Z-accuracy. A biased positioning of the model tree top will cause bias in the candidate positions. This sets demands on the quality of the images and the manual model tree measurement. (Table 25).

Ellipse size and position

The best case in hit-rate occurred with value 2.4 metres for parameter *EllipseWidth* (Table 26). In the performance tests, the interval for the parameter *EllipseWidth* was from 2.0 to 3.0 metres in plot S6. As the parameter value was changed from one to four metres, all performance measures in Table 26 show changes. For values larger than two metres, the commission error rate is below 6.3%, and positions are accurate in terms of mean differences and RMS errors.

Parameter *EllipseShift* is used to center the template in the direction of radial displacement. This corresponds to the direction of the Z-axis. A negative value means that the template is centred below the tree top and thus captures more of the crown in the image. The actual effect (shift in pixels) on the image is determined by the amount of radial displacement, which is determined by nadir angle. For near-nadir views, the parameter has almost no effect, and the template image

Table 26. Performance of 3D tree top positioning algorithm for different values of parameter EllipseWidth. Plot S6, model tree 88 and image set 612CIR.

EW, m	Hit-rate, %	Comm. error rate, %	Mean ΔX, m	Mean ΔY, m	RMSE (XY), m	Mean ΔZ, m	RMSE (Z), m
1	96.1	25.2	0.01	–0.35	0.71	0.73	1.26
1.2	94.5	24.4	–0.05	–0.33	0.70	0.70	1.16
1.4	92.9	22.8	0.00	–0.31	0.66	0.66	1.10
1.6	93.7	16.5	–0.03	–0.27	0.64	0.56	0.96
1.8	95.3	12.6	–0.05	–0.24	0.63	0.45	0.95
2	96.9	5.5	–0.09	–0.20	0.60	0.27	0.83
2.2	97.6	6.3	–0.10	–0.18	0.60	0.22	0.80
*2.4	98.4	3.1	–0.10	–0.15	0.59	0.12	0.81
2.6	94.5	4.7	–0.10	–0.11	0.59	0.13	0.81
2.8	92.9	3.9	–0.10	–0.08	0.59	0.18	0.82
3	92.9	3.9	–0.11	–0.08	0.60	0.22	0.87
3.2	89.8	3.1	–0.11	–0.05	0.60	0.27	0.89
3.4	89.0	3.9	–0.11	–0.04	0.61	0.29	0.91
3.6	85.8	2.4	–0.10	–0.03	0.60	0.28	0.95
3.8	81.1	2.4	–0.09	–0.01	0.60	0.33	0.94
4	77.2	1.6	–0.11	–0.01	0.60	0.38	1.02

Table 27. Performance of 3D tree top positioning algorithm for different values of parameter EllipseShift. Plot S6, model tree 88, and image set 612CIR.

ES, m	Hit-rate, %	Comm. error rate, %	Mean ΔX, m	Mean ΔY, m	RMSE (XY), m	Mean ΔZ, m	RMSE (Z), m
0.50	86.6	9.4	–0.05	–0.16	0.66	0.40	0.97
0.25	91.3	11.0	0.00	–0.17	0.65	0.52	0.98
0.00	91.3	11.8	0.00	–0.15	0.62	0.61	1.00
–0.25	92.1	5.5	–0.12	–0.23	0.65	0.58	1.07
–0.50	93.7	11.8	–0.02	–0.10	0.59	0.51	0.89
–0.75	97.6	7.9	–0.01	–0.17	0.60	0.20	0.74
–1.00	94.5	6.3	–0.08	–0.22	0.61	0.06	0.70
–1.25	97.6	5.5	0.01	–0.20	0.60	0.02	0.77
*–1.50	98.4	3.1	–0.10	–0.15	0.59	0.12	0.81
–1.75	94.5	3.1	–0.13	–0.23	0.63	0.21	0.81
–2.00	95.3	4.7	–0.05	–0.27	0.64	–0.11	0.84
–2.25	96.1	3.9	0.01	–0.26	0.64	–0.05	0.92
–2.50	93.7	9.4	–0.03	–0.28	0.66	–0.10	1.02

is centred on the tree top. In the optimum, the value for *EllipseShift* was –1.5 metres (Table 27). In the sensitivity tests, the parameter had a significant effect on the accuracy of Z. Parameter values below –0.75 metres resulted in low bias, but values between –0.5 and 0.5 metres resulted in large positive bias in Z. These findings are in line with those of Larsen (1998) who observed that the elliptic (synthetic) templates should be centred below the tree top for optimal results in template matching.

The best-case hit-rate was produced with the *EllipseHeight* value at 3.2 metres (Table 28). Low values for the parameter *EllipseHeight* caused bias in Z. This is explained by the parameter value for *EllipseShift* which was set at value –1.5 metres. For low values of *EllipseHeight*, the templates are circular in shape, and positioned such that in oblique views they no longer capture the tree top but instead the crown below the top. The maxima in the cross-correlation images are shifted down the crown. Thus, the candidate positions are shifted down. This resulted in the observed positive bias of Z. (Table 28).

Table 28. Performance of 3D tree top positioning algorithm for different values of parameter EllipseHeight. Plot S6, model tree 88, and image set 612CIR.

EH, m	Hit-rate, %	Comm. error rate, %	Mean ΔX, m	Mean ΔY, m	RMSE (XY), m	Mean ΔZ, m	RMSE (Z), m
2	96.9	7.9	–0.09	–0.14	0.62	0.59	1.09
2.4	96.9	7.1	–0.09	–0.16	0.61	0.46	1.02
2.8	96.9	3.9	–0.1	–0.15	0.60	0.26	0.88
*3.2	98.4	3.1	–0.1	–0.14	0.59	0.12	0.81
3.6	94.5	3.1	–0.1	–0.15	0.60	0.02	0.75
4	92.9	3.9	–0.08	–0.12	0.59	–0.05	0.74
4.4	89.0	3.9	–0.11	–0.11	0.60	–0.06	0.71
4.8	85.8	3.1	–0.12	–0.1	0.60	–0.07	0.72

Table 29. Performance of 3D tree top positioning algorithm for different values of parameter SpaceDepth. Plot S6, model tree 88, and image set 612CIR. The values of "Max hit-rate" indicate the maximum attainable hit-rate given the depth of the search space (SD), and the height of the hit cylinder, 6 metres.

SD, m	Hit-rate, %	Max hit-rate, %	Comm. error rate, %	Mean ΔX, m	Mean ΔY, m	RMSE (XY), m	Mean ΔZ, m	RMSE (Z), m	Trend in ΔZ×h, m/m
1	75.6	81.5	2.4	–0.09	–0.16	0.63	–0.08	1.25	0.87
2	81.1	85.6	2.4	–0.08	–0.13	0.62	0.04	1.18	0.74
3	85.8	90.8	1.6	–0.09	–0.14	0.61	0.10	1.04	0.60
4	89.8	93.8	0.0	–0.11	–0.14	0.61	0.15	0.94	0.46
5	91.3	94.9	0.0	–0.10	–0.13	0.60	0.13	0.87	0.38
6	93.7	99.0	1.6	–0.09	–0.13	0.59	0.11	0.82	0.29
7	96.1	99.5	2.4	–0.10	–0.14	0.59	0.11	0.80	0.24
8	97.6	100.0	2.4	–0.10	–0.14	0.59	0.10	0.81	0.21
9	97.6	100.0	2.4	–0.10	–0.14	0.59	0.11	0.80	0.18
*10	98.4	100.0	3.1	–0.10	–0.15	0.59	0.12	0.81	0.17
11	97.6	100.0	5.5	–0.10	–0.15	0.59	0.12	0.86	0.17
12	97.6	100.0	7.9	–0.10	–0.13	0.59	0.09	0.86	0.16
13	98.4	100.0	7.1	–0.10	–0.13	0.60	0.08	0.89	0.15
14	96.9	100.0	11.0	–0.10	–0.14	0.60	0.13	0.84	0.14

Search space depth and vertical position

In the optimum, the depth of the search space was 10 metres, and it was centred vertically at the height of the top of the model tree 88. This is indicated by the value of the parameter *SpaceAsymmetry* at the optimum, which was zero (Table 30). The depth of the search space had an effect on the Z-accuracy (Table 29). A low search space resulted in an averaging effect. This can be observed in the trend coefficient (*b*) of the regression model $\Delta Z = a + b \times h$. For example, at a parameter value of 10 metres, the coefficient is 0.17. For a four-metre deep search space, the coefficient increases to 0.46 m/m. Also, the RMSE of Z increases as the search space is lowered. This is a result of the averaging effect. When the search space is too deep, the commission error rate increases (cf. Fig. 8, p. 30, Fig. 14, p. 35). The first false tree tops appear at the lower and upper parts of the search space where epipolar lines of neighbouring trees intersect and produce clusters. The commission error rate was zero in a search space depth of between four and five metres, but at the expense of reduced hit-rate and accuracy of Z. This is also explained by the geometry: The search space is centred vertically at the correct position, and the 6-metre high hit-cylinders still allow hits from above and below. For a one to three-metre deep search space, some of the shortest and tallest trees start to produce commission errors. The model tree's height (18.0 m) is close to the mean of the discernible trees and therefore the mean difference in Z was not affected by the changes in the depth of the search space. (Table 29).

Table 30. Performance of 3D tree top positioning algorithm for different values of parameter SpaceAsymmetry. Plot S6, model tree 88, and image set 612CIR. The values of "Max hit-rate" indicate the maximum attainable hit-rate given the depth of the search space (SD), and the height of the hit cylinder, 6 metres.

SA, m	Hit-rate, %	Max hit-rate, %	Comm. error rate, %	Mean ΔX, m	Mean ΔY, m	RMSE (XY), m	Mean ΔZ, m	RMSE (Z), m	Trend in ΔZ×h, m/m
–4	90.6	97.9	13.4	–0.12	–0.13	0.63	0.68	1.18	0.32
–3	96.9	99.5	5.5	–0.13	–0.14	0.62	0.49	1.03	0.26
–2	97.6	100.0	4.7	–0.11	–0.14	0.61	0.30	0.86	0.18
–1	98.4	100.0	3.1	–0.10	–0.14	0.60	0.18	0.79	0.14
*0	98.4	100.0	3.1	–0.10	–0.15	0.59	0.12	0.81	0.17
1	96.9	100.0	5.5	–0.10	–0.14	0.59	0.00	0.88	0.22
2	91.3	99.0	8.7	–0.09	–0.14	0.59	–0.01	0.77	0.22
3	89.0	94.4	8.7	–0.08	–0.14	0.59	–0.16	0.81	0.27
4	85.0	87.7	10.2	–0.06	–0.14	0.59	–0.44	1.00	0.39

Table 31. Performance of 3D tree top positioning algorithm for different values of parameter GridDensity. Plot S6, model tree 88, and image set 612CIR.

GD, m	Hit-rate, %	Comm. error rate, %	Mean ΔX, m	Mean ΔY, m	RMSE (XY), m	Mean ΔZ, m	RMSE (Z), m
0.33	97.6	2.4	–0.11	–0.14	0.59	0.14	0.81
*0.5	98.4	2.4	–0.10	–0.15	0.59	0.12	0.81
0.67	92.1	2.4	–0.14	–0.15	0.63	0.16	0.89
0.83	86.6	3.1	–0.12	–0.15	0.66	0.13	0.88

The parameter *SpaceAsymmetry* adjusts the vertical position of the search space with respect to the model tree top's Z-value. If the model tree represents the mean height of trees, a value set at zero should produce best results. The arithmetic mean height of trees in plot S6 was 16.8 metres, and the field-measured height of tree 88 was 18.0 metres. It can be seen that a one-meter shift downward still produced a hit-rate of 98.4% (Table 30). Similarly, a one-metre shift upward caused a reduction in the hit-rate and an increase in the commission error rate. The tallest tree on plot S6 is 22.7 metres high. However, 86% of the discernible trees have a height between 13 and 21 metres. A ten-metre deep search space centred at 17 metres above the ground fills this space better than a space of equal depth a metre above. It can also be seen that a wrongly centred search space causes bias in Z-estimation. On average, a metre's change in the shift (*SpaceAsymmetry*) resulted in a 0.12-metre change in the mean of Z-differences. The parameter *SpaceAsymmetry* had an effect on the commission error rate, and the averaging in Z, both of which were minimised for the correct

vertical position of the search space. The correct position was interpreted here to correspond to the mean height of discernible trees.

Search space grid density

The parameter *GridDensity* defines the density of points in the search space. These points are clustered for tree top candidate locations. Since the search space is three-dimensional, *GridDensity* greatly affects the run-times. For the computation of ρ3D, each point requires the use of collinear equations and fiducial mark transformation, which are made up of several floating-point multiplications and divisions. *GridDensity* at a value of 0.33 metres results in 27 points per cubic metre of search space, whereas a spacing of 0.5 metres results in eight points. All points in the search space need to be computed for ρ3D-value and to be sorted and clustered. It is advisable to keep the density of the grid at a minimum. In the sensitivity test, four values of *GridDensity* were tried. At the 0.33-metre value, the optimum hit-

Table 32. Performance of 3D tree top positioning algorithm for different values of parameter XYthin. Plot S6, model tree 88, and image set 612CIR.

XYthin	Hit-rate, %	Comm. error rate, %	Mean ΔX, m	Mean ΔY, m	RMSE (XY), m	Mean ΔZ, m	RMSE (Z), m
1.0	97.6	29.9	−0.11	−0.13	0.58	0.10	0.75
1.2	97.6	13.4	−0.11	−0.14	0.59	0.12	0.80
1.4	98.4	7.1	−0.11	−0.14	0.59	0.07	0.80
1.6	98.4	3.9	−0.11	−0.15	0.59	0.12	0.81
*1.7	98.4	2.4	−0.10	−0.15	0.59	0.12	0.81
1.8	96.1	1.6	−0.11	−0.15	0.60	0.13	0.82
2.0	92.9	0.8	−0.09	−0.15	0.62	0.16	0.83
2.2	89.0	0.8	−0.07	−0.14	0.64	0.17	0.82
2.4	79.5	3.9	−0.09	−0.17	0.68	0.22	0.87
2.6	74.0	3.1	−0.09	−0.18	0.71	0.21	0.87
2.8	67.7	4.7	−0.11	−0.21	0.76	0.21	0.94
3.0	56.7	7.9	−0.06	−0.16	0.80	0.32	1.00

rate was changed only little. *GridDensity* values of 0.67 and 0.83 metres produced higher planimetric errors and lower hit-rates. The value for parameter *XYthin* at the optimum was 1.7 metres. There is likely a co-effect between parameters *GridDensity* and *XYthin*, which makes it difficult to interpret the effects that the changes of *GridDensity* caused. (Table 31).

Parameters controlling the clustering of ρ3D-data

Parameter *XYthin* controls the clustering of volumetric ρ3D-data by setting a minimum planimetric distance between two clusters. In the clustering, a list of points sorted according to ρ3D is searched through, and adjacent points are fused into existing clusters. Points with distances below *XYthin* are merged into existing clusters. This parameter should be set to a value that causes ρ3D values of one tree top to be merged into one and one cluster only. If the value is set too low, the maxima are split and it shows in increase of commission errors. Similarly, if the value is set too large, the number of clusters is reduced, and maxima produced by neighbouring trees are merged into positions somewhere between the trees. This results in a reduction of the hit-rate, an increase of the commission error rate, and an increase in positioning errors. These phenomena are seen in Table 32. Fig. 33 illustrates a correlogram obtained by analysing a near-nadir image
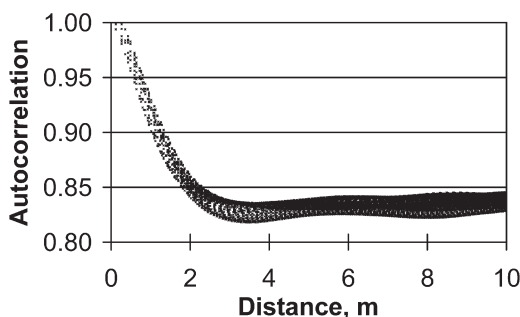

Fig. 33. Correlogram of a near-nadir 1:12000 image of plot S6. Autocorrelation values for lag-distances below 10 metres are included.

of plot S6. The values of *XYthin*, which produced satisfactory results, are located in the lower part of the slope, just before the correlation flattens. In the performance tests, the best cases of plot S6 had an average of 1.9 metres for parameter *XYthin* with a 0.35-metre standard deviation.

Parameter *Rlimit* gives the lower bound for ρ3D. A low value of *Rlimit* results in more clusters, and similarly a high value decreases the number of points from which the clusters are formed, and reduces the number of clusters. *Rlimit* is a parameter used for adjusting the interrelationship of hit-rate and commission error-rate. A low value produces clusters of low quality, i.e. false tree tops with weaker positioning accuracy, but at the same time increases the hit-rate. A balance is found by adjusting the parameter value. *Rlimit* had an effect

67

Table 33. Performance of 3D tree top positioning algorithm for different values of parameter Rlimit. Plot S6, model tree 88, and image set 612CIR.

Rlimit	Hit-rate, %	Comm. error rate, %	Mean ΔX, m	Mean ΔY, m	RMSE (XY), m	Mean ΔZ, m	RMSE (Z), m
0.25	98.4	26.0	–0.09	–0.16	0.64	0.02	1.00
0.27	97.6	18.9	–0.09	–0.16	0.63	0.06	0.94
0.29	98.4	11.8	–0.09	–0.15	0.62	0.08	0.94
0.31	98.4	7.1	–0.10	–0.15	0.61	0.09	0.90
0.33	97.6	6.3	–0.11	–0.15	0.59	0.12	0.80
*0.34	98.4	2.4	–0.10	–0.15	0.59	0.12	0.81
0.35	96.9	3.1	–0.10	–0.14	0.59	0.16	0.78
0.37	92.1	1.6	–0.10	–0.13	0.59	0.18	0.74
0.39	89.8	0.8	–0.11	–0.12	0.58	0.19	0.70
0.41	86.6	0.0	–0.13	–0.12	0.59	0.19	0.71
0.43	80.3	0.0	–0.14	–0.13	0.59	0.24	0.74
0.45	70.1	0.8	–0.15	–0.13	0.56	0.28	0.62
0.47	64.6	0.0	–0.17	–0.13	0.58	0.33	0.59
0.49	59.8	0.0	–0.17	–0.13	0.58	0.39	0.63
0.51	52.8	0.0	–0.19	–0.15	0.59	0.43	0.63
0.55	40.2	0.0	–0.18	–0.16	0.58	0.40	0.58
0.59	21.3	0.0	–0.18	–0.19	0.56	0.39	0.54
0.63	7.1	0.0	–0.11	–0.20	0.56	0.47	0.64
0.67	3.9	0.0	–0.12	–0.17	0.56	0.52	0.56
0.71	1.6	0.0	–0.51	–0.26	0.79	0.76	0.78
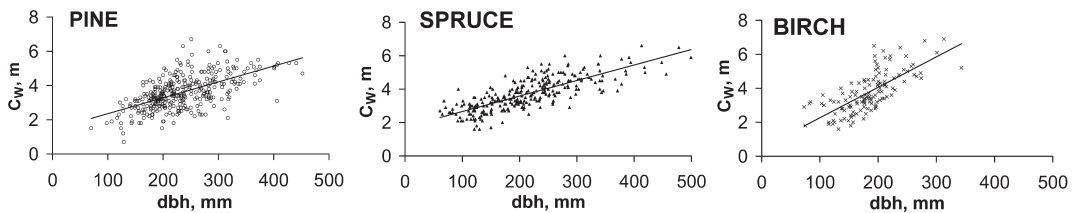
Fig. 34. Field-measured C_W plotted against field-measured dbh.

on the RMS error of XY and Z (Table 33). It also had an impact on ΔZ. For the largest tried values, positive bias was observed. It was interpreted that this was caused by the shape of the maxima on the correlation images of oblique views. These maxima were elongated asymmetrically in the direction of the radial displacement (cf. Fig. 17, p. 38). When the parameter *Rlimit* received a large value, points below the true tree top positions formed the clusters. This resulted in the positive bias of Z.

3.3 Manual Crown Width Measurements

3.3.1 Measurement Accuracy

The data set consisted of 13288 image observations of 715 discernible trees that had their crown width measured in the field (Fig. 34). On average, each tree was observed for photogrammetric crown width from 18.6 images.

The manual photogrammetric measurement of maximum crown width resulted in an underestimation (ΔC_W) of 0.53 metres on average (Table 34). The amount of underestimation was found to be correlated with the crown size (Fig. 35), and it varied between species, film type, and scale

Table 34. Descriptive statistics of crown width measurement data.

Species	N trees	N image obs	Mean C_W field, m	Mean $C_W\perp$ field, m	Mean ΔC_W, m	s ΔC_W, m	Mean relative height
Pine	346	5449	3.55	2.78	0.31	0.80	0.888
Spruce	245	3828	3.70	3.20	0.83	0.75	0.812
Birch	120	2038	3.79	3.12	0.50	0.82	0.910
Other	4	58	3.97	2.85	1.53	1.06	0.614
All	715	11373	3.65	2.99	0.53	0.82	0.864

ΔC_W = Field measured crown width (maximum) – Photo measured crown width, $C_W\perp$ = field measured crown width measured in perpendicular direction to C_W.

Table 35. Differences between field measured and photogrammetric crown widths (ΔC_W) by image scale and tree species.

Scale and Film	ΔC_W, m Pine	Spruce	Birch	Other	All
1:6000 COL	0.37	0.80	0.59	1.69	0.57
1:6000 CIR	0.44	0.88	0.62	1.60	0.64
1:12000 CIR	0.28	0.84	0.46	1.49	0.50
1:16000 CIR	0.22	0.82	0.36	1.32	0.43
All	0.31	0.83	0.50	1.53	0.53

(Table 34, Table 35).

The standard deviation of the differences in crown width was 0.82 metres. If it is assumed that the precision of field measurements is of the same order, the precision (standard error excluding bias) of manual photogrammetric measurements is approximately 0.6 metres.

The average relative height, scaled between zero and one, was 0.864 for the trees with field measured crown width (Table 34). It is natural that for spruce the average relative height is smaller than for the light-demanding pine and birch. On average, the photogrammetric observations underestimated crown widths by 0.53 metres, which corresponds to 14.5% of the mean of the field-measured crown widths, which was 3.65 metres. Observed differences were largest for spruce, 0.83 metres. This is most likely explained by the conical crown shape of spruce. The maximum crown width can occur below the sun-lit part of the crown and is therefore not well seen on the photograph. Crowns in the study material were asymmetric (Table 34), and this asymmetry in width explains partly the underestimation. In the field, the trees were measured for maximum crown diameter, which is required by the allometric models, but on the photographs, the direction
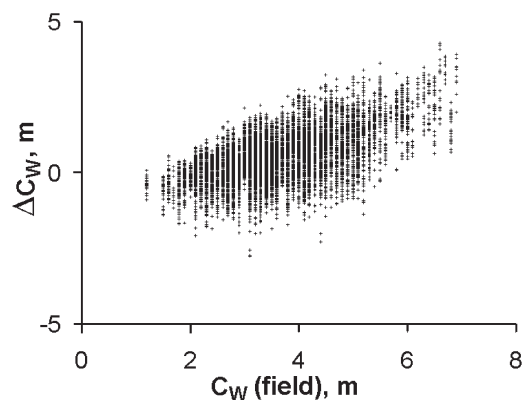
Fig. 35. Differences of photogrammetric and field measured crown widths, ΔC_W plotted against field-measured crown width. N = 11373.

was determined by the viewing geometry.

The underestimation of crown width was lowest for the smallest scales 1:16000 and 1:12000 (Table 35). In 12.2% of the cases, an observation could not be made because the operator was unable to discern the crown edges (Table 36). This proportion was 16.0% in the 1:6000 COL images and 9.8, 11.1, and 12.1% in the CIR images in scales

Table 36. Photogrammetric crown width measurements by observation types.

Observation type / class	N image obs	Mean ΔC_W, m	s ΔC_W, m	Mean relative height
Normal observation	10863	0.50	0.81	0.875
One edge visible, symmetry assumed	143	0.70	0.65	0.826
Unclear edges, observed	47	1.34	0.99	0.842
Tree occluded, only top visible	320	1.32	0.83	0.794
Total, successful crown width observations	11373	0.53	0.81	0.864
Tree occluded, no observation	299	–	–	0.675
Crown edges unclear, no observation	1616	–	–	0.842
Tree falls outside image extent, no observation	104	–	–	0.875
Total, all image observations	13392	–	–	0.864

Table 37. Proportions of successful manual photogrammetric crown width measurements by image scale and tree species.

Film and scale	N image obs	Succesful C_W photo measurements by species, %				
		Pine	Spruce	Birch	Other	All
1:6000 COL	2357	83.4	79.1	80.4	71.4	81.1
1:6000 CIR	2361	89.9	84.0	91.3	83.3	88.0
1:12000 CIR	3563	90.0	81.2	88.9	68.0	86.5
1:16000 CIR	3092	86.8	83.9	89.7	64.7	86.3
All	11373	87.7	81.9	87.9	71.6	85.6

1:6000, 1:12000, and 1:16000 respectively (data not shown). In small-scale images, the contrast is low due to the increase of the scattering and absorption of light. Also, the resolution is lower. Details that appear sharp in large-scale images become unclear as the scale decreases. A blurred crown edge in the image is possibly observed at a wrong position. Other possible causes for the unexpected effect of scale are the subjectivity of measurements and the failings in the experiment.

3.3.2 Measurability

The type of observation, a class, which reflects the ease of measurement and explains as to why an observation could not be made, was connected with the quality of the crown width observation and the relative height of the tree. The amount of underestimation in crown width was lowest, 0.50 metres, in the observations, which were classified as normal. In these cases, the operator could detect the crown edges without difficulties. For the other cases in which the measurement was

done, with uncertainty, the amount of underestimation was higher, from 0.70 to 1.34 metres. The mean relative height of trees was lowest in the class: Tree occluded, no observation. It seems therefore that the operator could interpret the images in 3D although all observations were made monoscopically. (Table 36).

The operator could make more crown width observations by using the CIR images than by using colour images (Table 37). The differences in measurability between species are probably explained in part by the differences in relative height. Spruce trees had on average lower relative heights and the probability for occlusion and shading is higher for the suppressed trees as shown in the discernibility tests. The contrast of crowns of different species on the photograph can also have an effect on the measurability. The overall effect of scale in the measurability of crown width is not significant. For CIR images in the scale of 1:6000, 88.0% of the tried measurements could be carried out. Correspondingly a measurability of 86.5% and 86.3% was achieved for the scales 1:12000 and 1:16000. It is plausible to assume that the measurability of crown width

Table 38. Proportions of observation types of photogrammetric crown width measurement by image-object-sun geometry classes. NN = near-nadir, ON = off-nadir, B = back-lighted, S = side-lighted, F = front-lighted.

| Observation type / class | Proportions, % | | | | | | |
| | Image-object-sun geometry class | | | | | | |
	NN-B	NN-S	NN-F	ON-B	ON-S	ON-F	All
Normal observation	91.9	88.5	91.1	77.6	73.3	83.9	81.8
One edge visible, symmetry assumed	0.6	0.5	0.4	1.8	1.8	0.4	1.1
Unclear edges, observed	0.1	0.3	0.2	0.5	0.5	0.2	0.4
Tree occluded, only top visible	1.0	1.0	0.9	5.8	2.9	1.5	2.4
Sub-total observed C_W	93.7	90.2	92.6	85.7	78.5	86.0	85.6
Tree occluded, no observation	0.6	1.0	1.4	3.9	3.5	1.0	2.3
Crown edges unclear, no observation	5.7	8.7	6.0	10.5	18.1	13.0	12.2
Total, %	100.0	100.0	100.0	100.0	100.0	100.0	100.0
Total, N	931	2294	1479	2086	4170	2328	13288
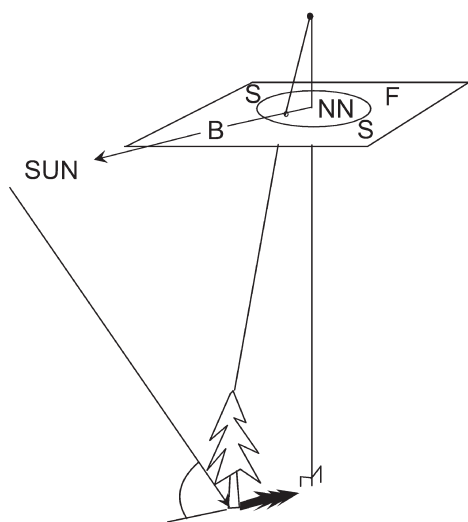
Fig. 36. Division of the photo-area in six classes of image-object-sun geometry. Near-nadir (NN) cases are inside the depicted circle and off-nadir (ON) fall outside. 90-degree wide back-lighted sector (B) is on both sides of the sun-vector, which is the projection of the sunray on the film plane. Front-lighted sector (F) is on the opposite side. Between these are the front-side and back-side lighted sectors (S) combined as one.

is related to the discernibility of a tree. Thereby, the results of Table 37 imply that more or less the same trees are discernible independent of the used scale of the CIR images.

In analysing the effect of image-object-sun geometry, the observations were classified accord-ing to nadir angle, tree-to-camera azimuth angle, and sun azimuth angles into six (two by three) classes (Fig. 3, p. 17, Fig. 36). Cases in which the nadir angle was below 25 degrees were put in class near-nadir and the remaining into class off-nadir. In addition, the photograph was divided in three sectors representing the back-, side-, and front-lighted cases. The side-lighted sector is 180 degrees wide, thus representing 50% of the image area. 48.6% of the observations were from this sector.

The proportion of unsuccessful photogram-metric C_W-measurements was highest in the two side-lighted classes ON-S and NN-S. Cases in which the tree is viewed either back-lighted or front-lighted did not differ much from each other, and were superior to the side-lighted views in both near-nadir and off-nadir views. The proportion of successful measurements was lower in off-nadir views than in near-nadir views. This is related to occlusion, since in oblique views of stands with variation in height, occlusion is present. (Table 38).

Logistic regression analysis was used to illus-trate the effect of nadir angle and the relative height on the measurability of crown width (Fig. 37). The results indicated that the probability of successful manual C_W measurement is dependent on both of these variables. Near-nadir views were better for the measurement of crown width, and the probability of measurability correlated with the relative height.
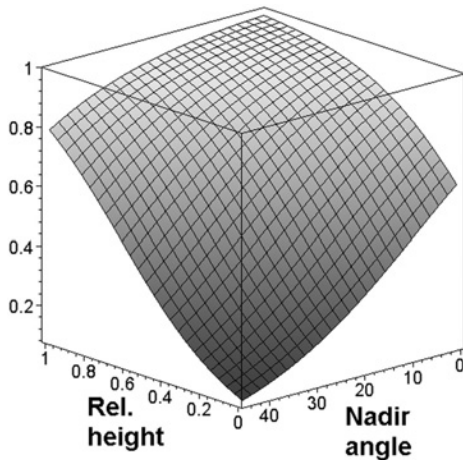
Fig. 37. Probability for successful photogrammetric crown width measurement as a function of relative height and nadir angle. Logistic regression, deviance = 10217.5, degrees of freedom = 13285, and P-value = 1.0.
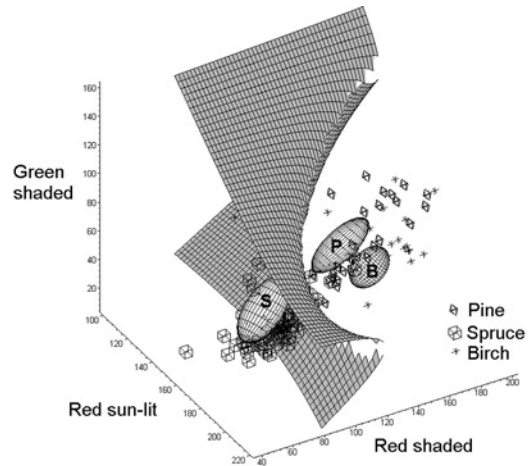

Fig. 38. Species classifications of plot MaPS2. Test set data consisting of 156 observations is plotted in the 3D-feature space. Ellipsoids represent variation in the training set data. The quadratic Bayesian decision surface between pine and spruce is drawn. It has a rupture due to inaccuracies in the plotting software.

3.4 Tree Species Classification with Simultaneous Use of Multiple Images

Species recognition by using two images simultaneously proved satisfactory in the three tested stands. This statement is based on the observed kappa-values (Kappa, e.g. Congalton et al. 1983, Haara and Haarala 2002). (Table 39, Table 40).

In stand MaPS2, the old and tall pine trees, from 120 to 145 years of age, were in many cases classified as spruce or birch (Table 39). The Bayesian classifier employing the estimated covariance matrices performed better in the recognition of pines. However, the overall results improved only marginally with the Bayesian classifier. On plot MaPS2, birches were also often classified incorrectly as pines. Pine and birch are situated close to each other in the feature space (Fig. 38). Fig. 38 also illustrates how spruce and pine separate well in the variable RED-shaded. Spruce had much lower pixel values in this channel compared to pine and birch. Pine and birch are separated in the direction of variable RED-sun-lit, in which the values for birch were higher.

In the young stands PS1 and PS2, the minimum-distance classifier produced species classifications in which 78.7% and 90.5% of the tested trees were correctly recognised. When interpreting the results, it should be remembered that the test sets and training sets consisted of the same birches sampled twice. On plot PS2, the classification produced the same number of pines, spruces, and birches as there was in the ground truth. On plot PS1, the proportions changed due to asymmetric misclassification and especially the share of birch was overestimated. (Table 40).

It is possible that the difference in results between plots PS1 and PS2 are in part explained by the image data (Table 10, p. 45). On plot PS2, the sun-lit crown patches were sampled from a CIR image in scale 1:6000, and the shaded part of the crown from a CIR image in scale 1:12000. On plot PS1, the reverse order of scales was employed. In addition, on plot PS1 both images viewed the trees with 29-degree nadir angles. On plot PS2, the images were near-nadir, back- and front-lighted views with 19 and 6-degree nadir angles.

Table 39. Results of species classification in plot MaPS2.

Species by minimum distance classification	Species – ground truth. Plot MaPS2		
	Pine (47)	Spruce (89)	Birch (20)
Pine	**26**	6	4
Spruce	11	**81**	1
Birch	10	2	**15**
	78.2% correct, kappa = 0.705		
Species by Bayesian Classification	Species – ground truth. Plot MaPS2		
	Pine (47)	Spruce (89)	Birch (20)
Pine	**31**	9	5
Spruce	9	**79**	1
Birch	5	1	**14**
	79.5% correct, kappa = 0.726		

Table 40. Results of species classification in plots PS1 and PS2.

Species by minumum distance classification	Species – ground truth. Plot PS1		
	Pine (47)	Spruce (62)	Birch (4)
Pine	**38**	11	1
Spruce	3	**48**	0
Birch	6	3	**3**
	78.7% correct, kappa = 0.719		
Species by minumum distance classification	Species – ground truth. Plot PS2		
	Pine (81)	Spruce (19)	Birch (5)
Pine	**77**	2	1
Spruce	3	**15**	1
Birch	1	2	**3**
	90.5% correct, kappa = 0.857		

Table 41. Error matrix of species recognition for model stand S2.

True species	Species by classification		Total
	Spruce	Birch	
Spruce	$0.85 + \varepsilon_1$	$0.15 \times \lambda_1$	1
Birch	$0.15 \times \lambda_2$	$0.85 + \varepsilon_2$	1

Table 42. Error matrix of species recognition for model stand MaPS3.

True species	Probability to be classified as			Total
	Pine	Spruce	Birch	
Pine	$0.80 + \varepsilon_1$	$0.12 \times \lambda_1$	$0.08 \times \lambda_1$	1
Spruce	$0.12 \times \lambda_2$	$0.80 + \varepsilon_2$	$0.08 \times \lambda_2$	1
Birch	$0.08 \times \lambda_3$	$0.08 \times \lambda_3$	$0.84 + \varepsilon_3$	1

3.5 Simulations of Photogrammetric Stand Cruising

In the simulations, the effect of biased crown width measurements and biased height measurements was studied as well as the effect of imprecise photogrammetric measurements and model estimation.

Plot S2 modelled a thinning stand. Parameters in the discernibility function were $a = -456.561$ and $b = 9.437$. All dominant, co-dominant, and intermediate trees are discernible applying this function (Fig 25, p. 48). Species recognition was programmed to produce, on average, 85% of correct recognition in model stand S2 (Table 41).

Model stand MaPS3 represented a regeneration stand. The parameters of the discernibility function (Eq. 7) were $a = -4.351$ and $b = 3.12$. For trees with a height greater or equal to the dominant height (relative height = 1), the probability of being discernible is 0.987 when applying this function. The error matrix for the species recognition process used in the model stand MaPS3 is presented in Table 42.

On average, 138.6 trees out of 281 trees in the thinning stand, and 671 out of 789 trees in the mature stand were discernible in the simulations. Total volume was underestimated in both stands with unbiased measurements (Table 43). This is due to non-discernible trees. The discernibility function applied in the simulations gave comparable results (manual discernibility analysis, Table 12, p. 53, Table 14, p. 54) in both stands.

The systematic errors in total volume resulting from biased C_W and height measurements can be considerable as seen in Table 43. One metre in C_W in the model stand S2 corresponds to 24% relative error in C_W. The intervals in relative volume error are on average ± 19% in classes of height bias. Thus, the relative bias in C_W resulted in an almost one-to-one relationship with the relative error in total volume. The mean basal area weighted height of all trees in stand S2 is 17.4 metres. One metre height error thus corresponds to 5.7% in relative value. On average, the intervals in relative volume error are ±12.3% in C_W bias classes. In

Table 43. Means of 200 simulated total volume, saw wood volume, and pulp wood volume estimates, relative to true values, as a function of biased C_W and height measurements. Model stands S2 and MaPS3. Measurement errors: $\sigma(C_W) = 0.6$ m, $\sigma(h) = 1.0$ m.

		Bias in crown width estimates, m								
		1.00	0.75	0.50	0.25	0.00	−0.25	−0.50	−0.75	−1.00
		Stand S2. Total volume (true value 43.79 m³)								
	1.0	65.3	69.6	73.9	77.9	82.2	86.1	90.4	94.7	98.5
	0.5	70.1	74.5	78.9	83.5	87.8	92.0	96.7	101.1	105.7
	0.0	75.1	79.6	84.6	89.1	93.5	98.6	103.2	108.2	112.8
	−0.5	80.0	85.2	90.2	95.3	99.9	105.3	110.4	115.2	119.9
	−1.0	85.6	90.8	96.3	101.5	106.7	111.8	117.1	122.3	127.6
		Stand MaPS3. Total volume (401.0 m³)								
	1.0	66.5	71.3	76.0	80.7	85.6	90.6	95.5	100.5	106.0
	0.5	69.9	74.7	79.8	84.6	89.7	94.7	100.0	105.3	110.6
	0.0	73.3	78.4	83.4	88.7	94.1	99.2	104.8	110.4	115.8
	−0.5	76.8	82.0	87.3	92.7	98.3	104.0	109.3	115.2	120.8
	−1.0	80.1	85.7	91.3	97.1	102.6	108.3	114.5	120.3	126.3
		Stand S2. Saw wood volume (24.16 m³)								
	1.0	49.2	56.4	63.3	69.8	77.3	84.3	92.0	100.2	107.1
	0.5	56.6	63.7	70.7	78.9	86.4	94.0	102.8	111.3	120.0
	0.0	64.2	71.6	80.2	88.1	96.0	105.7	114.2	123.9	133.1
	−0.5	72.0	80.7	89.3	98.3	107.1	117.5	127.3	136.8	145.9
	−1.0	80.8	89.8	99.7	109.1	119.0	128.7	139.2	149.4	160.0
		Stand MaPS3. Saw wood volume (316.0 m³)								
	1.0	56.6	63.3	69.9	76.5	83.6	90.8	97.9	105.3	113.0
	0.5	60.7	67.4	74.6	81.5	88.9	96.0	103.7	111.3	118.8
	0.0	64.7	71.9	79.1	86.6	94.4	101.8	109.8	117.8	125.4
	−0.5	69.1	76.3	83.8	91.6	99.6	107.9	115.5	123.9	131.8
	−1.0	73.0	80.9	88.8	97.2	105.1	113.3	122.2	130.4	138.8
		Stand S2. Pulp wood volume (17.84 m³)								
	1.0	88.2	89.4	90.8	92.1	92.6	93.0	93.2	92.9	93.1
	0.5	90.1	91.6	93.0	93.5	94.2	94.4	94.2	93.7	93.3
	0.0	92.0	93.5	94.3	94.8	95.1	94.8	94.6	93.9	92.9
	−0.5	93.6	94.9	95.8	96.2	95.9	95.3	94.6	93.7	93.0
	−1.0	95.4	96.3	96.8	96.7	96.5	96.0	95.0	93.9	92.7
		Stand MaPS3. Pulp wood volume (81.15 m³)								
	1.0	103.0	100.9	98.9	96.3	93.2	89.8	86.7	83.3	80.3
	0.5	103.7	101.8	99.4	96.3	93.0	90.1	86.4	83.5	80.2
	0.0	104.7	102.6	99.4	96.7	93.1	89.7	86.5	82.9	80.3
	−0.5	105.3	103.1	100.2	97.0	93.5	89.9	86.7	83.0	80.0
	−1.0	106.3	103.7	100.7	97.1	93.6	90.0	85.9	83.2	80.0
		1.00	0.75	0.50	0.25	0.00	−0.25	−0.50	−0.75	−1.00

Bias in height estimates, m

Bias in crown width estimates, m

the model stand MaPS3, one metre corresponds to 1.9% of the mean height and 20% of the mean crown width. On average, the intervals of volume error over C_W bias classes are ±8.5% and ±21.3% over height bias classes. The relative effect of biased height measurements was stronger than the effect of biased C_W measurements in both stands. (Table 43).

In stand S2, the volume of spruce was underestimated by 14% and the volume of birch was

Table 44. Means of 200 simulated mean diameter and mean height (basal area weighted) estimates, relative to true values, as a function of biased C_W and height measurements. Stands S2 and MaPS3. Measurement errors: $\sigma(C_W) = 0.6$ m, $\sigma(h) = 1.0$ m.

	Bias in crown width estimates, m								
	1.00	0.75	0.50	0.25	0.00	–0.25	–0.50	–0.75	–1.00
Stand S2 Mean diameter (214 mm)									
1.0	94.1	96.6	99.2	101.5	104.0	106.2	108.6	111.1	113.3
0.5	95.9	98.3	100.8	103.4	105.7	108.0	110.6	112.9	115.5
0.0	97.5	100.1	102.6	105.0	107.3	110.0	112.4	115.0	117.4
–0.5	99.2	101.8	104.3	106.8	109.2	111.8	114.5	116.8	119.2
–1.0	100.9	103.5	106.1	108.6	111.1	113.6	116.1	118.6	121.2
Stand MaPS3. Mean diameter (280 mm)									
1.0	89.9	92.4	94.8	97.2	99.6	102.2	104.5	107.1	109.7
0.5	91.1	93.6	96.2	98.5	101.0	103.4	105.9	108.4	111.0
0.0	92.4	94.9	97.4	99.8	102.4	104.8	107.3	109.9	112.3
–0.5	93.7	96.1	98.6	101.0	103.6	106.1	108.6	111.2	113.7
–1.0	94.7	97.4	99.8	102.4	104.9	107.4	110.1	112.5	115.1
Stand S2. Mean height (17.4 m)									
1.0	102.1	102.0	101.7	101.5	101.3	101.1	100.9	100.8	100.5
0.5	104.9	104.6	104.4	104.3	104.0	103.8	103.6	103.5	103.4
0.0	107.6	107.4	107.2	107.0	106.7	106.6	106.4	106.3	106.1
–0.5	110.4	110.1	109.9	109.7	109.5	109.3	109.3	109.0	108.9
–1.0	113.0	112.9	112.7	112.5	112.2	112.1	111.9	111.7	111.6
Stand MaPS3. Mean height (22.6 m)									
1.0	98.4	98.3	98.1	98.1	97.9	97.8	97.7	97.7	97.6
0.5	100.6	100.4	100.4	100.2	100.1	100.0	99.9	99.8	99.7
0.0	102.7	102.6	102.5	102.3	102.3	102.1	102.0	102.0	101.9
–0.5	104.9	104.7	104.6	104.5	104.4	104.3	104.2	104.1	104.0
–1.0	107.0	106.9	106.7	106.6	106.5	106.4	106.4	106.2	106.2
	1.00	0.75	0.50	0.25	0.00	–0.25	–0.50	–0.75	–1.00
	Bias in crown width estimates, m								

Bias in height estimates, m (left vertical axis label)

overestimated by 48% with unbiased measurements (Table 45). This is due to the differences in the allometric models (Eq. 4), which predict dbh with species, C_W, and height. In the simulations, 15% of the spruce were misclassified as birch and vice versa. Since the proportions of total volume are 87% for spruce and 13% for birch (Table 2), it is understandable that the volume of spruce was underestimated and the volume of birch overestimated. In stand MaPS3, the smaller strata were also overestimated because of the errors of species classification (Table 42). The overestimation of spruce and birch was 16% and 380%, respectively. Similarly, the volume of pine was underestimated by 17% (data not shown).

With unbiased C_W and height measurements, saw wood volume in the thinning stand S2 was underestimated by 4% and by 5.6% in the stand MaPS3. The discernibility curve for stand S2 gave a high probability of discernibility to all dominant, co-dominant, and intermediate trees. The underestimation by 4% is explained by the non-linear effects that errors in species classification and the measurement errors of C_W and height have on the estimation of dbh and saw wood volume (cf. Fig. 24, p. 48). Biased C_W and height estimates cause considerable bias in saw wood volume. Pulp wood volume was underestimated in stand S2 because a portion of the intermediate trees was not discernible. In model stand MaPS3,

Table 45. Means of simulated estimates of stand attributes relative to true values (Δ, %) and the coefficients of variation (CV, %). Stand S2 with varying species recognition accuracy (randomness through elements ε_i in Table 41 not included). Unbiased measurements of C_W and height. Measurement errors: $\sigma(C_W) = 0.6$ m, $\sigma(h) = 1.0$ m.

Species recognition accuracy	Vtot		Vspruce		Vbirch		Vs		Vp	
	Δ, %	CV, %	Δ, %	CV, %	Δ, %	CV, %	Δ, %	CV, %	Δ, %	CV, %
0.75	91.2	2.4	78.8	6.7	174.6	13.3	90.9	5.6	96.4	2.9
0.80	92.3	2.4	82.4	6.3	158.7	14.5	93.6	5.3	95.4	2.9
0.85	94.0	2.2	86.0	5.2	148.0	13.4	96.7	4.6	95.4	2.9
0.90	95.0	2.0	89.7	4.3	130.0	12.5	99.4	4.2	94.2	2.8
0.95	96.6	1.9	93.9	3.5	114.8	12.0	102.8	3.8	93.7	2.2

the pulp wood volume was overestimated only if the crown width measurements produced underestimates by 0.5 metres or more. This is also explained by the non-linearities of grading (cf. Fig. 24, p. 48). With unbiased measurements, the pulp wood volume was underestimated by 6.9% because of the omission errors. (Table 43).

In model stand S2, the basal area weighted mean-diameter of trees is overestimated even with unbiased measurements by 7.3% (16 mm). It is explained in part by the fact that the small trees are not measurable in the photographs. The model used for predicting the dbh with estimates on species, C_W, and height is also non-linear and causes part of the observed bias. Basal area weighted mean-height of trees is overestimated by 6.7% (1.1 m) with unbiased measurements. A portion of small trees is non-discernible, and the mean height is therefore overestimated. It is clear that bias in height estimates has a direct impact on the estimate of the mean height. Bias in C_W also has a small effect on the mean height. This is explained by the weighting with the square of dbh. On plot MaPS3, the omission errors cause the mean diameter and height to be overestimated even if the measurements are unbiased. (Table 44).

In order to demonstrate the importance of accurate species recognition results for the model stand S2 were computed with varying accuracy of species recognition (Table 45). A high accuracy

Table 46. Coefficients of variation in percentage computed from 200 simulations with unbiased measurement errors. Model stands S2 and MaPS3. Measurement errors: $\sigma(C_W) = 0.6$ m, $\sigma(h) = 1.0$ m. Species recognition accuracy, see Table 41 and Table 42.

Variable	Stand S2	Stand MaPS3
	Coefficient of variation, %	
Vtot	2.2	1.7
Vpine	–	7.4
Vspruce	6.1	13.0
Vbirch	15.7	22.2
Vs	4.7	2.4
Vp	2.8	2.3
Mean diameter	1.1	0.8
Mean height	0.5	0.3

(0.9–0.95) is needed in mixed stands for the reliable estimation of the small strata.

Coefficients of variation were computed from the simulations in which the measurement errors had zero expectances (Table 46). The random errors cancel each other, and high precision was observed as can be expected. If the forest were measured by using plots instead of full mapping of trees, an element of sampling error would be included in the results. Such simulations were not performed.

4 Discussion

4.1 Tree Discernibility

It seems inevitable that in most cases photogram-metric stem number estimates based on individual tree positions will be underestimates. Overestimates can be caused by commission errors only. The results of tree discernibility implied that in most cases the probability of discernibility for the suppressed, shortest trees is very small. These trees are occluded with a high probability in oblique views by the dominant trees and by the shadows of neighbouring trees. The height distribution of trees and the stand structure seem to determine largely what portion of trees is potentially measurable. In managed stands with only one crown-layer and a narrow height distribution, the underestimation in stem number will be lower. In stands with bimodal or wide height distribution, the stem number will be underestimated considerably. In the study material there were no samples of seed tree stands or young stands with single remnant trees, nowadays left in the forest for bio-diversity reasons. In such stands, it is possible that a larger portion of the smallest trees is discernible, since the upper canopy is sparse.

The analysis of discernibility indicated that a large portion of trees that constitute the commercial stem volume is measurable with manual image-matching by using CIR photographs in scale 1:6000. The lowest proportion for total volume was observed in an unmanaged 60-year old spruce stand with high growing stock and large height variation. In that stand, 88% of total volume, 98% of saw wood volume, and 82% of pulp wood volume were discernible. In the other tested stands, the proportions of discernible total volume varied from 92% to 100%. In stands with bimodal or wide height distribution, the pulpwood volume is inevitably underestimated if the pulp-wood resides in the suppressed and intermediate trees. This was demonstrated in plot MaPS4, a stand in which there was an upper layer of old

pine trees and an understorey of spruce. In it, 94% of the total volume, but only 77% of the pulpwood volume was measurable.

The volume of saw wood resides in the largest stems. In the tests, these trees were discernible with a high probability, and thus it seems possible to assess the saw wood volume without notable underestimation. The observed proportions of discernible saw wood volume ranged from 96% to 100%, and they were in all stands higher than the proportion of discernible total volume. The proportion of discernible pulp wood volume ranged from 77% to 100%. It was close to the proportion of discernible total volume in the thinning stands, but lower in the mature stands. In mature stands, the non-discernible intermediate trees with high proportion of pulp wood volume were the cause for this.

The results of discernibility were obtained by using manual image-matching and four to six CIR images in scales 1:6000 and 1:12 000. Wide-angle cameras viewed the stands from different directions with 60% side and forward overlaps (1:6000). In some cases, substitute images in the scale of 1:12 000 were used if the photo-strip in scale 1:6000 did not cover the field plot. With support from the field data, the operator knew where to look for the smallest trees. This means that the results (level of discernibility) are attainable only under optimal conditions and that the results represent upper bounds. In the images used in the discernibility analysis, the sun elevation was 35 degrees, which is close to the typically required minimum of 33 degrees. The number of trees shaded by larger trees can be expected to be lower for a higher sun elevation. In addition, it can be assumed that less occlusion is present in images that are taken with a normal angle camera that has a longer focal length. Also, the results would have been different for a smaller number of views. The stands in which discernibility was tested were subjectively selected and do not represent the full

variation in factors affecting the discernibility. Thus the results obtained in this study should be generalised with caution. For example, in mixed stands, different species can form separate canopy layers, and in these stands, the underestimation of a particular species can be considerable.

The underestimation in stem number can be considerable and the photogrammetric stem count is an unreliable estimate for the true stem number. On the other hand, if the shape and position of the discernibility function can be estimated, it would be possible to correct the estimate of stem count for the intermediate and suppressed trees. This calibration, however, would require that the discernibility function be known with high reliability. Without field observations it can be difficult. Active remote sensing methods such as laser scanning could perhaps provide information about the small trees.

The findings on tree discernibility when using multiple image-matching of aerial images are in accordance with results of earlier studies on stereoscopic interpretation (e.g. Talts 1977) and laser ranging (see Section 1.3.1, Persson et al. 2002).

4.2 Automated 3D Tree Top Positioning and Tree Height Estimation

3D positioning of tree tops is of great importance in the context of the proposed photogrammetric individual tree measurement schema (Fig. 1, p. 8). In it, tree top positions are supposed to benefit the processes of crown width measurement and species recognition. The results of the performance tests imply that a portion of the tree tops can be mapped in 3D accurately without a multitude of commission errors. Manual image-matching by using multiple image-matching or stereoscopic measurements can be used to complete and correct the set of detected tree tops.

Best case hit-rates of 100% were observed in three tested stands. In these stands, the semi-automatic positioning method was able to locate all of the tree tops which had been determined as discernible and without more than 5% of commission errors. These stands are characterised by low variation in tree height and a regular pattern of trees. The best case hit-rates were higher in the three tested managed stands than in the

unmanaged counterparts. The unmanaged stands usually have a higher stem number so there will also be a greater need for later manual editing of the positionings. In the unmanaged stands the spatial pattern of trees is likely less regular, and there can be more variation in tree height, crown dimensions, and species selection. These are all likely causes for the inferior performance.

The number and scale of images had an effect on the results. Image-pair sets were inferior to image sets that consist of four or more images. The theoretical image sets with up to seven or eight images, as well as the scale-combination sets with six images in two scales, produced best performance. In many cases, the effect of scale was such that better performance was observed for the large-scale image sets. However, it is difficult to draw conclusions about the effect of image scale because the 3D top positions of model trees were the same for all tested image combinations, and they were obtained using four to six images in scale 1:6000. In a real situation, the operator measures the model tree with the image material available. Also, the use of downsampled images in the scale of 1:6000 complicated the interpretation of the effects of scale. Operational tests will be needed to further evaluate the effect of scale on the performance of the method. The viewing angle of the images was shown to have an effect on the performance. In many cases, the theoretical image sets consisting of images with high nadir angle (oblique views) were inferior to the sets with same number of images, which had a smaller average nadir angle. The probability of occlusion is higher in oblique views. Performance of the positioning algorithm was better in CIR images than in colour images.

The proposed 3D positioning method relies on a set of parameters, which affect the performance. Exact proposals for their optimal tuning are not given in this study. In the method, a model tree is selected, measured for 3D tree top position, and used for template acquisition. Template matching relies on successful realization of these tasks. The objective is to acquire cross-correlation images with sharp local maxima at the correct 2D image locations. The results of the sensitivity analysis and the experience gained during the development of the method suggest that a small tree, which is likely occluded in oblique views, is not optimal.

Nor is a tree with exceptional crown. The optimal position of the template with respect to the crown pattern on the image seems to be such that the template is centred below the tree top. Thus, the template captures more of the crown than the background. This is in line with results by Larsen and Rudemo (1998) which apply to spruce.

The sensitivity analysis showed that changes in the metric parameters, which affect the depth and vertical position of the search space, cause predictable and interpretable changes in the performance of 3D tree top positioning algorithm. Manual measurement of the model tree (top position) proved crucial. Measurement errors in the Z-coordinate were shown to map almost one-to-one to the candidate positions. This sets high demands on the quality of the manual measurement and on the quality of the image material. In addition, a wrongly set depth or position of the search space has an effect on the accuracy of Z, hit-rate and commission error-rate. In order to apply the proposed method for positioning of tree tops, the search space must be correctly set in 3D to contain the tree tops of discernible trees. Hit-rate will be low and commission error-rate high if the search space is positioned above or below the canopy. The positions will get averaged in Z if the depth of the search space is too low.

At best, the RMSE of XY-errors (planimetric positioning accuracy for the trees with a hit, inside the hit-cylinders) of the algorithm was approximately 0.5–0.6 m. This is approximately 0.4–0.5 m if the estimated imprecision of the field measurements is subtracted. The RMSE of Z-coordinate was at best 0.7–0.8 m. This corresponds to 0.5–0.6 m if the imprecision of Z in the ground truth is deducted. As stated, the positions can be biased in Z due to inaccurate model tree measurement. In all, it seems plausible to state that the method works at the individual tree level. It may be possible to establish continuous forest inventory that operates at the single tree level and is based on the tree positions.

There are limitations and prerequisites. The orientation of the images has to be accurate, as the 3D tree top positioning method relies on geometric constraints. Also, it seems that large-scale images are required. Large-scale images allow reliable measurement of the model tree, and they can be used for the quality control and for the edit-

ing of the false and erroneous tree top positions. However, the method is not restricted to the use of images in one scale only. Image sets with images in different scales produced in many cases best results in the performance tests. Since the costs of image material are largely determined by the scale, it would maybe be advisable to perform aerial photography in two scales and such that the large scale images have less image overlap.

Very high-resolution airborne laser scanning (ALS) has been shown to produce similar or even better positioning and height measurement accuracy for single trees (e.g. Hyyppä et al. 2001, Persson et al. 2002). However, even with ALS there seems to be a need for a calibration of the height estimates. Echoes that are expected to return from the ground are actually returned from the ground flora, and unless very high resolution is used, the uppermost parts of tree tops are not hit by the beam (Persson et al. 2002). Requirements for high resolution, small beam divergence, and narrow near-nadir scanning angle all add of costs of laser scanning.

4.3 Measurement of Crown Width

The allometric models that predict dbh from tree height and crown width are based on the assumption that the tree is measured for the maximum crown width. Even on ground the crown width cannot be measured unambiguously. Trees can have single exceptionally long branches and crowns can be asymmetric due to crown competition. Thus, the measurements from the ground or from an image are inherently inaccurate, susceptible to bias, and imprecise. The allometric relationships between crown dimensions and stem size form the basis of the indirect estimation. Many factors that affect the relationships are possibly not accounted for in the current models. These factors can be related with the site type, stand-history, or age and to estimate these factors only by using the aerial photographs, can be difficult. From this, it seems apparent that very high accuracy for dbh or volume estimates cannot be expected at the single tree level even if the exact crown dimensions are known.

Large systematic underestimation of crown width was observed in the tests of manual pho-

togrammetric measurement of crown width. The amount of underestimation varied between tree species, and was largest for spruce, 0.8 metres. The underestimation correlated with the field measured crown width so that the absolute underestimation was largest for the trees with large field measured crown width. Unexpectedly the underestimation was smallest for the small-scale images in scales 1:12 000 and 1:16 000.

Near-nadir views proved best for visual determination of crown width. An observation of the crown width was possible in over 90% of the near-nadir cases. Off-nadir observations, particularly those in the side-lighted regions of the photograph, were found less fit for manual measurement of crown width. For these off-nadir and side-lighted views, which represent approximately 39% of the photo-area (wide-angle camera), the proportion of successful measurements was as low as 78.5%. Differences in the measurability were also observed between front-lighted, side-lighted, and back-lighted photo-areas. The results imply that there are possibly areas better suited for the automatic measurement of crown width. Small trees will likely pose a challenge should the automation of crown width measurement be tried, because of the lower probability of discernibility.

One operator was used in the tests. There is an element of subjectivity involved in the manual measurements. The results obtained are, thus, tentative and should be interpreted with caution.

High-sampling-rate airborne laser scanning data, with small footprint size, will likely be superior in comparison to passive image data (cf. Persson et al. 2002). Shadows do not cause a problem with ALS data as they seem to do in aerial images. Problems caused by overlapping crowns, occlusion, and imprecision of the allometric models are shared by both ALS data and aerial images.

4.4 Species Recognition

This work presented a new method for species recognition by using multiple CIR aerial images and spectral classification. This was not an initial objective for this work, but rather a by-product. The Kappa-coefficients in the three tested stands ranged from 0.71 to 0.86, and the overall recognition accuracy from 78% to 90%. Under similar forest conditions and quite comparable image material, but with smaller tree sets, Haara and Haarala (2002) obtained Kappa-values from 0.40 to 0.86 by using monocular images and segmentation. It is too early to draw conclusions about the superiority of either approach. However, especially for separating between pine and spruce, the suggested method proved efficient. Misclassification between pine and spruce was the main source of errors in the work by Haara and Haarala (2002).

The proposed species recognition strategy relies on the accurate 3D tree top positions. In the tests, the tree top positions were obtained by means of manual image-matching, and the operator traversed the image for the proper location so that the crowns were sampled for pixels from the sun-lit and of the shaded parts of the crown. The automation of the sampling procedure remained unsolved. It is probable that an increased position inaccuracy will worsen the accuracy of species recognition. Training data was local and from the same stand. It can be argued if such data collection scheme is cost-efficient in practice. There are problems related to the continuously varying image-object-sun geometry, film development, weather conditions, and phenology of trees, which will all have to be accounted for if spectral classification is attempted. Normalisation of images, which are taken under varying photographic conditions (weather, sun elevation, exposure, development), is probably difficult (cf. Haara and Haarala 2002). In the context of the proposed species recognition method, the normalisation could perhaps be done 'via ground' by using the mapped trees of the training set. Their spatial density should be high enough so that for each image there would be available several samples from various parts of the image. However, it remained unclear how far in the image-object-sun-metrics the training data is still valid. In addition, it remained unclear if the training sets should be collected separately for trees of different age and vigour. Concerning the phenology of trees, it is plausible that little can be done with respect to the timing of photography (Haara and Haarala 2002, Fig. 4) although it is likely that phenology has an effect on species recognition accuracy.

The species recognition accuracy will most

likely be inferior in stands that are more diverse. Improvement in species recognition can be expected with the introduction of digital aerial cameras if their spectral resolution is superior to that of the films. Species recognition methods that are based on the use of airborne laser scanning data have relied on the use of statistical measures of the 3D data and on the intensity of the echoes (Brandtberg et al. 2003, Holmgren 2003). Holmgren (2003) reports of 95% overall classification accuracy for separating Scots pine and Norway spruce by using high resolution (5 points per m^2) laser data from a flying height of 130 metres.

4.5 Photogrammetric Single Tree Measurements in the Estimation of Stand Attributes

This study was confined to the assessment of timber resources. The appraisal of timber resources is the core element of forest inventories. However, the list of variables of interest in a forest inventory can be extensive depending on the information needs.

The results of the simulations, which on their part were based on the findings of this study, imply that an inventory scheme, which uses photogrammetric individual tree measurements, full mapping of trees, and indirect estimation can provide precise distribution estimates such as sums and means of the volumes, height and diameter of trees. However, these estimates of timber resources are susceptible to large systematic errors. This is due to the imperfections of the allometric models and likely biased measurements. Inherent underestimation is also unavoidable because not all trees in a stand are discernible. The accuracy of species classification needs be high if accurate estimates of timber resources by species are required in the mixed stands. In comparison to the accuracy of customary standwise field inventory (e.g. Poso 1983, Laasasenaho and Päivinen 1986), results for the basic stand attributes can be more accurate, should photogrammetric stand cruising be applied. Prerequisites for this are field visits, which would provide calibration data.

It is not always sufficient for the end-user of the data that the sums and means are correct. For example, in pre-harvest timber cruising, it can be desirable to get an accurate estimate of the diameter-height distribution per species (Uusitalo 1995). This requires that the photogrammetric measurements and subsequent model estimates are accurate at the tree level and that the averaging effect is compensated for, or avoided. Averaging is inherently present in the estimates of allometric regression models, and averaging was observed in the 3D tree top position estimates. Very accurate estimates at the tree level cannot be expected even if the image measurements on species, crown width, and tree height were perfect because of the imprecision of the allometric models.

4.6 Costs and Applicability

The appraisal of the costs of an inventory scheme that utilises photogrammetric individual tree measurements, is determined largely by the material costs of photography and the amount of field-work and manual photogrammetric work.

High quality is required for the exterior orientation of the images. The use of satellite positioning has reduced the need of ground control points, which are expensive to measure and mark in the field. Automatic methods for the solution of interior and exterior orientation can be used to trim down the costs. Large-scale images are required. The largest scale tested for this study was 1:6000, and it seems that a least part of the image material should be in this scale to enable reliable manual measurements. Metric aerial cameras were used in this study. Such cameras are not necessarily required, but the camera to be used needs to be calibrated for imperfections. Aerial photography is typically done only under clear sky conditions in the summertime. In this respect, airborne laser scanning is much more flexible, although if leaf-on data is required, the data acquisition is restricted to the summer season for laser scanning and photography alike.

The current material costs of aerial photography (for large projects) in Finland are approximately 120 € per scanned and orientated image. The costs are approximately 2–3 €/ha for images in the scale of 1:6000 assuming 60% and 20% overlaps. In this study, images in scales 1:12000 and 1:16000 were used in combination with images in 1:6000. The costs for such medium-scale material are

approximately 1–2 €/ha assuming 60% forward and 60% side overlaps. In a given area, there is only a certain proportion of forest, in which it is reasonable to use the individual tree approach. This will add to the per hectare costs. On the other hand, the image material may be valid for other purposes as well.

To strive for the full mapping of trees is possibly too ambitious, since in a real situation the tree top positioning algorithm will not provide the best observed (see Section 3.2.1) hit-rates of 75–100%. The operator needs to complete the missed trees. This can be time-consuming. In the tests for tree discernibility, tree tops were measured with a rate of 40–80 trees per hour. The rate of height measurements in the field is approximately 15–20 trees per hour. In a stand with 600 discernible trees per hectare, the complementary editing of the missed trees and commission errors can thus take up to 2–3 hours. If full mapping of trees is replaced by sampling, the costs of operator work can be reduced significantly. However, the accuracy of the results will worsen because of the element of sampling error. The required sampling rate for a stand will largely be determined by the within-stand variation (cf. Talts 1977). In this respect, the photogrammetric approach of forest inventory does not differ from the conventional methods. However, for the system to be operational and cost-efficient, the automation of species recognition and the measurement of crown size need to be solved.

Field visits seem inevitable, since the estimates are susceptible to systematic errors. Non-discernibility of trees, biased crown width and height measurements, and allometric models are the sources of systematic errors. In addition, it can be appropriate to have a reliable training set for species recognition. Even for sole timber cruising, such qualitative observations of stems can be needed which are impossible to obtain from the aerial photographs (Uusitalo 1995).

The proposed methodology combines expert knowledge in surveying, photogrammetry, digital image analysis, and forest mensuration. This study presents tools and methods to be incorporated in an interactive, semi-automatic image-based interpretation system. For the system to be applicable, the degree of automation should be increased.

4.7 Elevation Models

In this study it was assumed that an accurate elevation model is available for height estimation and for the estimation of the search space used by the semiautomatic 3D tree top positioning algorithm. This assumption is questionable.

In Finland, basic maps have elevation contour lines at intervals of 2.5, 5, and 10 metres. Raster DEMs have been interpolated by using these data. The National Land Survey of Finland reports of an analysis in which the standard deviation of elevation differences between DEM and geodetic points (N = 62876) was 1.39 metres and a mean absolute error of 1.76 metres (Maanmittauslaitos 1997). There were differences between map sheets. This reflects the photogrammetric method by which the data was originally collected. The raster DEMs have a 25-metre resolution. Thus, it is clear that they cannot represent well breaklines or small-scale topographic variation. The modelled topography is flattened out. The accuracy of the DEMs derived from basic maps will not suffice for the methods presented in this study.

Airborne laser scanning (ALS) can be used for terrain modelling of wooded areas (Kraus and Pfeifer 1998). ALS can provide elevation accuracy in the range between 0.5 and 2 centimetres per 100 metres of flying height (Baltsavias 1999). A combined flight with a passive camera and laser scanner could perhaps be used for data acquisition (cf. Baltsavias 1999). In this way, the terrain elevation would be obtained from the ALS-data, and the images would be used for tree measurements. The ALS-data could also provide an approximation for the 3D search space required by the 3D tree top positioning algorithm (e.g. Næsset 1997). Integrated ALS and passive sensing requires careful flight planning. The field of view (FOV) of ALS is typically restricted to 20–40 degree scan angles, whereas aerial cameras have FOV from 60 to 80 degrees (Baltsavias 1999). The flying heights for ALS is typically from 200 to 1000 metres, whereas aerial images in scale 1:6000, and smaller, are taken from 900 metres and above. The current costs of ALS data acquisition are approximately 2–3 €/ha using an aeroplane at the flying height of 900 metres. If the aim is to try individual tree extraction from the ALS data, a lower flying height and/or speed

is required.

The topographic aerial photographs, which are taken in early spring under leaf-off conditions, are an alternative for the estimation of elevation. In CIR images, the ground is barely detectable and trees are emphasised. Panchromatic topographic images are better in this respect and could possibly be used for the calibration of an existing DEM.

4.8 General Conclusions and Suggestions for Future Research

In this study, an attempt to study the whole photogrammetric measurement and estimation scheme was tried. 3D positioning of tree tops by using multiple image-matching is the core of the scheme upon which other measurement processes are expected to be founded on. As such, the idea of estimating the characteristics of single trees with aerial photographs is not novel. This study tried to answer questions that are concerned with the automation of the photogrammetric measurements. An investigation for the upper bounds was performed. Tree discernibility tests implied that at least in the managed stands a large portion of the commercial timber is measurable should semi-automatic or manual methods for the tree detection be applied. Accurate position estimation of tree tops was proven possible in both the semi-automatic method and in the manual image-matching. Tests in the manual measurement of crown width revealed that these measurements are likely to be imprecise and inaccurate. A method for species recognition, which uses multiple images and spectral classification was demonstrated, and the tentative results imply that the proposed approach can possibly make species recognition more reliable in comparison to existing methods that operate on monocular images. The estimation of the characteristics of single trees is indirect, and the allometric models are inherently imprecise and susceptible to systematic errors. Very high estimation accuracy at the single tree level cannot be expected. The simulations demonstrated that high precision for the stand attributes is possible by applying full mapping of the stand.

There are parts in the measurement and estima-

tion scheme that should be studied further and developed for better methods should the approach be applied in practice.

The semi-automatic 3D tree top positioning algorithm is likely applicable only in an area where the tree crowns do not exhibit large variation and the variation in tree height is restricted. These areas could be stands or sub-stands. Automatic delineation of such inventory strata, or problematic areas could be incorporated to the 3D tree top positioning algorithm. The delineation could perhaps be carried out by using segmentation of orthoimages combined with auxiliary information on the spatial variation of stand height. Stand height information could be assessed by using automatic image-matching of stereo pairs (Næsset 2002), by using multiple image-matching (Grün and Baltsavias 1988) or by using the ranging laser data (Hyyppä and Inkinen 1999).

The templates that are captured from the images are applicable only locally in the varying image-object-sun geometry of the images. Further studies will be needed for testing the applicability of templates in the image-object-sun metrics, and the applicability of synthetic templates (e.g. Larsen 1997).

Template matching that uses a single-sized template is not invariant to the size of crowns. In a stand where the crowns exhibit large variation, the use of multi-scale templates could be possible to overcome the problem. However, the whole image-matching strategy would have to be reconsidered in such a case.

The 3D tree top positioning algorithm relies on a number of parameters, which need to be optimised by the operator. Further studies should address the objective of finding ways for quick acquisition of good approximate values.

Automatic measurement of crown width remained unsolved. It may be well assumed that the 3D positions of tree tops will facilitate the task by providing the number of crowns and seed values for the image locations. Multiple images can possibly be used to control the estimation. Consistency of the estimates of different images could perhaps be used for quality control. Model based matching (e.g. Tarp-Johanssen 2001), least-squares matching (Kraus 1997), and image segmentation methods (e.g. Gougeon 1995) are possible solutions to the problem of automating

crown width measurements.

The proposed method for species recognition assumes that the images are traversed for the correct image locations from the tree top locations where the sun-lit and shaded parts of crown can be sampled for pixel values. The automatic implementation of this can be challenging. With respect to species recognition and spectral classification of multiple CIR images, the requirements of the training sets need to be investigated. A method is needed for linking the field-mapped tree set with the trees positioned by using the aerial photographs. The need for image normalisation in the context of the spectral classification should be looked into.

The integration of laser scanning and aerial photography can possibly be used to solve problems related with the DEM and the setting of the search space. Methods are needed for the calibration of photogrammetric measurements and model estimates. Finally, more tests in practice will be needed, since the field and image material for this study was limited. Young stands were completely lacking from the data set. Also, it seems likely that mixed stands and unmanaged stands will be challenging for the application of the methodology. In this study, a wide-angle camera was used. Normal angle cameras exhibit less perspective distortion and are possible a better choice. In the near future digital cameras will enter the market and possibly offer features that will be of use.

Acknowledgements

References

Åge P.J. 1983. Mätning och tolkning i flygbilder för skogsinventering. LMV-Rapport 1983:5. Lantmäteriet. Gävle. Sweden. ISSN 0280-5731. 44 p. (In Swedish).

Aldred A.H. 1964. Wind-sway error in parallax measurements of tree height. Photogrammetric Engineering 30(5): 732–734.

— 1976. Measurement of tropical tree on large-scale aerial photographs. For. Manage. Inst. Ottawa, Ontario. Information Report FMR-X-86. Can. For. Service. 38 p.

— & Sayn-Wittgenstein, L. 1972. Tree diameters and volumes from large-scale aerial photographs. For. Manage. Inst. Ottawa, Ontario. Information Report FMR-X-40. Can. For. Service. 39 p.

— & Hall, J.K. 1975. Application of large-scale photography to a forest inventory. The Forestry Chronicle 51(1). 7 p. A reprint.

Alphen van, B.J. 1994. Forest border detection on digital images. University of Helsinki. Department of Forest Resource Management. Master's thesis. 40 p.

Anttila, P. 1998. Analyyttisellä stereoplotterilla ilmakuvilta tulkittujen puukohtaisten tunnusten tarkkuus. Master's thesis. University of Joensuu, Faculty of Forestry. 36 p. (In Finnish).

— & Lehikoinen, M. 2002. Kuvioittaisten puustotunnusten estimointi ilmakuvilta puoliautomaattisella latvusten segmentoinnilla. Metsätieteen aikakauskirja 3/2002: 381–389. (In Finnish).

Avery, G. 1958. Helicopter stereo-photography of forest plots. Photogrammetric Engineering 24(4): 617–624.

Axelsson, H. 1972. Information om skoglig flygbildteknik. Nämnden för skoglig flygbildteknik. 42 p. (In Swedish)

Bäckström, H. & Welander, E. 1948. En preliminär undersökning rörande möjligheterna att skilja olika trädslag på flygbilder. Svenska skogsvårdsföreningens tidskrift 3: 180–200. (In Swedish).

Baltsavias, E.P. 1999. A comparison between photogrammetry and laser scanning. International Society of Photogrammetry and Remote Sensing. Journal of Photogrammetry and Remote Sensing 54(2–3): 83–94.

Bickford, C.A., Mayer C.E. & Ware K.D. 1963. An efficient sampling design for forest inventory: the northeastern forest resurvey. Journal of Forestry 59(10): 761–763.

Bilker, M. & Kaartinen, H. 2001. The quality of real-time kinematic (RTK) GPS positioning. Reports of the Finnish Geodetic Institute 2001(1). 25 p.

Brandtberg, T. 1999. Automatic individual tree based analysis of high spatial resolution aerial images on naturally regenerated boreal forests. Canadian Journal of Forest Research 29: 1464–1478.

— 2002. Individual tree-based species classification in high spatial resolution aerial images of forests using fuzzy sets. Fuzzy Sets and Systems 132: 371–387.

— & Walter, F. 1999. An algorithm for delineation of individual tree crowns in high spatial resolution aerial images using curved edge segments at multiple scales. In: Hill, D.A. & Leckie, D.G. (Eds.). Proceedings of Int. Forum on automated Interpretation of High Spatial Resolution Digital Imagery for Forestry, Feb 1998. Victoria, Canada: 41–51.

— , Warner, T.A., Landerberger, R.E, McGraw, J.B. 2003. Detection and analysis of individual leaf-off tree crowns in small footprint, high sampling density lidar data from the eastern deciduous forest in North America. Remote Sensing of Environment 85: 290–303.

Case, J.B. 1980. Automation in photogrammetry. In: International Society of Photogrammetry and Remote Sensing. International Archives for Photogrammetry and Remote Sensing, Vol. XXIII, Part B2, Commission II. Hamburg 1980. p. 38–49.

Cohen, B.W., Spies, T.A. & Bradshaw, G.A. 1990. Semivariograms of digital imagery for analysis of conifer canopy structure. Remote Sensing of Environment 34: 167–178.

Congalton, R.G., Oderwald, R.G. & Mead, R.A. 1983. Assessing Landsat classification accuracy using

discrete multi-variate analysis statistical techniques. Photogrammetric Engineering and Remote Sensing 49(12): 1671–1678.

Cramer, M. 1999. Direct geocoding – is aerial triangulation obsolete? In: Fritsch, D. & Spiller, R. (Eds.). Photogrammetric Week '99. Herbert Wichmann Verlag, Heidelberg 1999. p. 59–70.

— , 2001. On the use of direct georeferencing in airborne photogrammetry. Proc. 3rd Int. Symp. On Mobile Mapping Technology, January 2001, Cairo. Digital publ. on CD, 13 p.

— , Stallman, D. & Haala, N. 2000. Direct georeferencing using GPS/inertial exterior orientations for photogrammetric applications. International Archives for Photogrammetry and Remote Sensing, Vol. XXXII/B Amsterdam, 2000. p. 198–205.

Dralle, K. 1997. Locating trees by digital image processing of aerial photographs. PhD-thesis. Danish Forest and Landscape Research Institute and Dept. of Mathematics, The Royal Veterinary and Agricultural University. March, 1997. 117 p.

— & Rudemo, M. 1996. Stem number estimation by kernel smoothing of aerial photos. Canadian Journal of Forest Research 26: 1228–1236.

— & Rudemo, M. 1997. Automatic estimation of individual tree positions from aerial photographs. Canadian Journal of Forest Research 27: 1728–1736.

El-Hakim, S.F. & Ziemann, H. 1982. A step-by-step strategy for gross-error detection. In: International Society of Photogrammetry and Remote Sensing. International Archives for Photogrammetry and Remote Sensing. Vol. 24-III. Helsinki 1980. p. 145–153.

Ericsson, O. 1984. Beståndsinventering med flygbild. Summary: Stand inventory by Aerial Photogrammetry. Forskningsstiftelsen Skogsarbeten. Redogörelse NR 8 1984. 19 p. (In Swedish).

Fent, L., Hall, R.J. & Nesby, R.K. 1995. Aerial films for forest inventory: optimizing film parameters. Photogrammetric Engineering and Remote Sensing 61(3): 281–289.

Fish, S. 2000. Combining geostatistics and geographic information systems to provide locally specific estimates of basal area and volume per hectare from forest inventory plots. Master's thesis. University of Helsinki, Department of Forest Resource Management. 89 p.

Flesch, T.K. & Wilson, J.D. 1999. Wind and remnant tree sway in forest cutblocks. II. Relating measured tree sway to wind statistics. Agr. and For. Meteorology 93: 243–258.

Förstner, W. 1982. On the geometric precision of digital correlation. International Archives for Photogrammetry and Remote Sensing 24(3): 176–189.

Fryer J.G. 1989. Camera calibration in non-topographic photogrammetry. 2nd edition. American Society for Photogrammetry and Remote Sensing. p. 59–69.

Gagnon, P.A., Agnard J.P. & Nolette, C. 1993. Evaluation of a soft-copy photogrammetry system for tree-plot measurements. Canadian Journal of Forest Research 23: 1781–1785.

Gates, D.M. 1980. Biophysical ecology. Springer-Verlag, New York Inc. 611 p.

Gerrard, D.J. 1969. Error propagation in estimating tree size. Photogrammetric Engineering 35(4): 355–362.

Gong, P., Sheng, Y. & Biging, G.S. 2002. 3D model-based tree measurement from high-resolution aerial imagery. Photogrammetric Engineering and Remote Sensing 68(11): 1203–1212.

Gonzalez, R.C. & Woods, R.E. 1993. Digital image processing. Addison-Wesley Publishing Company. 716 p.

Gougeon, F.A. 1995. A crown-following approach to the automatic delineation of individual tree crowns of high spatial resolution aerial images. Canadian Journal of Remote Sensing 21(3): 274–284.

— , Leckie, D.A., Paradine, D. & Scott, I. 1999. Individual tree crown species recognition: the Nahmint study. In: Hill, D.A. & Leckie, D.G. (Eds.). Proceedings of Int. Forum on automated Interpretation of High Spatial Resolution Digital Imagery for Forestry, Feb 1998. Victoria, Canada: 209–223.

Gruen, A. 1982. Phototriangulation with analytical plotters using natural tie points. In: International Society of Photogrammetry and Remote Sensing. International Archives for Photogrammetry and Remote Sensing. Vol. 24-III. Helsinki 1980. p. 145–153.

Grün, A. & Baltsavias, E. 1988. Geometrically constrained multiphoto matching. Photogrammetric Engineering and Remote Sensing 54(5): 633–651.

Haara, A. & Haarala, M. 2002. Tree species classification using semi-automatic delineation of trees on aerial images. Scandinavian Journal of Forest Research 17: 556–565.

— & Nevalainen, S. 2002. Detection of dead or defoliated spruces using digital aerial data. Forest Ecology and Management 160: 97–107.

Hall, R.J. & Aldred, A.H. 1992. Forest regeneration appraisal with large scale aerial photographs. The Forestry Chronicle 68(1): 142–150.

Hearn, D. & Baker, M.P. 1997. Computer graphics. C version. 2nd edition. Prentice Hall 652 p.

Helava, U. 1978. Digital correlation in photogrammetric instruments. Photogrammetrica 34: 19–41.

— 1991. State of the art in digital photogrammetric workstations. The Photogrammetric Journal of Finland 12(2): 65–76.

van den Heuvel, F.A. 1998. 3D reconstruction from single image using geometric constrains. International Society of Photogrammetry and Remote Sensing. Journal of Photogrammetry and Remote Sensing 53: 354–358.

Hobrough, G. 1959. Automatic stereoplotting. Photogrammetric Engineering and Remote Sensing 25(5): 763–769.

Holmgren, J. 2003. Estimation of forest variables using airborne laser scanning. Doctoral dissertation. Acta Universitatis Agriculturae Sueciae. Silvestria 278. SLU, Umeå, Sweden. 43 p.

Holopainen, M. 1998. Forest habitat mapping by means of digitized aerial photographs and multispectral airborne measurements. Publications of the Department of Forest Resource Management 18. University of Helsinki. 48 p.

Horn, H.S. 1971. The adaptive geometry of trees. Princeton University Press, Princeton 144 p.

Horn, B.K.P. 1983. Noncorrelation methods for stereo matching. Photogrammetric Engineering and Remote Sensing 49(4): 535–536.

Hyppänen, H. 1996. Spatial autocorrelation and optimal spatial resolution of optical remote sensing data in boreal forest environment. International Journal of Remote Sensing 17(17): 3441–3452.

Hyyppä, J. & Inkinen, M., 1999. Detecting and estimating attributes for single trees using laser scanner. The Photogrammetric Journal of Finland 16(2): 27–42.

Hyyppä, J., Kelle O, Lehikoinen, M & Inkinen, M. 2001. A segmentation-based method to retrieve stem volume estimates from 3-D tree height models produced by laser scanners. IEEE Transaction on Geoscience and Remote Sensing 39(5): 969–975.

Ilvessalo, Y. 1950. On the correlation between crown diameter and the stem of trees. Communicationes Instituti Forestalis Fenniae 38(2). 32 p.

Jakobsons, A. 1970. Sambandet mellan trädkronans diameter och andra trädfaktorer, främst brösthöjdsdiametern: analyser grundade på riksskogstaxeringens provträdsmaterial. Stockholms skoghögsskolan, institutionen för skogstaxering. Rapporter och uppsatser 14. 75 p. (In Swedish).

Jain, A.K. 1989. Fundamentals of digital image processing. Prentice-Hall international editions. 567 p.

Jain, R., Kasturi, R. & Schunck, B. 1995. Machine vision. McGraw-Hill international editions. 549 p.

Jensen, R. & Köhl, M. 1992. Sampling design and data analysis of the second Swiss national forest inventory. Proc. of Ilvessalo Symposium on National Forest Inventories, Finland 17–21 August 1992. (Organized by IUFRO S4.02). Metsäntutkimuslaitoksen tiedonantoja – The Finnish For. Res. Inst. Research Papers 444: 61–69.

Jiyu, L., Xiaoming, C., Deren, L., Guang, W., Jingnian, L., Wei, L., & Jinxiang, Z. 1996. GPS kinematic carrier phase measurements for aerial photogrammetry. International Society of Photogrammetry and Remote Sensing. Journal of Photogrammetry and Remote Sensing 51(5): 230–242.

Johnson, E.W. 1958. The effect of photographic scale on precision of individual tree-height measurement. Photogrammetric Engineering 24(1): 142–152

Jonsson, B., Jacobsson, J. & Kallur, H. 1993. The forest management planning package. Theory and application. Studia Forestalia Suecica 189. 56 p.

Jupp, D.L.B., Strahler, A.H. & Woodcock C.E. 1988. Autocorrelation and regularization in digital images. I. Basic theory. IEEE Transaction on Geoscience and Remote Sensing 26(4): 463–473.

Kalliovirta, J. 2003. Laserelaskoopin tarkkuus ja tehokkuus. Summary: The accuracy and efficiency of laser-relascope. Master's thesis. University of Helsinki. Department of Forest Resource Management. 60 p. (In Finnish).

— & Tokola, T. 2003. Functions for estimating stem diameter and age of tree using the crown length, height and existing stand register information. Manuscript for journal publication.

Kangas, A. 1994. Classical and model based estimators for forest inventory. Silva Fennica 28(1): 3–14.

Kamara, H.M. 1989. An introduction to non-topographic photogrammetry. In: Non-topographic photogrammetry. 2nd edition. American Society for Photogrammetry and Remote Sensing. p. 1–6

Key, T., Warner, T.A., McGraw, J. & Fajvan M.A. 1999. An evaluation of the relative value of spectral and phenological information for tree crown classifica-

tion of digital images in the eastern deciduos forest. In: Hill, D.A. & Leckie, D.G. (Eds.). Proceedings of Int. Forum on automated Interpretation of High Spatial Resolution Digital Imagery for Forestry, Feb 1998. Victoria, Canada: 243–250.

Kiema, P. 1990. Latvusten projisointi numeerisen ilmakuvan koordinaatistoon yksittäisen puun numeerisen ilmakuvatulkinnan menetelmässä. Master's thesis. University of Helsinki. Department of Forest Mensuration and Management. 76 p. (In Finnish).

Konecky, G. 1981. Development of photogrammetric instrumentation and its future. Finnish Society of Photogrammetry, 50th Anniversary Publication. p. 21–48.

Korpela, I. 2000. 3-d matching of tree tops using digitized panchoromatic aerial photos. University of Helsinki. Department of Forest Resource Management. Licentiate thesis. 109 p.

Kovats, M. 1997. A large-scale aerial photographic technique for measuring tree heights on long-term forest installations. Photogrammetric Engineering and Remote Sensing 63(6): 741–747.

Kraus, K. 1993. Photogrammetry. Volume 1. Fundamentals and standard processes. Dummler Bonn. 397 p.

— 1997. Photogrammetry. Volume 2. Advanced methods and applications. Dummler Bonn. 466 p.

— & Pfeifer, N. 1998. Determination of terrain models in wooded areas with airborne laser scanner data. International Society of Photogrammetry and Remote Sensing. Journal of Photogrammetry and Remote Sensing 53(2): 193–203.

Kujala, V. 1958. Mäntykasvit – Pinaceae. In: Jalas, J. (Ed.), Suuri kasvikirja I. Otava, Helsinki. p. 129–152. (In Finnish).

— 1965. Koivukasvit – Betulaceae. In: Jalas, J. (Ed.), Suuri kasvikirja II. Otava, Helsinki. p. 68–101. (In Finnish).

Kvarnbrink, T. & Thunberg, A. 1952. Inblickbarhet i stereomodell över skog. Ett modellförsök. Tekniska högskolan i Stockholm. Available from KTH, The Royal Institute of Technology, Stockholm. 172 p. (In Swedish).

Laasasenaho J. 1982. Taper curve and volume functions for pine, spruce and birch. Communicationes Instituti Forestalis Fenniae 74. 74 p.

— & Päivinen, R. 1986. Kuvioittaisen arvioinnin tarkistamisesta. Summary: On the checking of inventory by stands. Folia Forestalia 664. 19 p. (In Finnish).

Larsen, M. 1997. Crown modeling to find tree top positions in aerial photographs. In: Proceedings of the third International Airborne Remote Sensing Conference and Exhibition, Copenhagen, Denmark. ERIM international. Vol 2: 428–435.

— 1999a. Finding an optimal match window for spruce top detection based on an optical tree model. In: Hill, D.A. & Leckie, D.G. (Eds.). Proceedings of Int. Forum on automated Interpretation of High Spatial Resolution Digital Imagery for Forestry, Feb 1998. Victoria, Canada: 55–63.

— 1999b. Individual tree top position estimation by template voting. Presentation (re-print) at the Fourth International Airborne Remote Sensing Conference and Exhibition / 21st Canadian Symposium on Remote Sensing, Ottawa, Canada, 21–24 June 1999. 8 p.

— 1999c. Jittered match windows voting for tree top positions in aerial photographs. In: Proceedings of the 11th Scandinavian Conference on Image Analysis, Kangerlussuauq, Greenland. June 7–11 1999. Vol 2: 889–894.

— & Rudemo, M. 1997. Using ray-traced templates to find individual trees in aerial photographs. Proceedings of the 10th Scandinavian Conference on Image analysis. Lappeenranta, Finland. June 9–11, 1997: 1007–1014.

— & Rudemo, M. 1998. Optimizing templates for finding trees in aerial photographs. Pattern Recognition Letters 19(12): 1153–1162.

Leckie, D.G. 1990. Advances in remote sensing technologies for forest surveys and management. Canadian Journal of Forest Research 20: 464–483.

Lindeberg T. 1994. Scale-space theory in computer vision. Kluwer academic publishers. 423 p.

Lillesand, T. & Kiefer, R. 1979. Remote sensing and image interpretation. John Wiley & Sons, Inc. 612 p.

Lyons, E.H. 1961. Preliminary studies of two camera low-elevation stereo-photography from helicopters. Photogrammetric Engineering and Remote Sensing 27(1): 72–76.

Lyytikäinen, H.E. 1972. Ilmakuvien tulkinta. TKY/ Otapaino 321. 91 p. (In Finnish).

Maanmittauslaitos 1997. Korkeusmallin tarkkuutta tutkittu. Uutisia. Positio – Paikkatiedon erikoislehti 3/1997. Maanmittauslaitos. 32 p. (In Finnish).

Maltamo, M., Tokola, T. & Lehikoinen, M. 2001. Estimating stand characteristics by combining single tree pattern recognition of digital video imagery

and a theoretical diameter distribution model. Forest Science 49(1): 98–109.

McGlone J.C. 1989. Analytic data reduction schemes in non-topographic photogrammetry. In: Non-topographic photogrammetry. 2nd edition. American Society for Photogrammetry and Remote Sensing. p. 37–58.

Methley, B.D.F. 1986. Computational models in surveying and photogrammetry. Blackie & Son Ltd. Glasgow. 346 p.

Meyer, P., Staenz, K. & Itten, K.I. 1996. Semi-automated procedures for tree species recognition in high spatial resolution data from digitized colour infrared-aerial photography. International Society of Photogrammetry and Remote Sensing. Journal of Photogrammetry and Remote Sensing 51: 155–165.

Mitchell, K.J. 1975. Stand description and growth simulation from low-level stereo photos of tree crowns. Journal of Forestry 1/1975: 12–16.

Muinonen, E., Maltamo, M., Hyppänen, H. & Vainikainen, V. 2001. Forest stand characteristics estimation using a most similar neighbor approach and image spatial structure. Remote Sensing of Environment 78: 223–228.

Murtha, P.A. 1972. A guide to air photo interpretation of forest damage in Canada. Canadian Forestry Service. Publication No. 1292. 62 p.

Næsset, E. 1992a. Tolkning av treslagsfordeling i infrarøde og pankromatiske flybilder. Interpretation of tree species mixture on infrared and panchromatic aerial photos. Norwegian Forest Research Institute: Meddelelser fra / Communicationes of Skogsforsk 44(10). 20 p. (In Norwegian).

— 1992b. Effekten av målestokk, filmtype og brenvidde ved toklkning av treslagsfordeling i flybilder. The effect of scale, type of film and focal length upon interpretation of tree species mixture on aerial photos. Norwegian Forest Research Institute: Meddelelser fra / Communicationes of Skogsforsk 45(5). 28 p. (In Norwegian).

— 1993. Tolkning av bestandsmiddelhøyde, kronedekning og treslag i flybilder fra sommer og høst. Interpretation of stand mean height, crown closure and tree species on aerial photographs from summer and autumn. Norwegian Forest Research Institute: Meddelelser fra / Communicationes of Skogsforsk 46(11). 28 p. (In Norwegian).

— 1997. Determination of mean height of forest stands using airborne laser scanner data. International Society of Photogrammetry and Remote Sensing. Journal of Photogrammetry and Remote Sensing 52: 49–56.

— 1998. Determination of stand volume in practical forest inventories based on field measurements and photo-interpretation: the Norvegian experience. Scandinavian Journal of Forest Research 13: 246–254.

— 1999. Point accuracy of combined pseudorange and carrier phase differential GPS under forest canopy. Canadian Journal of Forest Research 29: 547–553.

— 2002. Determination of mean tree height of forest stands by digital photogrammetry. Scandinavian Journal of Forest Research 17(5): 446–459.

— , Skråmo, G. & Tomter, S.M. 1992. Norske erfaringer med bruk av flybiler ved skogregistering. (Summary: Forest surveying by means of aerial photographs: the Norwegian experiences). In: Næsset, E. (Ed.), Skogsregistering og skogsbruksplanlegging. Aktuelt fra Skogforsk 13–1992, Dept. of Forest Sciences, Agric. Univ. of Norway, Ås. p. 3–12. (In Norwegian).

— & Jonmeister, T. 2002. Assessing point accuracy of DGPS under forest canopy before data acquisition, in the field and after postprocessing. Scandinavian Journal of Forest Research 17(4): 351–358.

— & Økland, T. 2002. Estimating tree height and tree crown properties using airborne scanning laser in a boreal nature reserve. Remote Sensing of Environment 79: 105–115.

Nelson, R., Swift, R. & Krabill, W. 1988. Using airborne lasers to estimate forest canopy and stand chracteristics. Journal of Forestry Oct 1988: 31–38.

Nilson, T. & Ross, J. 1996. Modeling radiative transfer through forest canopies: implications for canopy photosynthesis and remote sensing. In: Gholz, H.L., Nakane, K. & Shimoda, H. (Eds.), The use of remote sensing in the modelling of forest productivity. Kluwer Acad. Publ., Dordrecht, The Netherlands, p. 23–60.

Nyyssönen A. 1955. On the estimation of the growing stock from aerial photographs. Communicationes Instituti Forestalis Fenniae 46(1): 1–57.

— 1962. The use of aerial photography in inventories of tropical forests. Publication of the Finnish Society of Photogrammetry 3: 1–4.

— 1979. Assessment of forest resources for forest management. Silva Fennica 13(3): 269–277.

—, Poso, S. & Keil, C. 1968. The use of aerial photographs in the estimation of some forest characteristics. Acta Forestalia Fennica 82.4. 35 p.

Oker-Blom [Stenberg], P. 1986. Photosynthetic radiation regime and canopy structure in modeled forest stands. Acta Forestalia Fennica 197. 44 p.

Olofsson, K. 2002. Detection of single trees in aerial images using template matching. ForestSAT Symposium, Heriot Watt University, Edinburgh, August 5–9 2002. 6 p.

Päivinen, R. 1987. Metsän inventoinnin suunnittelumalli. Joensuun yliopiston luonnontieteellisiä julkaisuja 11. University of Joensuu. 179 p. (In Finnish).

Persson, A., Holmgren, J. & Soderman, U. 2002. Detecting and measuring individual trees using an airborne laser scanner. Photogrammetric Engineering and Remote Sensing, 68(9): 925–932.

Petrie, G. 2003. Airborne digital frame cameras. The technology is really improving. *GEOInformatics*. Oct/November 2003: 18–27.

Pinz, A. 1999a. Tree isolation and species classification. In: Hill, D.A. & Leckie, D.G. (Eds.). Proceedings of Int. Forum on automated Interpretation of High Spatial Resolution Digital Imagery for Forestry, Feb 1998. Victoria, Canada: 127–139.

— 1999b. Austrian forest inventory system. In: Hill, D.A. & Leckie, D.G. (Eds.). Proceedings of Int. Forum on automated Interpretation of High Spatial Resolution Digital Imagery for Forestry, Feb 1998. Victoria, Canada: 375–381.

Pitkänen, J. 2001. Individual tree detection in digital aerial images by combining locally adaptive binarization and local maxima methods. Canadian Journal of Forest Research 31: 832–844.

Pollock, R.J. 1994. A model-based approach to automatically locating individual tree crowns in high-resolution images of forest canopies. Presentation at the first International Airborne Remote Sensing Conference and Exhibition, Strasbourg, France, 11–15 September 1994. 13 p.

— 1996. The automatic recognition of individual trees in aerial images of forests based on a synthetic tree crown model. PhD-thesis in computer science. The University of British Columbia. 158 p.

Pope R. B. 1957. The effect of photo scale on the accuracy of forest measurements. Photogrammetric Engineering 23(1): 869–873.

Poso, S. 1972. A method of combining photo interpretation and field samples in forest inventory. Communicationes Instituti Forestalis Fenniae 76(1). 133 p.

— 1983. Kuvioittaisen arvioimismenetelmän perusteita. Summary: Basic features of forest inventory by stands. Silva Fennica 17(4): 313–349. (In Finnish).

— & Kujala, M. 1971. Ryhmitetty ilmakuva- ja maasto-otanta Inarin, Utsjoen ja Enontekiön metsien inventoinnissa. Summary: Groupwise sampling based on photo and field plots in forest inventory of Inari, Utsjoki and Enontekiö. Folia Forestalia 132: 1–40. (In Finnish)

—, Wang, G. & Tuominen, S. 1999. Weighting alternative estimates when using multisource auxiliary data for forest inventory. Silva Fennica 33(1): 41–50.

Pouliot, D.A., King, D.J., Bell, F.W. & Pitt, D.G. 2002. Automated tree crown detection and delineation in high-resolution digital camera imagery of coniferous forest regeneration. Remote Sensing of Environment 82: 322–334.

Pukkala, T. & Kolström, T. 1991. Effect of spatial pattern of trees on the growth of a Norway spruce stand. A simulation model. Silva Fennica 25(3): 117–131.

Räsänen, P., Heiskanen, J., Miettinen, J., Sunden T. & Torpo, J. 1992. Metsänhoitotieteen opetuskoealat Hyytiälässä. University of Helsinki. Department of Forest Ecology Publications 4. 108 p. (In Finnish).

Ripley, B.D. 1981. Spatial statistics. John Wiley & Sons. 252 p.

Rohde, W.G. & Olson, C.E. 1972. Multispectral sensing of forest tree species. Photogrammetric Engineering March 1972: 1209–1215.

Rosenholm, D. 1980. Image correlation algorithms. International Archives for Photogrammetry and Remote Sensing 23(B2): 139–158.

Salmenperä, H. 1973. Avaruuskolmiointimenetelmät. Technical University of Tampere. 104 p. (In Finnish).

Sarjakoski, T. 1981. Concept of completely digital stereoplotter. The Photogrammetric Journal of Finland 8(2): 95–100.

— 1989. Digitaalinen stereokuvakartta – tulevaisuuden karttatuote? Maanmittaus 1/1989: 93–110. (In Finnish).

Sarvas, R. 1938. Ilmavalokuvauksen merkityksestä metsätaloudessamme. Über die Bedeutung Luftfotogrammetrie in unserer Waldwirtschaft. Silva

Fennica 48. 49 p. (In Finnish with German summary).

— 1964. Havupuut. WSOY, Porvoo. 518 p. (In Finnish).

Savioja, M. 1991. Havupuumetsikön stereokojeavusteisesta arvioinnista. Maanmittaus 2/91: 4–14. (In Finnish).

Sayn-Wittgenstein, L. 1978. Recognition of tree species on aerial photographs. Forest Management Institute. Ottawa, Ontario. Information report FMR-X-188. Canadian Forest Service. Dept. of the Environment. 97 p.

— & Aldred, A., H. 1972. Tree size from large-scale photos. Photogrammetric Engineering Oct 1972: 971–973.

Schenk, T. 1999. Digital photogrammetry. Volume I. Terrascience, Laurelville OH, USA. 428 p.

— & Toth C. 1992. Conceptual issues of softcopy photogrammetric workstations. Photogrammetric Engineering and Remote Sensing, 58(1): 101–110.

Secilla, J.P., Narciso, G. & Carrascosa J. 1987. Locating templates in noisy environments. In: Proceedings of the 5th Scandinavian Conference on Image Analysis. Stockholm, June 1987. IAPR Vol. 1: 101–108.

Sheng, Y., Gong, P. & Biging, G.S. 2001. Model-based conifer-crown surface reconstruction from high-resolution aerial images. Photogrammetric Engineering and Remote Sensing 67(8): 957–965

Smith, J.L. 1986. Evaluation of the effects of photo measurement errors on predictions of stand volume from aerial photography. Photogrammetric Engineering and Remote Sensing 52(3): 401–410.

Sonka, M., Hlavac, V. & Boyle, R. 1998. Image processing, analysis and machine vision. 2nd edition. PWS Publishing. 770 p.

Spencer, R.D. & Hall, R.J. 1988. Canadian large-scale aerial photographic systems (LSP). Photogrammetric Engineering and Remote Sensing 54(4): 475–482.

Spurr, S.H. 1960. Photogrammetry and photo-interpretation. The Ronald Press Company, New York, 1960. 472 p.

St-Onge, B.A. & Cavayas, F. 1995. Estimating forest stand structure from high-resolution imagery using the directional variogram. International Journal of Remote Sensing 16(11): 1999–2021.

Ståhl, G. 1994. Optimizing the utility of forest inventory activities. Dissertation. Swedish Univ. of Agric. Sciences. Section of Forest Mensuration and Management. Report 27. Umeå 1994. 46 p.

Stenberg P. 1996. Metsikön rakenne, säteilyolot ja tuotos. University of Helsinki. Department of Forest Ecology Publications 15. 68 p. (In Finnish).

Stolze, P. 2001. Finding single trees in aerial images. Master's thesis. Dept. of Economics and Natural Resources. RVAU Copenhagen. 97 p.

Strahler, A.H. 1997. Vegetation canopy reflectance modeling – recent developments and remote sensing perspectives. Remote Sensing Reviews 15: 179–194.

Schwidefsky K. & Ackermann F. 1978. Fotogrammetria. Otakustantamo. 384 p. (In Finnish).

Talts, J. 1977. Mätning i storskaliga flygbilder för beståndsdatainsamling. Summary: Photogrammetric measurements for stand cruising. Royal College of Forestry. Department of forest mensuration and management. Research notes NR 6 – 1977. 102 p. (In Swedish).

Tarp-Johanssen, M.J. 2001. Locating individual trees in even-aged oak stands by digital image processing of aerial photographs. PhD Thesis. Dept. of Mathematics and Physics. RVAU. Copenhagen, Denmark. 158 p.

Tomppo, E. 1986. Models and methods for analyzing spatial patterns of trees. Communicationes Instituti Forestalis Fenniae 138. 65 p.

— 1992. Multi-source national forest inventory of Finland. In: Proc. of Ilvessalo Symposium on National Forest Inventories, Finland 17–21 August 1992. (Organized by IUFRO S4.02). Metsäntutkimuslaitoksen tiedonantoja – The Finnish For. Res. Inst. Research Papers 444: 52–60.

— , Henttonen, H. & Tuomainen, T. 2001. Valtakunnan metsien 8. inventoinnin menetelmä ja tulokset metsäkeskuksittain Pohjois-Suomessa 1992–94 sekä tulokset Etelä-Suomessa 1986–92 ja koko maassa 1986–94. Metsätieteen aikakauskirja IB/2001: 99–248. (In Finnish).

Tötterström, S. 2000. GPS RTK-network ja virtuaalitukiasema (VRS). GPS-mittauksen uusi ulottuvuus. Maankäyttö (5/2000): 41–43. (In Finnish).

Uusitalo J. 1995. Pre-harvest measurement of pine stands for sawing production planning. University of Helsinki. Publications of the Department of Forest Resource Management 9. 96 p.

Uuttera, J., Haara, A., Tokola & T. Maltamo, M. 1998. Determination of the spatial distribution of trees from digital aerial photographs. Forest Ecology

and Management. 110: 275–282.

Varjo, J. 1997. Change detection and controlling forest information using multitemporal Landsat TM imagery. Acta Forestalia Fennica 258. 64 p.

Willingham, J.W. 1957. The indirect determination of forest stand variables from vertical aerial photographs. Photogrammetric Engineering 23(1): 892–893.

Woodcock, E.C. & Strahler, A.H. 1987. The factor of scale in remote sensing. Remote Sensing of Environment 21: 311–332.

Worley, D.P. & Landis, G.H. 1954. The accuracy of height measurements with parallax instruments on 1:12000 photographs. Photogrammetric Engineering 20(1): 823–829.

Wulder, M., Niemann, K.O. & Goodenough, D.G. 2000. Local maximum filtering for the extraction of tree locations and basal area from high spatial resolution imagery. Remote Sensing of Environment 73: 103–114.

Zheng Y.-J. 1993. Digital photogrammetric inversion: theory and application to surface reconstruction. Photogrammetric Engineering and Remote Sensing 59(4): 489–498.

Total of 176 references